NASA/CR -1998- 207722

IN-93-CR
084830

300 GEV OBSERVATIONS OF UNIDENTIFIED EGRET SOURCES
A SEARCH FOR TEV COUNTERPARTS TO BATSE GAMMA-RAY BURSTS

Grant NAG5-3581

Final Report

For the period 15 November 1996 to 14 November 1997

Principal Investigator

Dr. Trevor C. Weekes

March 1998

Prepared for
National Aeronautics and Space Administration
Washington, DC

Smithsonian Institution
Astrophysical Observatory
Cambridge, Massachusetts 02138

The Smithsonian Astrophysical Observatory
is a member of the
Harvard-Smithsonian Center for Astrophysics

1. Extraordinary Astronomy

There are few things more intriguing in high energy astrophysics than the study of the highest energy particles in the universe. Where and how these particles achieve their extreme energies is of interest not only to the astrophysicist but also to the particle physicist. At GeV and TeV energies the problem is manageable since the physics is known and the acceleration processes feasible. But the energy spectrum extends to $10^{20} Ev$ and there the problem of their origin is both more difficult and interesting; in fact at these high energies we do not even know what the particles are.

The study of the origin and distribution of relativistic particles in the universe has been a challenge for more than 80 years but it is only in recent years that the technology has become available to really address the question. Although something can be learnt from studies of composition and energy spectrum, the origins (and thence the acceleration mechanisms) can only come from the direct study of the neutral particle component (in this respect the highest energy particles are effectively neutral since they are virtually undeflected). The feasible channels of investigation are therefore the study of the arrival directions of: (1) TeV photons (covered by the following U.S. experiments: STACEE, Whipple/VERITAS, MILAGRO and, to some extent, by EGRET/GLAST); (2) neutrinos of TeV energy and above (AMANDA/KM3); (3) the highest energy cosmic rays (HiRes, Auger).

While these studies represent a form of astronomy they are the astronomy of the *extraordinary universe*, the universe populated by the most dynamic and physically exciting objects, the universe of the high energy astrophysicist whose cosmic laboratories represent conditions beyond anything that can be duplicated in a terrestrial laboratory. This extraordinary astronomy may say little about the normal evolution of stars and galaxies but it opens windows into cosmic particle acceleration where new and strange physical processes take place.

2. Role of Whipple Collaboration

The Whipple Gamma Ray Collaboration was formed in 1982 with the aim of improving the sensitivity of the ground-based atmospheric Cherenkov technique by the use of imaging cameras on large optical detectors. The approach was successful and the discipline of ground-based TeV astronomy was established. The first confirmed galactic source was discovered by the Whipple Collaboration as were the first two extragalactic sources. The technique has now matured and several new and important astrophysical results have been produced.

The γ-ray group of the Smithsonian Astrophysical Observatory is a key component of the Whipple Gamma Ray Collaboration. With all its members resident in Arizona, all its activities are devoted to research in ground-based γ-ray astronomy.

3. The Crab Nebula

TeV observations of the Crab Nebula made at the Whipple Observatory over the last decade indicate no evidence for flux variability in the energy range from 400 GeV to more than 10 TeV, making this object a valuable standard candle for calibration purposes.

The spectrum of the Crab Nebula exhibits a remarkably broad dynamic range, spanning the energy range from less than 10^{-4}eV to at least 5x10^{13} eV. Gould (Gould 1965) postulated that the entire spectrum (then not even known to extend to X-ray energies) could be explained by a Compton-synchrotron model. From the lowest radio frequencies up to sub-GeV energies, the spectrum is dominated by the synchrotron emission of relativistic electrons with energies extending up to 1 PeV; these are now believed to be accelerated by the pulsar wind. The GeV-TeV photons arise from inverse Compton scattering of synchrotron photons or other low energy photons (e.g. the microwave background) in the nebula by the relativistic electrons.
Over the dynamic range 500 GeV to 5 TeV the spectrum is well represented by a power law of the form $J = (3.2 \pm 0.7).10^{-7} \times (E/1TeV)^{2.49\pm0.06\pm0.05}$ m^{-2}s^{-1}TeV^{-1} (Mohanty et al. 1998). A recent observation by CANGAROO at low elevations provides data in the energy region > 7 TeV, which suggests that a power law spectrum might extend up to 50 TeV. However, the air shower array limits at energies greater than 100 TeV fall below the extrapolation. If this linear power law is extrapolated to lower energies, it passes more than a decade above the upper EGRET point at 5 GeV. A form which is quadratic in Log (E) (Hillas et al. 1998) satisfies both the GeV and TeV data and is consistent with upper limits at energies greater than 100 TeV. This spectrum implies a magnetic field in the nebula of 160μG, close to the equipartition value.

4. Supernova Remnants: Shell-type

The canonical theory of cosmic ray origins suggests that they emanate in shell-type SNRs. High energy γ-ray observations can indicate which SNRs have a large content of relativistic cosmic ray hadrons, and TeV γ-ray observations, in particular, have the sensitivity and angular resolution to reduce background confusion. EGRET measurements of SNRs are not definitive because the detector has low angular resolution at 100 MeV and measurements are masked by gas clouds. Collisions of cosmic ray nuclei with the interstellar medium result in the production of neutral pions which subsequently decay into γ-rays. These processes result in a secondary γ-ray spectrum which follows the primary cosmic ray spectrum at energies above ~10 GeV up to ~1/10 of the maximum proton energy of ~ 100 TeV.
Calculations indicate that the luminosity of nearby SNRs should be sufficient for detection by the most sensitive VHE γ-ray telescopes. If there is a density enhancement from a molecular cloud, current ACTs and EGRET should already be able to detect the γ-ray emission from some objects. For a source spectral index of α=2.1, Drury et al. (1994) estimate the integral γ-ray flux at earth to be

$$F(>E) \approx 9 \times 10^{-11} \left(\frac{E}{1\ \mathrm{TeV}}\right)^{-1.1} \left(\frac{\theta E_{SN}}{10^{51}\mathrm{erg}}\right) \left(\frac{d}{1\ \mathrm{kpc}}\right)^{-2} \left(\frac{n}{1\ \mathrm{cm}^{-3}}\right)\ \mathrm{cm}^{-2}\mathrm{s}^{-1} \qquad (1)$$

where θ is defined as the fraction of the supernova energy E_{SN} converted into cosmic rays, d is the distance to the SNR, and n is the average density of the ISM around the remnant.
Assuming $\theta \approx 0.15$, a fairly conservative value for the average density of $n \approx 0.2\mathrm{cm}^{-3}$ and the canonical value $E_{SN} \approx 10^{51}$ ergs, gives a flux $F(>200\ \mathrm{GeV}) \approx 1.6 \times 10^{-11}(d/1\ \mathrm{kpc})^{-2}$ – photons cm^{-2}s^{-1}. This flux lies close to the sensitivity limit of the current generation of TeV telescopes.
For several of the unidentified EGRET sources there is now evidence for an association with a SNR (γ-Cygni, IC443 and W44. Observations by the Whipple telescope do not confirm the

Table 1: SNR Upper Limits

Source	EGRET Flux x$10^{-7} cm^{-2} s^{-1}$	Whipple Upper Limit x$10^{-11} cm^{-2} s^{-1}$
W44	5.0	<3.0
W51	<3.2	<3.6
γ-Cygni	12.6	<2.2
W63	<1.9	<6.4
Tycho		<0.8
IC443	5.0	<2.1

expected extension of the γ-ray spectrum[?]Buckley et al. 1998). Some of these limits are listed in Table 1. They lie a factor of ten below the predicted spectrum, but there is still significant uncertainty in the remnant parameters so that the canonical model is not yet in jeopardy. It is also possible that the EGRET associations with the SNR are incorrect. Although not yet definitive, the upper limits require that the source spectrum for IC443 and γ-Cygni be steeper than $E^{-2.4}$; this would imply that the additional steepening of the cosmic ray spectrum due to propagation effects in the galactic disk should be -0.3 rather than the preferred value of -0.6.

5. Pulsars

A likely source of TeV γ-rays is radio pulsars; this is particularly so since more than six of them have been detected as γ-ray emitters by CGRO. There were also unconfirmed reports of pulsed emission from several early TeV experiments. The most convincing detection, a steady pulsed signal from the Crab pulsar, was from the Durham group (Dowthwaite et al. 1984); the observed flux was $\sim 1 \times 10^{-11}$ cm^{-2}s^{-1} at 1 TeV. More sensitive observations show that less than 5% of the total TeV flux is pulsed (Gillanders et al. 1997). Evidence for the detection of a pulsed signal was also suggested for the Vela pulsar and for the Geminga pulsar. However, observations with more sensitive imaging ACTs failed to confirm these early results.

An extensive search by the Whipple group for emission for the two other EGRET pulsars (Geminga: Gillanders et al. 1997; PSR 1951+32 Srinivasan et al. 1997a) that are visible in the northern hemisphere failed to find any evidence for emission. No TeV pulsed signal has been detected from the other (southern) CGRO pulsars, PSR B1706-44 and PSR B 1055−52 either. No TeV observations have been reported yet on PSR B0656+14.

The upper limits for the TeV flux from the EGRET γ-ray pulsars are below the fluxes extrapolated from the GeV region of EGRET detection assuming a power law spectrum of constant index. The emission from the pulsar magnetosphere seems to turn off or to fall off steeply in VHE region. It has been have argued that the pulsed component will extend to VHE energy in outer gap models.

The analysis of pulsars is not trivial since it is necessary to ascertain that the system timekeeping is sound, that the absolute timing is accurate, that the pulsar emphemeris (usually based on radio observations) is correct, and that the times of arrival are barycentered and folded correctly.

Table 2: Whipple Limits from Gamma Ray Pulsars

pulsar		EGRET HE flux (10^{-7} cm^{-2} s^{-1})	Group	VHE Flux (10^{-12} cm^{-2} s^{-1})	E_{th} (TeV)
Crab	unpulsed	7.7 ± 0.8	Whipple	8.8 $(E/TeV)^{-1.69}$	0.4
	pulsed	23	Whipple	< 0.2	0.25
Geminga	unpulsed	–	Whipple	< 8.9	0.5
			Whipple	< 5	0.5
1951+32	pulsed	1.6 ± 0.2	Whipple	<5.4	0.3

Once a periodic γ-ray pulsar signal has been detected, then all systems are verified; however a null result leaves the suspicion that one or more of the above may have been incorrect.
To verify all components of the Whipple pulsar data taking and analysis, the telescope was converted into an optical telescope to observe the optical pulsar in the Crab Nebula. This was achieved by stopping down the central pixel of the 10m camera and recording the output on a scaler readout every 1 millisec. Folding the data taken over a ten minute observation at the predicted pulsar period revealed the familiar double-peaked light- curve of the Crab pulsar with the main peak exactly at the predicted phase (Srinivasan et al. 1997b). The null results reported above can therefore be treated with confidence.

6. Unidentified EGRET Sources

Despite extensive searches for counterparts at long wavelengths for the 30 odd low latitude unidentified EGRET sources close to the galactic plane, no identifications have been made and their nature is unknown. A search for counterparts at high energies is justified because many of the sources exhibit flat spectra and the imaging ACTs have good source location capabilities. The Whipple telescope has been used to observe a number of these (Buckley et al. 1997) but no significant emission has been seen.

7. Bursts

A feature of γ-ray astronomy has been that as the energy is increased there is an increase in the degree of temporal variation. As seen above, in AGN studies, TeV variations with doubling times as short as 15 minutes have been observed. It would not be unexpected that TeV γ-ray bursts would be observed, either as the tail end of classical γ-ray bursts or as a manifestation of a new phenomenon.
There are a number of exotic suggestions that justify a search for γ-ray bursts at TeV energies. These include emission from the decay of primordial black holes(PBHs) and cosmic strings. Most models predict a final explosion of energy when all possible evaporation channels are available, but the number of degrees of freedom of emission is a highly controversial issue. Upper limits have already been set to the PBH density by atmospheric Čerenkov and air shower array experiments under various assumptions.

Predictions have been made that (i) non-conducting cosmic strings acquire cusps that are smoothed out by emitting bursts of TeV γ-rays over ill-defined time-scales and that (ii) superconducting strings with a saturated current produce a jet of fermions which decay to TeV γ-rays over a 1 second period. In general these predictions have sufficient free parameters that non-detections are not serious limitations; however the exciting new physics that a positive detection would indicate fully justify the search for new burst phenomena as TeV detectors are developed with improved flux sensitivity.

Since August 1992, the Whipple collaboration has searched for bursts on a one second time-scale, both on-line and in the archival data-base. The methodology required for a search of this nature (where the source can come from anywhere in the field and the onset is unknown) is unlike that used in the search for point sources and required the development of new analysis techniques (Connaughton et al. 1998). The number of bursts of 3 or more per 1 second was compared with the expectation value and no significant excess was obtained over the 4 years of the data-base. From this null result a reliable limit to the density of PBHs could be derived.

Although the serendipitous overlap of an atmospheric Čerenkov telescope with its limited field of view with a classical BATSE- detected burst is unlikely, there is some hope of detecting the delayed high energy component seen in some bursts. It is possible to make rapid follow-up observations of BATSE bursts using source positions distributed on the BACODINE network. The effectiveness of these observations is limited by the restricted duty-cycle of ACTs, by the imprecise position locations of the bursts, by the slew speed of the telescope and by its limited field of view. Nonetheless observations by the Whipple Collaboration of 16 BATSE positions, one acquired within two minutes of the reported BATSE burst time, have been reported (Connaughton et al. 1997; Boyle et al. 1997). However in no case did the FOV of the telescope overlap the complete error box in source position uncertainty. No evidence of TeV emission is found and upper limits to the high-energy delayed or extended emission were derived based on assumptions of the source positions.

References

Boyle, P.J. et al., Proc. 25th ICRC (Durban, South Africa), 3, 61 (1997).

Buckley, J. H. et al. 1998, A& A, in press.

Buckley, J. H. et al. 1997b, Proc. 25th ICRC (Durban), 3, 237.

Carter-Lewis, D.A. et al. 1997 Proc. 25th ICRC (Durban), 3, 161.

Connaughton, V., et al., ApJ, 479, 859 (1997).

Connaughton, V., et al., Astroparticle Phys. (in press) (1998).

Dowthwaite, J.C. et al., Astrophys.J. 286, L35 (1984)

Drury, L.O'C., Aharonian, F.A., Volk, H.J., Astron.Astrophys. 287, 959 (1994).

Gillanders, G.C., et al., Proc. 25th ICRC (Durban, South Africa) 3, 185 (1997).

Gould, R.J., Phys.Rev.Lett. 15, 511 (1965).

Hillas, A.M. et al., ApJ, in press (1998).

Mohanty, G. et al., Astroparticle Phys. (in press) (1998).

Srinivasan, R. et al., Astrophys. J., 489, 170 (1997a).

Srinivasan, R. et al., Proc. Workshop on A.C.T.s (Kruger Park, South Africa), Aug. 1997, in press.(1997b)

Appendix A.

Selected Reprints/Preprints.

(1) Connaughton, V., Akerlof, C. W., Barthelmy, S., Biller, S. D., Boyle, P., Buckley, J. H., Carter-Lewis, D. A., Catanese, M., Cawley, M. F., Cline, T., Fegan, D. J., Finley, J., Fishman, G. J., Gaidos, J. A., Gehrels, N., Hillas, A. M., Kouveliotou, C., Lamb, R. C., Lessard, R., McEnery, J., Meegan, C., Mohanty, G., Porter, N. A., Quinn, J., Rose, H. J., Rovero, A.C., Samuelson, F., Schubnell, M. S., Sembroski, G., Srinivasan, R., Weekes, T. C., Wilson, C. and Zweerink, J. "A Search for TeV Counterparts to BATSE Gamma-ray Bursts", ApJ (1997) 479, 859.

(2) Connaughton, V., Akerlof, C.W., Biller, S.D., Buckley, J.H., Carter-Lewis, D.A., Catanese, M., Cawley, M.F., Fegan, D.J., Gaidos, J.A., Hillas, A.M., Lamb, R.C., Lessard, R., McEnery, J., Mohanty, G., Porter, N.A., Quinn, J., Rose, H.J., Rovero, A.C., Samulson, F., Schubnell, M.S., Sembroski, G., Srinivasan, R., Weekes, T.C., Wilson, C. and Zweerink, J.; 1996, Astroparticle Physics (submitted) A Search for TeV Gamma-ray Bursts on a 1-second Time-scale.

(3) Boyle, P.J., Buckley, J.H., Burdett, A.M., Bussons Gordo, J., Carter-Lewis, D. A., Catanese, M., Cawley, M. F., Fegan, D. J., Finley, J. P., Gaidos, J. A., Harris, K., Hillas, A. M., Krennrich, F., Lamb, R. C., Lessard, R., Masterson, C., McEnery, J. E.,Mohanty, G., Moriarty, P., Quinn, J., Rodgers, A. J., Rose, H. J., Samuelson, F. W., Sembroski, G. H., Srinivasan, R., Weekes, T. C., and Zweerink, J. "Large Search for TeV Counterparts in Gamma Ray Bursts" Proceedings of the 25th International Cosmic Ray Conference (Durban, South Africa), Publ. Potchefstroom University, Eds. M.S.Potgieter, C.Raubenheimer, D.J. van der Walt; (1997) 3, 61.

(4) Carter-Lewis, D. A., Biller, S., Boyle, P.J., Buckley, J.H., Burdett, A.M., Bussons Gordo, J., Catanese, M., Cawley, M. F., Fegan, D. J., Finley, J. P., Gaidos, J. A., Hillas, A. M., Krennrich, F., Lamb, R. C., Lessard, R., Masterson, C., McEnery, J. E., Mohanty, G., Quinn, J., Rodgers, A. J., Rose, H. J., Samuelson, F. W., Sembroski, G. H., Srinivasan, R., Weekes, T. C., West, M., and Zweerink, J. "Spectrum Of TeV Gamma Rays from the Crab Nebula" Proceedings of the 25th International Cosmic Ray Conference (Durban, South Africa), Publ. Potchefstroom University, Eds. M.S.Potgieter, C.Raubenheimer, D.J. van der Walt; (1997) 3, 161.

(5) Gillanders, G.G., Boyle, P.J., Buckley, J.H., Burdett, A.M., Bussons Gordo, J., Carter-Lewis, D. A., Catanese, M., Cawley, M. F., Fegan, D. J., Finley, J. P., Gaidos, J. A., Hillas, A. M., Krennrich, F., Lamb, R. C., Lang, M. J., Lessard, R., Masterson, C., McEnery, J. E., Mohanty, G., Moriarty, P., Quinn, J., Rodgers, A. J., Rose, H. J., Samuelson, F. W., Sembroski, G. H., Srinivasan, R., Weekes, T. C., and Zweerink, J. " A Search for TeV Gamma-ray Emission from the Crab Pulsar" Proceedings of the 25th International Cosmic Ray Conference (Durban, South Africa), Publ. Potchefstroom University, Eds. M.S.Potgieter, C.Raubenheimer, D.J. van der Walt; (1997) 3, 185.

(6) Srinivasan, R., Buckley, J. H., Carter-Lewis, D. A., Catanese, M., Cawley, M. F., Colombo, E., Fegan, D. J., Finley, J. P., Gaidos, J. A., Hillas, A. M., Krennrich, F., Lamb, R. C., Lessard, R., McEnery, J., Moriarty, P., Quinn, J., Rodgers, A., Rose, H. J., Sembroski, G., Weekes, T. C., Wilson, C. L. "Very High Energy Observations of PSR B1951+32" Proceedings of the 25th International Cosmic Ray Conference (Durban, South Africa), Publ. Potchefstroom University, Eds. M.S.Potgieter, C.Raubenheimer, D.J. van der Walt; (1997) 3, 205.

(7) Lessard, R., Boyle, P.J., Buckley, J.H., Bradbury, S. M., Burdett, A.M., Bussons Gordo, J., Carter-Lewis, D. A., Catanese, M., Cawley, M. F., Fegan, D. J., Finley, J. P., Gaidos, J. A., Hillas, A. M., Krennrich, F., Lamb, R. C., Masterson, C., McEnery, J. E., Mohanty, G., Moriarty, P., Quinn, J., Rodgers, A. J., Rose, H. J., Samuelson, F. W., Sembroski, G. H., Srinivasan, R., Weekes, T. C., and Zweerink, J. "Constraints on Cosmic-ray Origin Theories from TeV Gamma-ray Observations" Proceedings of the 25th International Cosmic Ray Conference (Durban, South Africa), Publ. Potchefstroom University, Eds. M.S.Potgieter, C.Raubenheimer, D.J. van der Walt (1997) 3, 233.

(8) Buckley, J.H., Boyle, P.J., Bradbury, S. M., Burdett, A.M., Bussons Gordo, J., Carter-Lewis, D. A., Catanese, M., Cawley, M. F., Fegan, D. J., Finley, J. P., Gaidos, J. A., Hillas, A. M., Krennrich, F., Lamb, R. C., Lessard, R., Masterson, C., McEnery, J. E., Mohanty, G., Quinn, J., Rodgers, A. J., Rose, H. J., Samuelson, F. W., Sembroski, G. H., Srinivasan, R., Weekes, T. C., and Zweerink, J. "A Search for TeV Emission from Unidentified Sources in the Galactic Plane" Proceedings of the 25th International Cosmic Ray Conference (Durban, South Africa), Publ. Potchefstroom University, Eds. M.S.Potgieter, C.Raubenheimer, D.J. van der Walt (1997) 3, 237.

(1)

A Search for TeV Gamma-Ray Bursts on a 1-second Time-Scale

V.Connaughton[1,2,8], C.W.Akerlof[3], S.Biller[4], P.Boyle[2], J.Buckley[1], D.A.Carter-Lewis[5], M.Catanese[5], M.F.Cawley[6], D.J.Fegan[2], J.Finley[7], J.Gaidos[7], A.M.Hillas[4], R.C.Lamb[5], R.Lessard[2], J.McEnery[2], G.Mohanty[5], N.A.Porter[2], J.Quinn[2], H.J.Rose[4], M.S.Schubnell[3], G.Sembroski[7], R.Srinivasan[7], T.C.Weekes[1], C.Wilson[7], J.Zweerink[5]

[1] *Whipple Observatory, Harvard-Smithsonian CfA, U.S.A.*

[2] *University College, Dublin, Ireland*

[3] *University of Michigan, U.S.A.*

[4] *University of Leeds, United Kingdom.*

[5] *Iowa State University, U.S.A.*

[6] *St.Patrick's College, Maynooth, Ireland*

[7] *Purdue University, U.S.A.*

[8] *Contact address: ES84, Marshall Space Flight Center, AL 35812, U.S.A.*

Abstract

Although atmospheric Cherenkov telescopes have restricted fields of view their fluence sensitivity warrants a search for gamma-ray burst phenomena. A search for 400 GeV gamma-ray bursts on a 1s time-scale using archival data taken between 1988 and 1992 with the Whipple Collaboration 10m reflector is presented. No evidence of such bursts is found. Bursts of TeV gamma rays have been predicted from exotic astrophysical objects such as Primordial Black Holes and Cosmic Strings. An upper limit to the number density of exploding PBH of $3.0 \pm 1.0 \times 10^6$ $\mathrm{pc}^{-3}\mathrm{yr}^{-1}$ is calculated.

Contact: Valerie Connaughton, ES 84, Marshall Space Flight Center, AL 35812. vc@msfc.nasa.gov. tel: (205) 544 6494 FAX: (205) 544 5800.

PACS Codes: 95.75.-z, 95.85.Pw, 98.70.Rz, 98.62.Nx

Keywords: TeV Astronomy - Gamma-Ray Bursts - Primordial Black Holes.

1 Introduction

The detection of gamma-ray bursts with peak luminosity at MeV energies has been one of the most exciting discoveries in high energy astrophysics [9]. Although still unexplained after 30 years of intense research the phenomenon has inspired searches for counterparts at a variety of wavelengths [14]. It has also opened the possibility that there might be similar phenomena that have peak luminosity at other wavelengths; here we consider a TeV search for such phenomena on time-scales of one second using the Imaging Atmospheric Cherenkov Technique.

The Whipple Observatory Gamma Ray Collaboration has been involved in searches for gamma-ray bursts since 1978; initially multi-element first generation systems over long baselines were used [17]. The development of the Imaging Atmospheric Cherenkov Technique has significantly improved the sensitivity for the detection of point sources [25]. The Whipple 10m imaging camera has successfully detected TeV emission from several point sources - the Crab Nebula [24], Markarian 421 [19] and Markarian 501 [20]. It has been the most sensitive instrument of its kind for source-centered observations but its off-axis sensitivity has not so far been fully characterized [1].

Here the response of the Whipple 10m reflector to non-source-centered gamma rays is assessed using shower simulations, and a method is developed to search for gamma-ray bursts of one second duration. We report on a search through 4 years of the Whipple database.

There are a number of exotic suggestions that justify a search for gamma-ray bursts in this parameter space. These include emission from the decay of primordial black holes (PBHs) [13] and cosmic strings [22]. The cosmological and physical importance of PBHs is well-established [12]. As the PBH evaporates, its temperature increases in proportion to the mass loss. Most models predict a final explosion of energy when all possible evaporation channels are available, but the number of degrees of freedom of emission is a highly controversial issue, and ranges from the conservative standard elementary particle model, where it reaches a maximum once the three generations of fermions are free to be produced, to the runaway Hagedorn model where the number of emission modes increases exponentially beyond this [12]. For the conservative model an optimum time-scale of 1 s is found for observing the explosion of a PBH using the Whipple 10m telescope. During this final second 9.1×10^{28} photons are emitted above 0.4 TeV.

The fluence sensitivity of the detector over this time-scale is of order 10^{-9} erg cm^{-2} which is comparable to or better than that achieved in most bands of the gamma-ray spectrum. The sensitivity of the technique is compared to that achieved in searches by other gamma-ray experiments, operating at energy thresholds higher than the Whipple instrument.

2 The Whipple 10m Telescope

Situated at an altitude of 2.3 km on Mt.Hopkins in Arizona, the telescope operated by the Whipple Collaboration has been used as an imaging device since 1982; the camera has been improved from a 37 to a 109 element imaging system during that time. The telescope consists of a 10-metre dish (with 248 front-coated mirrors) on an alt-azimuth mount and a camera containing 109 photomultipliers (PMTs). The inner 91 PMTs are 1.1cm diameter tubes (Hamamatsu R1398) and are connected via amplifiers to trigger discriminators. An outer ring of 18 tubes is independent of the trigger logic and contributes only to the imaging of the event. Until 1993, these outer tubes were 5cm tubes giving a total field-of-view of 3.75°. They have been replaced by the smaller tubes so that the camera field-of-view is now 3°. The arrangement of PMTs in the focus box prior to 1993 is shown in Figure 1 and a detailed description of the instrument can be found in [5].

The camera is triggered if the signal in two or more PMTs exceeds a preset threshold in a 10 nsec time interval. When the system is triggered i.e. an event is registered, the light level in each PMT is recorded over a 25 nsec gate width. The trigger rate during the epoch of the observations reported here was typically 8 events per second. The time is derived from a GPS clock and is recorded with each event with an accuracy of 0.1 msec. The deadtime is 1.5 msec and the distribution of time differences of successive events from a 60 minute data file taken at a telescope elevation of 80° is shown in Figure 2.

The digitized images of the Cherenkov light are analyzed off-line. A typical image recorded by the present camera is shown at various stages of processing in Figure 3. Moment-fitting routines are used to define each image by an ellipse whose parameters define the event (shown in Figure 4). The event is accepted as a potential gamma-ray event or rejected as a hadron-initiated event depending on the values of these parameters. The axis of the image is defined by minimizing the signal-weighted sum of the squares of the perpendicular angular distances of the pixels. The rms spread of light perpendicular to and along this axis define the semi-minor and semi-major axes of the ellipse and these are known as the *width* and *length* of the image. Image compactness is defined by *concentration*, which is the fraction of the sum over all non-zero pixels of the cleaned image in digital counts (known as *size*) contained in the two or three brightest pixels. The other parameters shown in Figure 4 relate to the orientation of the image axis relative to the source position in the field-of-view.

If the position of the source is known (usually at the centre of the field of view) then the orientation of the image relative to that direction is important for source detection. A combination of shape and orientation parameters has been used by the Whipple Collaboration to reject 99.7% of recorded background while keeping 50% of gamma-rays; the set of selection parameters that are most useful for observations of a point-source in the centre of the field of view are called Supercuts and are defined elsewhere [21]. A comparison of the *width* and

length domains for photons (simulated) and real background (data taken with the telescope pointed at the zenith) can be seen in Figures 5.

The success of Supercuts and the Imaging Atmospheric Cherenkov Technique in the detection of point sources owes much to Monte Carlo simulations of photon and background hadron-initiated cascades. Owing to the impossibility of testing the atmospheric Cherenkov detector at an accelerator, analytical models and simulation of phenomena are used to optimize instrumental design and in the development of analysis techniques. Data taken during observations of the Crab Nebula, which plays the role of a TeV gamma-ray standard candle, are used to perfect new techniques.

3 Off-axis Sensitivity of 10m reflector

The characteristics of the 10m reflector in point-source mode of operation are well understood and defined [5]. What is less well characterized is the sensitivity of the instrument when an area of the sky is probed for a source without knowing its exact position, i.e., where each point in the field-of-view is a potential source. It has been demonstrated experimentally that the system is sensitive to a point source of gamma rays up to 1° off-axis [1], [10]. In the work reported here the response over the full field-of-view of the 10m reflector is investigated, using simulations, in order to use the instrument as a relatively wide field burst detector.

3.1 The off-axis Triggering and Imaging of Gamma Rays

The geometrical field-of-view of the 10m camera between 1988 and 1992 was 3.75°, but the imaging technique allows reconstruction of images whose origins lie outside this area. Conversely, some of the images of showers from sources on the edge of the camera face may fall outside the field-of-view so that the camera has reduced collection area for such sources.

In order to assess the sensitivity of the instrument for sources lying at various distances from the centre of the camera, a database of nearly 8000 simulated gamma-ray- induced showers of energies ranging from 0.2 TeV to 0.8 TeV was compiled using a simulation program based on the KASCADE code of Kertzmann and Sembroski [15]. The Whipple collaboration has used several different simulation codes in the various research institutions (e.g. MOCCA at the University of Leeds) and comparison of the simulations shows that they are in agreement with each other to within 10% in the Cherenkov light yields and image parameter distributions that they produce.

The response of the instrument to the simulated gamma-ray showers is gauged by mapping each Cherenkov photon in a shower from the mirrors onto the imaging camera and building up an event for each shower.

Displacing the focus box from its position at the focus of the reflector and constructing events as they appear to this displaced camera is equivalent to simulating the response of the camera to sources at an offset from the centre equal to the displacement of the camera but in the opposite direction. The response of the camera to gamma-ray showers from sources with 0° to 2.5° offsets from the centre was investigated by successively displacing the camera at 0.25° intervals along an arbitrary line, 17° from an axis through the centre of a row of PMTs. A different source displacement angle may be chosen without affecting the results. The treatment of simulated images is identical to that subsequently applied to real data. The parameterization and cutting procedures execute rapidly relative to the shower and instrument simulations, and it was possible to experiment with a variety of parameters and analysis methods before deciding on a suitable gamma-ray burst search method.

As the source position moves further away from the centre of the camera, less Cherenkov light falls on the detector at a given impact parameter. The software trigger is a requirement that two of the inner 91 tubes register at least 40 photo-electrons and the percentage of events triggering the system at each impact parameter is shown in Figure 6 for source offsets of (a) 0°, (b) 0.75° and (c) 1.5°.

By weighting the fraction according to impact parameter value (the collection area is bigger at larger impact radii), a value for the trigger efficiency over the field of view, equivalent to the effective area of the detector for each source offset, is calculated:

$$\text{Trigger efficiency} = \frac{\sum_i 2\pi r_i \phi_i \delta r}{7 \times 10^4} \qquad (1)$$

where r_i $(=i)$ is the radius of the annulus at impact parameter i, thickness $\delta r = 2$ metres, and ϕ_i is the fraction of the 20 showers at radius r_i which would trigger the telescope. The summing integer i is incremented from 12 to 200 in steps of 2. At impact parameters below 10 metres, the showers tend to saturate the central tube, and the Cherenkov light pool falls off rapidly beyond 150 metres, so that we define an ideal detector as one which is triggered by all showers with impact parameters between 10 and 150 metres, and which fails to register any events falling outside that area. The trigger efficiency is divided by 7×10^4 m^2 to give the efficiency relative to this arbitrary ideal detector. An efficiency of greater than 1 is, therefore, possible since showers lying beyond 150 metres may trigger the system. This procedure was implemented for all 4 shower energies, and the results are shown in Figure 7. Above threshold (> 0.4 TeV) the instrument would register over half of the gamma-ray showers from sources out to 1° away from the centre, but it is obviously more efficient at detecting those nearer the centre than at large offsets.

Image parameters have traditionally been used, in some combination of shape and orientation cuts, to discriminate against the hadronic background. In this search, however, only the shape parameters are relevant since there is

no preferred direction due to the unknown position of the source in the field-of-view. The most successful shape selection was found to involve cuts in *length* and *width*, using the values derived for Supercuts:

$$0.073° < \textit{width} < 0.15°$$
$$0.16° < \textit{length} < 0.30°$$

Figure 8 shows the percentage of 0.4 TeV events at offsets (a) 0°, (b) 0.75° and (c) 1.5° which trigger the camera and satisfy these image shape requirements. Combining the percentages for each impact parameter produces the results which are shown in Figure 9. Above the detector energy threshold, the collection area for gamma rays is fairly flat, and showers from sources which are up to half a degree off-axis are still selected over 50% of the time. There are two competing effects which explain the shape of the curves: at high energies, showers with large impact parameters produce enough Cherenkov light to trigger the telescope more often than distant low energy showers, but the Supercuts selection is biased towards small showers, so that the higher energy showers are less likely than the low energy events to survive the *width* and *length* cuts regardless of impact parameter. At large source offsets the fraction of events selected decreases with shower energy even though the high energy events appear to trigger the camera more often than at lower energies. If the showers triggering the system at these large offsets are examined, it can be seen that they are the longest images in the high-energy databases.

Observations of the Crab Nebula at angular offsets from the centre of the field-of-view of the 10m telescope were used to confirm the efficiency curves derived from these simulations. The Crab Nebula is a steady source of TeV gamma rays, and by comparing the rate of gamma rays measured after applying the Supercuts selection technique to data from September 1996 at offsets ranging from 0° to 1.5°, one obtains the efficiency for gamma ray collection displayed in Figure 10. The errors in Figure 10 reflect the variation in event rates for the offset observations, and are large owing to the small exposure time: only 1 hour of source observations were made at a source offset of 0.5° from the centre of the field-of-view, 1.5 hours at 1.0°, and 2 hours at 1.5° offset. Because the field-of-view of the telescope was smaller when these offset observations were made compared to that simulated in this study, a perfect correlation is not expected, and one anticipates that the efficiency at larger source offsets be slightly lower relative to source-centered observations than in the simulations.

3.2 Orientation of gamma-ray images

The orientation of the ellipse fitted to each image is represented by its major axis, and the most likely point-of-origin of the shower progenitor on the field-of-view lies on this axis at a distance d in degrees related to the ellipticity of the image:

$$d = 2 - 2(width/length) \tag{2}$$

This algorithm was developed based on simulations of gamma-ray showers from sources at the centre of the field-of-view, and was found to be accurate to about 0.3° either side of this point [1] for source-centered observations. The relation between the image, its centre, and the most likely point-of-origin are shown in Figure 11.

Because the ellipses derived from the moment-fitting routines are symmetrical, the point-of-origin may lie either side of the centre of the image. The following equations are used:

$$\begin{aligned} \sqrt{(y_{or} - y_{cen})^2 + (x_{or} - x_{cen})^2} &= 2 - 2 \times width/length \\ y_{or} &= m \times x_{or} + c \end{aligned}$$

to find the most likely points-of-origin x_{or}, y_{or} on both sides of the centre of light x_{cen}, y_{cen} along the major axis $y = m \times x + c$. The distance

$$\sqrt{(y_0 - y_{or})^2 + (x_0 - x_{or})^2} \tag{3}$$

where x_0, y_0 are the true positions of the simulated source, is a measure of how well Equation 2 finds the point-of-origin of a shower. The tolerance is defined as the maximum allowed value of this distance, in degrees. A range of tolerance levels from 0.1° to 0.7° was explored to determine the off-axis efficiency of the point-of-origin determination, and the results are displayed in Figure 12. The total efficiency Φ for each energy was obtained by combining source positions and weighting each efficiency (ϕ_r) according to source offset (r). The efficiency values featured are relative to an ideal detector with $\phi_r = 1$ at each source offset where the gamma-ray images are selected and their origin is correctly determined so that $\Phi = \sum \phi_r r / \sum r$ with r varying from 0.25° to 2.5°. The efficiency curve is fairly constant as the source is moved away from the centre and appears independent of impact parameter and photon energy.

Real background data were subjected to the same analysis so that the effect of varying the point-of-origin tolerance value on background acceptance could be assessed. It was found that in looking for bursts of 3 or more events over a 1-second time-scale, the highest signal to noise ratio could be obtained with a tolerance level of 0.425°. This selection criterion enables 66 ± 5% of shape-selected simulated events (over the impact parameter range 12 to 200 metres and source offset 0° to 2.5°) to be correctly located. The shaded areas in Figure 11 show the regions from which the imaged events could have originated with this tolerance value.

It is then possible to apply this calculated off-axis response of the detector to the search for counterparts to the delayed component of BATSE bursts (reported elsewhere [7]) and to the serendipitous detection of gamma-ray bursts during the normal operation of the gamma-ray telescope (described below).

4 Searches for 1 s TeV Gamma-Ray Bursts

The archival data of the Whipple Observatory taken with the 10m reflector with an energy threshold above 0.4 TeV between September, 1988 and September, 1992 were used for this search. In general these observations were in the form of files of (approximately) 28 minute duration containing information on each event (the arrival time, the outputs of the 109 ADCs from the 109 pixels, and other housekeeping data). Examinination of the observing logs allowed the identification and rejection of 1% of the data including (i) observations made when there were instrumentation problems (ii) data taken with discriminator thresholds or high-voltage values significantly different from those used in normal operation, and (iii) observations made while testing new or experimental configurations (for example, experiments with filters). A further 1% of the files were rejected because of obvious anomalies, such as a large number of bright stars in the field-of-view, or because they were taken at a telescope elevation less than 35° above the horizon. Following rejection of unsuitable data, 2217 hours of observations comprised the database. The database was divided according to the event rate of candidate gamma rays. Variation in event rates was caused by differences in zenith angle, mirror reflectivity and discriminator settings. The elevation of the source under observation is known to affect the energy threshold of the detector, and also influences the appearance of both gamma and hadronic images. A larger depth of atmosphere must be penetrated by the extensive air shower particles if they are to produce light lower in the atmosphere, so that a telescope pointed close to the zenith is sensitive to lower energy showers than if it is operated nearer the horizon. Consequently, the raw event rates decrease with increasing zenith angle - this relationship is shown in Figure 13(top). Despite this overall fall in event rates at low elevations, the Cherenkov image on the camera face is narrower on the horizon than at the zenith, and this effect results in more hadronic events being selected as gamma rays on the basis of the *width* parameter. Figure 13(bottom) shows the variation of image-selected event rate with telescope elevation.

Nearly 80% of observations were made with the telescope elevation above 55°, where data rates and image characteristics are fairly homogeneous. These observations form the bulk of the 1759 hours of data which had an average rate of < 0.2 candidate gamma-ray events per second, and comprise the largest of the three subsets of the Whipple database. The rest of the data was divided according to the average event rate; rate = 0.2 to 0.4 per second (394 hours) and rate > 0.4 events per second (64 hours). Standard routines were used to

flat-field the data, tubes with bright stars in their field-of-view were turned off in hardware or software, and the image parameters were calculated as described in [21]. The events were then characterized by these image parameters (and their arrival times). The evenness of the camera response across the field-of-view is illustrated in Figure 14, showing the distribution of event centroids in camera coordinates (degrees from centre) for a 60 minute observation.

4.1 The Burst Search

Initially the events were culled to include only those events whose images satisfied the gamma-ray event criteria. Events which survived the *width* and *length* cuts described above were included in a reduced data set which was submitted to a search for bursts of 3 or more events in a 1s time interval.

The arrival time of the first event was taken as the possible start of a 1s burst and was compared to the time of the second event. If the time difference was under 1s, the next event was examined. If not, the start of the time window was moved to the arrival time of the second event. The window was moved through the file until all events in a file have been processed, and the total number of bursts with from 3 to 10 shape-selected events in the file is obtained. No candidate bursts were found with more than 4 events. The number of 3- and 4-fold burst events are shown in Table 1 in the column headed "obs". A background (control) file was generated from each real data file by scrambling the events in each parameterized file, while maintaining the original time sequence. When the background file was subjected to the burst-search program, the image-selected events were the same as those picked from the real data file, but in a random order and attached to the original arrival times of other events. The number of 3- and 4-fold bursts thus found is shown in Table 1 headed "exp". The difference between the observed and the expectation is expressed in terms of the standard deviation, σ defined as $(\text{obs} + \text{exp})^{1/2}$. In no case is the difference statistically significant.

Table 1: Frequency of gamma-ray burst candidates in Whipple database vs. expected burst frequency (no common origin sought).

Event rate	Hours of	3-event burst			4-event burst		
/sec (cut)	Data	exp	obs	σ	exp	obs	σ
0.0-0.2	1759	4747	4762	+0.15	234	245	+0.50
0.2-0.4	394	13463	13679	+1.31	1308	1286	-0.43
> 0.4	64	10597	10539	-0.40	1800	1724	-1.28
Total	2217	28807	28980	+0.72	3342	3255	-1.07

To this point no use has been made of the fact that the events in the putative 3- and 4-fold bursts must come from the same point in the sky. Hence all the bursts were subjected to the common origin selection described above. Less than 2% of the putative bursts passed this selection. These are listed as before

in Table 2; the expectation is derived by applying the common origin selection to the scrambled events.

Again no excess of 3- or 4-fold bursts of candidate gamma-ray events on a 1-second time-scale is found in the 2217 hours of the Whipple database. Two candidate four-fold events are shown in Figure 15. If a TeV component to a background of bursters exhibiting activity on a 1 s time-scale exists, then the number of these bursts is low and below the sensitivity of the instrument in its current form.

Table 2: Frequency of gamma-ray burst candidates in Whipple database vs. expected burst frequency (with common origin).

Event rate	Hours of	3-event burst			4-event burst		
/sec (cut)	Data	exp	obs	σ	exp	obs	σ
0.0-0.2	1759	62	73	+0.95	0	2	1.41
0.2-0.4	394	230	232	+0.09	8	5	-0.83
> 0.4	64	236	257	+0.95	12	5	-1.70
Total	2217	528	562	+1.03	20	12	-1.41

5 Upper Limit to Density of Exploding PBH

Based on the null results obtained in this search an upper limit to the local density of exploding PBHs can be calculated using the flux of TeV photons predicted by the standard model and presented in [12].

Previous results of searches for exploding PBH by the Whipple Collaboration used extrapolated values of collection area and solid angle [18], [16], [23], [6]. The work presented here involves a search over a larger archival database (2217 hours) for bursts on a longer time-scale (1 s) with a lower energy threshold (0.4 TeV); hence the sensitivity should be greater. In addition the sensitivity is calculated more rigorously than in previous experiments. In the earlier Whipple experiments the sampling distance was calculated from the trigger efficiency rather than gamma-ray collection area. Our new Monte Carlo simulations indicate that in calculating limits from data taken after 1988 (when the imaging system was introduced), the sampling distance was overestimated. In addition, a constant gamma-ray sensitivity over the field-of-view was assumed and the sensitive volume integrated the estimated sampling distance over the solid angle of the camera. A more realistic sensitive volume based on Monte Carlo simulations is used in this search. Table 3 shows the sampling distances and sensitive volumes for a 3- photon burst in the 10m reflector for source offsets out to 2° given the gamma-ray flux calculated in [12]. The second column shows the collection area for a source at a particular point in the camera and column 3 shows the maximum distance at which a PBH can be detected. The volume probed, V_i, is calculated by integrating over the solid angle, Ω_i, covered by the

Table 3: Sensitivity of 10m Reflector for 0.4 TeV γ after applying *width* and *length* cuts at source offsets out to 2°.

Source Offset from Center (°)	Collection Area (10^4m^2)	Sampling Distance (pc)	Sensitive Volume ($\times 10^{-6}$ pc^3)
0.00	5.39 ± 0.89	0.38 ± 0.15	1.09 ± 0.07
0.25	5.07 ± 0.89	0.37 ± 0.15	3.03 ± 0.20
0.50	3.69 ± 0.95	0.32 ± 0.16	3.27 ± 0.41
0.75	2.73 ± 0.94	0.27 ± 0.16	2.75 ± 0.57
1.00	2.14 ± 0.82	0.24 ± 0.15	2.48 ± 0.61
1.25	1.52 ± 0.78	0.20 ± 0.14	1.75 ± 0.60
1.50	1.15 ± 0.62	0.18 ± 0.13	1.51 ± 0.57
1.75	0.70 ± 0.48	0.14 ± 0.11	0.82 ± 0.40
2.00	0.31 ± 0.37	0.09 ± 0.10	0.25 ± 0.34
Total sensitive volume			16.95 ± 3.77

annulus (or circle for a source at the centre) described by the source offset: $V_i = \frac{r^3}{3}(\Omega_i - \Omega_{i-1})$. This volume is nearly 8 times smaller than the volume estimate in Nolan et al. [16] although the hardware system is identical and the analysis and burst search methods used in this work are more sensitive.

The corresponding distances and volumes accessible to the reflector can be calculated for the detection of bursts of 4 photons in 1 s. The excess (or deficit) of bursts obtained over expectation in the sensitive volume in each of the three data groups in the archive is used to find the 99.9% maximum likelihood upper limit to the frequency of exploding PBH per year per cubic parsec (Table 4). More sensitive upper limits are obtained from air shower experiments which operate at higher energies and have longer exposure times; these are shown in Table 5.

Table 4: Upper Limits to Exploding PBH Frequency from Archival Search.

Hours of Data	3-event Burst		4-event Burst	
	Volume $\times 10^{-5}$ pc^3	Limit $\times 10^6$ pc^{-3}yr^{-1}	Volume $\times 10^{-5}$ pc^3	Limit $\times 10^6$ pc^{-3}yr^{-1}
1759	1.67 ± 0.38	14.13 ± 3.3	1.07 ± 0.26	3.0 ± 1.0
394		96.2 ± 23.0		20.4 ± 5.3
64		745 ± 170		117 ± 30

Models other than those derived from standard elementary particle theory have also been invoked to describe the final stages of evaporation of a PBH. Those propose a faster process with more degrees of freedom than the standard model - the Hagedorn model, in which the number of degrees of freedom increases exponentially with the number of emitted particles, predicts the most catastrophic explosion, of 6.0×10^{34} erg, lasting only 10^{-7} seconds, and comprised mainly of 250 MeV photons. A larger volume is accessible to searches

Table 5: Standard elementary particle upper limits to PBH density.

Experiment	Energy (TeV)	Reference	Limit $pc^{-3}yr^{-1}$
CYGNUS	50	Alexandreas et al. 1993 [2]	6.1×10^5
AIROBICC	20	Funk et al. 1995 [11]	8.9×10^5
Tibet	10	Amenomori et al. 1995 [3]	4.6×10^5

for this type of event than for PBH exploding according to the standard model. Upper limits to Hagedorn-type PBH explosions are, therefore, more restrictive, and are given in [17] and [8].

6 Conclusions

A method is described of using an atmospheric Cherenkov telescope to search for gamma-ray bursts on short time-scales. The application of this method to the search for counterparts to classical gamma-ray bursts detected by the BATSE experiment is described elsewhere [7]. Here it is applied to a search through a four year database accumulated by the Whipple telescope in its routine discrete source observing program. The minimum detectable fluence (6×10^{-9} erg-cm^{-2} in one second) is comparable with that of BATSE at much lower energies and compares favorably with all other gamma-ray experiments currently in operation.

Null results are obtained and an upper limit to the PBH density is derived, where the PBH is exploding via the standard model. This limit of $3.0 \pm 1.0 \times 10^6$ $pc^{-3}yr^{-1}$ is better than that obtained from previous searches using the Whipple 10m reflector. It is not, however, as stringent as the PBH limits obtained with wide field air shower experiments. The low duty cycle and small field-of-view of atmospheric Cherenkov telescopes makes them less efficient than air shower experiments like the MILAGRO water-Cherenkov telescope [4] which have a large field-of-view and longer exposures. Telescopes with rapid slew speeds are, nevertheless, well-suited for the detection of very high energy counterparts to BATSE-type bursts [7].

Acknowledgements

We acknowledge the technical assistance of Teresa Lappin and Kevin Harris. This research is supported by grants from the US Department of Energy and by NASA, by PPARC in the UK, and by Forbairt in Ireland.

References

[1] Akerlof C.et al. *Ap.J., 1991*, **377**, L97

[2] Alexandreas D.et al., *Proc.23rd ICRC, Calgary 1993*, **1**, 428

[3] Amenomori M. et al., *Proc.24th ICRC, Rome 1995*, **2**, 112

[4] Barwick S. et al., *Proc.24th ICRC, Rome 1995*, **2**, 436

[5] Cawley M.F. et al., *Exp.Astron., 1991*, **1**, 173

[6] Connaughton V. et al. *AIP Conf.Proc.307 GRB, 1993 (Huntsville, AL), eds. G.J. Fishman, J.J. Brainerd and K. Hurley*, 470

[7] Connaughton V. et al., *ApJ, 1997*, **479**, 859

[8] Fichtel C. et al., *AIP Conf.Proc.384 GRB, 1995 (Huntsville, AL), eds. C. Kouveliotou, M.S. Briggs and G.J. Fishman*, 368

[9] Fishman, G.J. & Meegan, C., *Annu. Rev. Astron. Astrophys., 1995*, **33**, 415

[10] Fomin V.P. et al., *Astropart.Phys., 1994*, **2**, 137

[11] Funk B. et al., *Proc.24th ICRC, Rome 1995*, **2**, 104

[12] Halzen F. et al., *Nature, 1991*, **353**, 807

[13] Hawking S.W., *Nature, 1974*, **248**, 30

[14] Hurley, K. 1996, Space Sc. Rev., 75, 43

[15] Kertzmann M.P. and Sembroski G.S., *Nuc.Inst.Meth.A 1994*, **343**, 629

[16] Nolan K. et al., *Proc.21st.ICRC, 1990 (Adelaide)*, **2**, 150

[17] Porter N.A. and Weekes T.C., *MNRAS, 1978*, **183**, 285

[18] Porter N.A. and Weekes T.C., *Nature, 1979*, **277**, 199

[19] Punch M.et al. *Nature, 1992*, **358**, 477

[20] Quinn J. et al., *Ap.J., 1996*, **452**, 588

[21] Reynolds P.T. et al., *Ap.J., 1993*, **404**, 206

[22] Samura T. and Kobayakawa K., *Proc.23rd ICRC, Calgary 1993*, **1**, 128

[23] Sommers P. and Elbert J.W., *J.Phys., 1987*, **G13**, 553

[24] Vacanti G. et al. *Ap.J., 1991*, **377**, 467.

[25] Weekes, T.C., *Space Sci.Rev., 1996*, **75**, 1

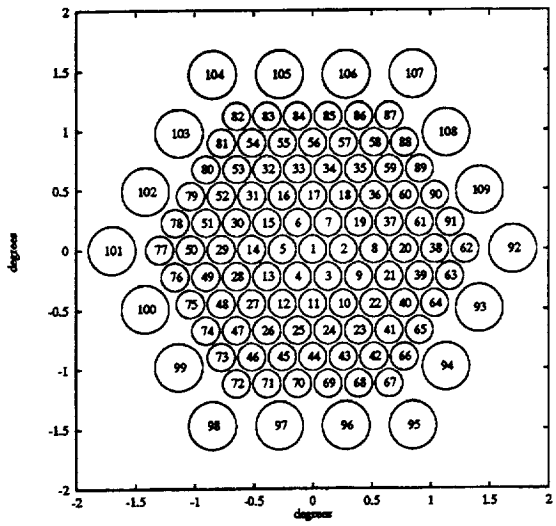

Figure 1: Arrangement of photomultiplier tubes in focus box of 10m reflector.

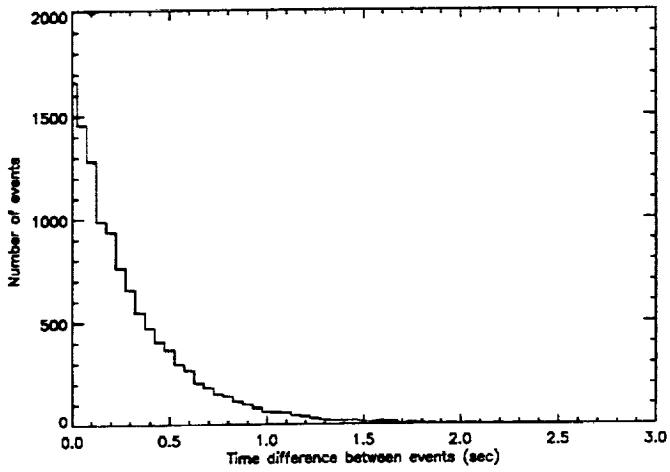

Figure 2: Arrival time difference distribution of successive events in a 60 minute data file.

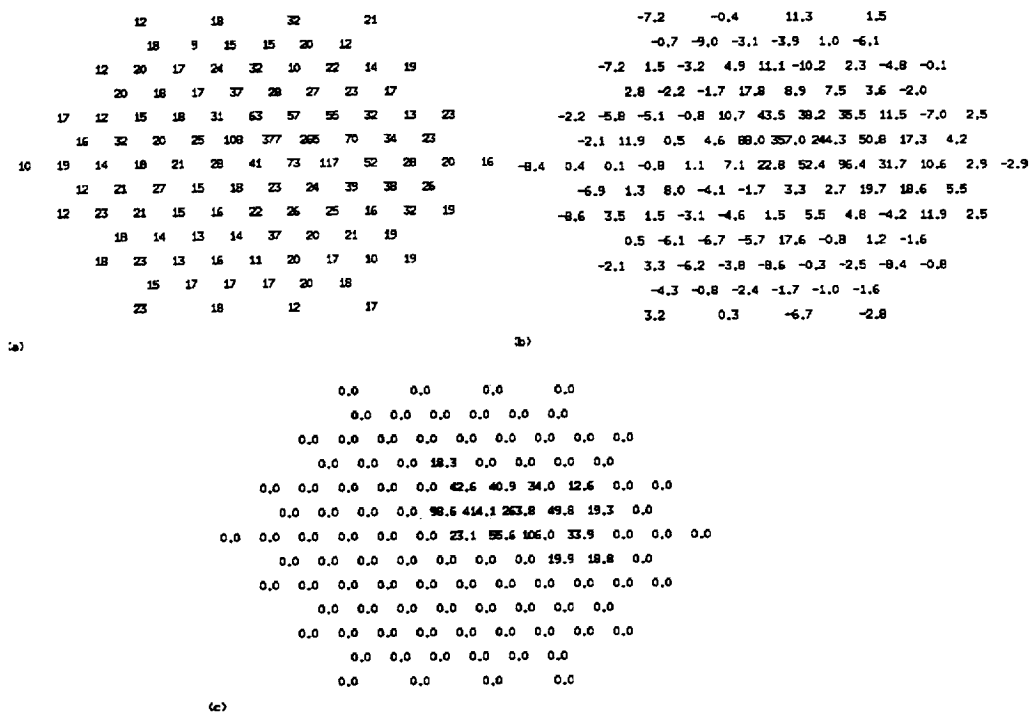

Figure 3: 10m image (a) before and (b) after flat-fielding, and (c) after cleaning.

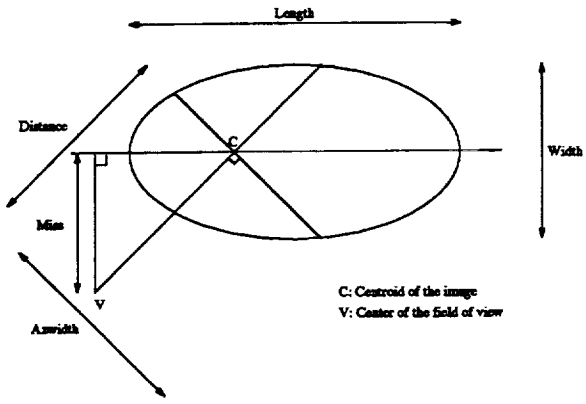

Figure 4: Representation of Image Parameters.

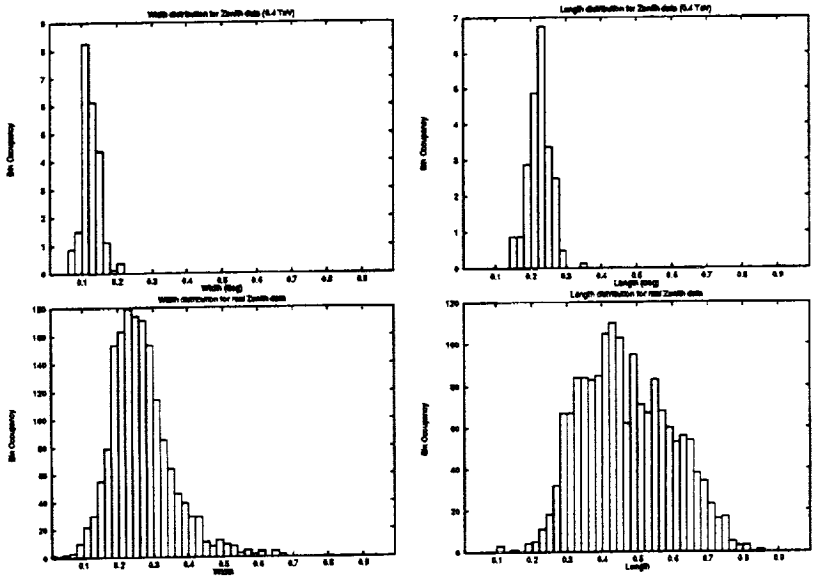

Figure 5: Width (left) and Length (right) distributions for simulated 0.4 TeV photon from the zenith (top) and real zenith (bottom) showers.

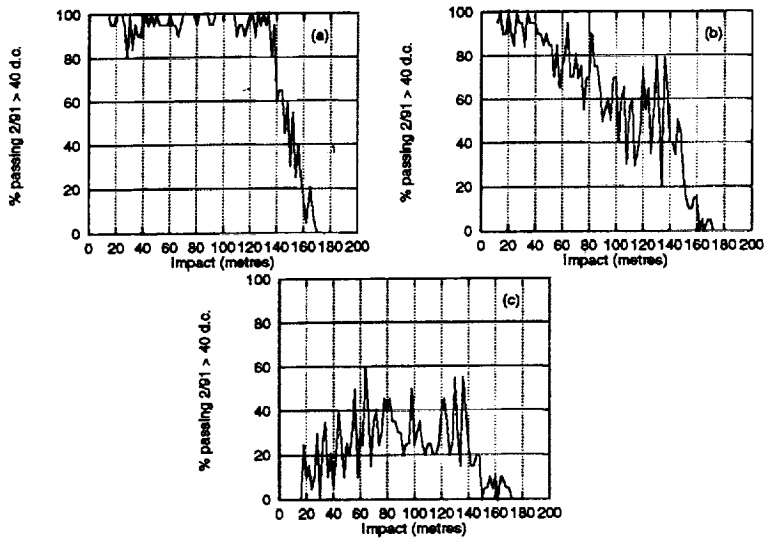

Figure 6: Percentage of events which trigger 10m reflector as a function of impact parameter for source offsets (a)0°, (b)0.75°,(c)1.5° for 0.4 TeV showers.

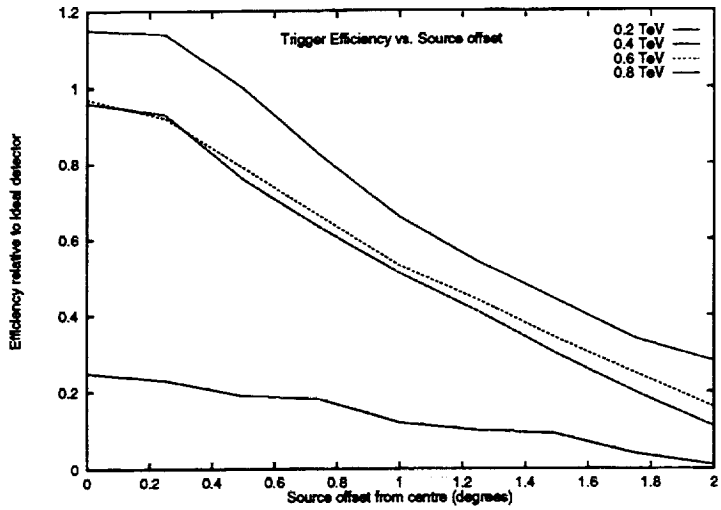

Figure 7: Trigger efficiency of 10m reflector as a function of source offset and energy. An efficiency of 1 is that of an ideal detector which has a 100 % trigger rate for showers of impact parameters between 10 and 150 metres, and no triggers outside this range. This is equivalent to a collection area of 7×10^4 m^2.

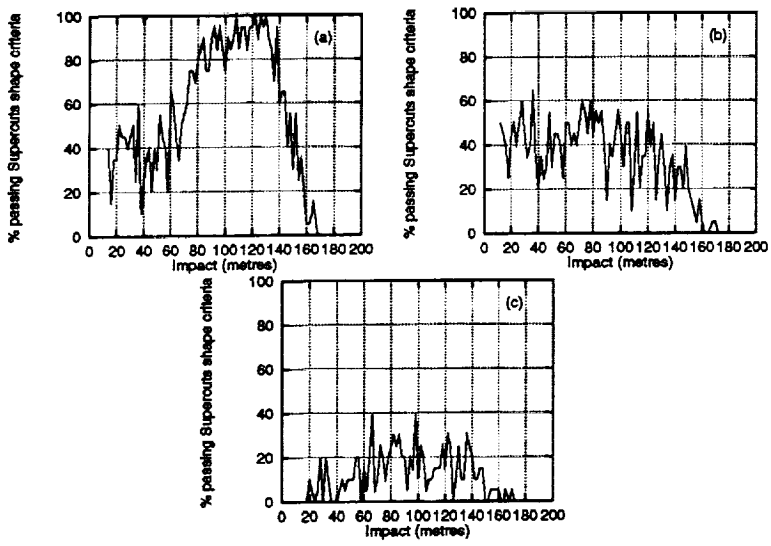

Figure 8: Percentage of events which survive Supercuts shape cuts as a function of impact parameter for source offsets (a)0°,(b)0.75°,(c)1.5° for 0.4 TeV showers.

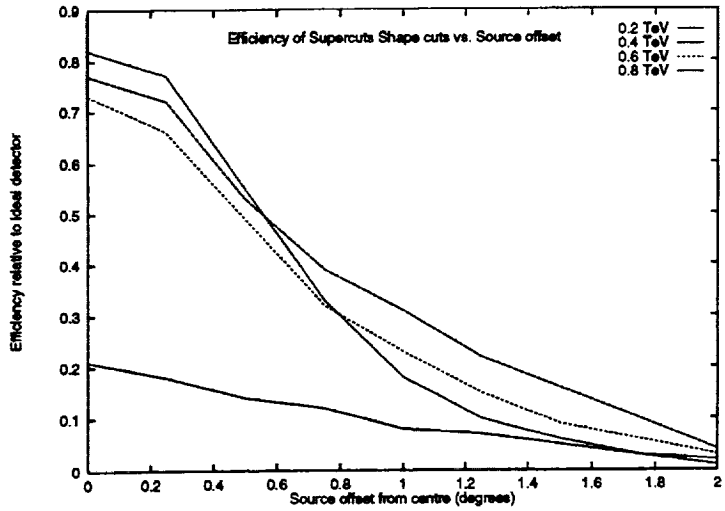

Figure 9: Ability of 10m reflector to detect gamma rays as a function of source offset and energy. *Width* and *Length* cuts are made on all events that trigger the system. An efficiency of 1 is that of an ideal detector which has a 100% trigger and image selection rate for showers with impact parameters between 10 and 150 metres and none outside. This is equivalent to a collection area of 7×10^4 m^2.

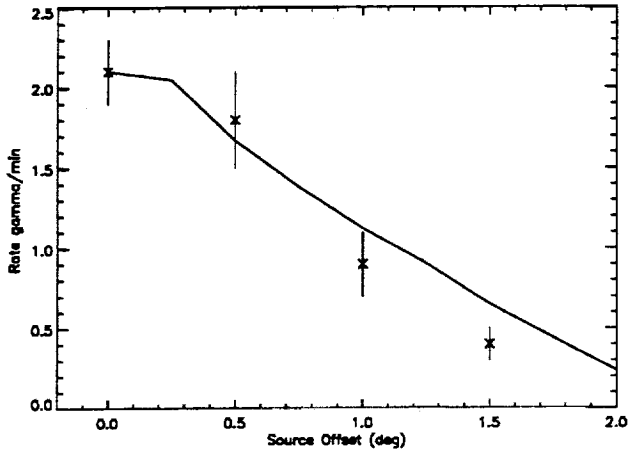

Figure 10: Efficiency curve from simulations (solid line) compared to gamma-ray rate measured from Crab Nebula (x) as a function of source offset.

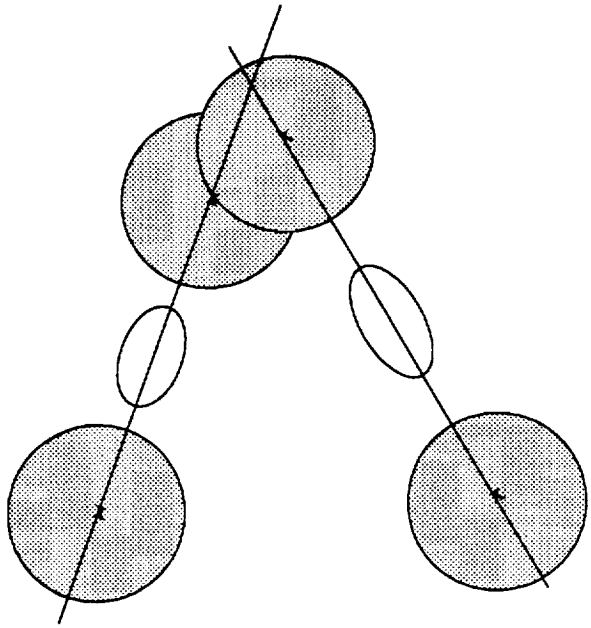

Figure 11: Illustration of the most likely points-of-origin (x) along the major axes of two events (ellipses). The shaded circles indicate the uncertainty associated with these positions.

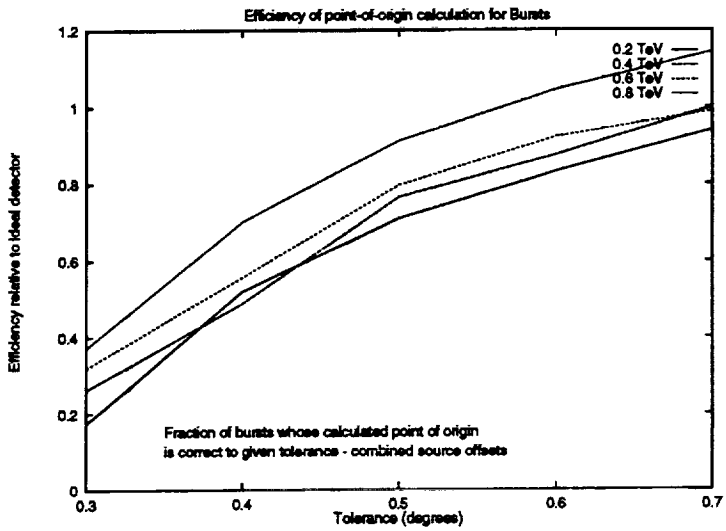

Figure 12: Efficiency of point-of-origin determination from $d = 2 - 2 \times width/length$ along the major axis. The tolerance on the x-axis is the value by which this calculated point-of-origin is allowed to vary from the actual source position.

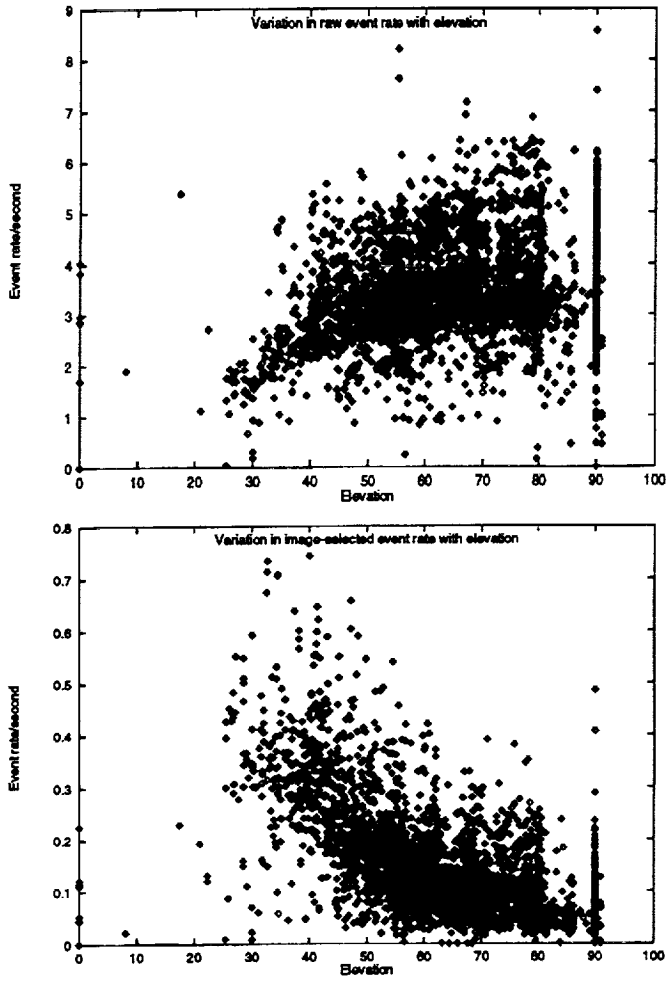

Figure 13: Variation of event rate with elevation raw event rate (top) and event rate after selection via image *width* and *length* cuts (bottom).

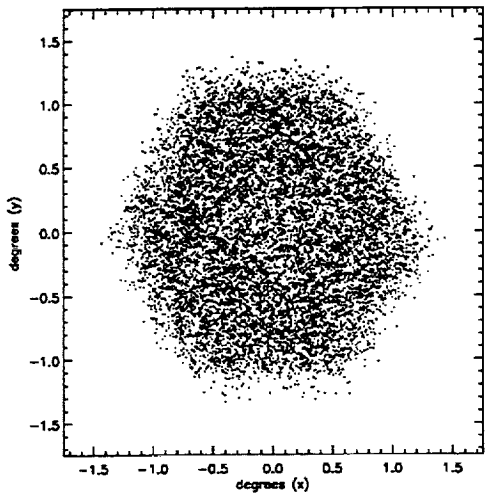

Figure 14: Event centroid distribution of events in a 60 minute data file.

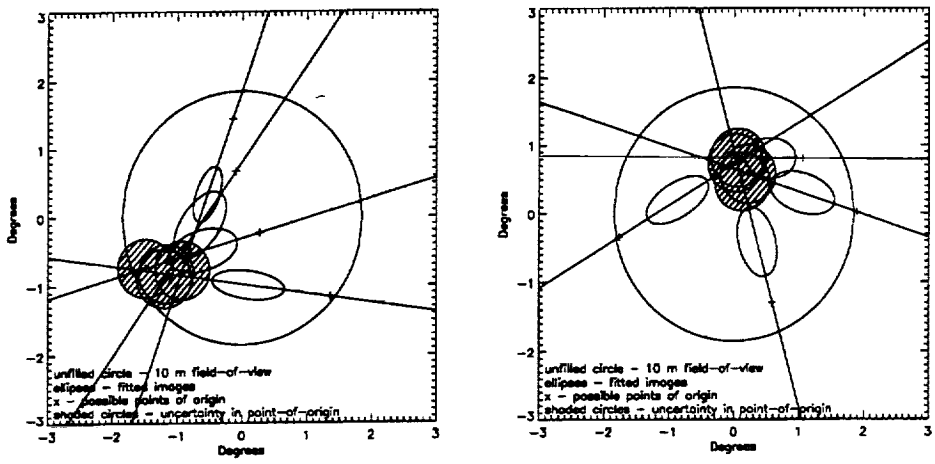

Figure 15: Two bursts of four events from real data in 1-second with a possible common point-of-origin.

ELSEVIER

Astroparticle Physics 8 (1998) 179–191

Astroparticle Physics

A search for TeV gamma-ray bursts on a 1-second time-scale

V. Connaughton [a,b,*], C.W. Akerlof [c], S. Biller [d], P. Boyle [b], J. Buckley [a], D.A. Carter-Lewis [e], M. Catanese [e], M.F. Cawley [f], D.J. Fegan [b], J. Finley [g], J. Gaidos [g], A.M. Hillas [d], R.C. Lamb [e], R. Lessard [b], J. McEnery [b], G. Mohanty [e], N.A. Porter [b], J. Quinn [b], H.J. Rose [d], M.S. Schubnell [c], G. Sembroski [g], R. Srinivasan [g], T.C. Weekes [a], C. Wilson [g], J. Zweerink [e]

[a] *Whipple Observatory, Harvard-Smithsonian, CA, USA*
[b] *University College, Dublin, Ireland*
[c] *University of Michigan, USA*
[d] *University of Leeds, UK*
[e] *Iowa State University, USA*
[f] *St.Patrick's College, Maynooth, Ireland*
[g] *Purdue University, USA*

Received 20 May 1996; revised 10 October 1997; accepted 10 October 1997

Abstract

Although atmospheric Cherenkov telescopes have restricted fields of view, their fluence sensitivity warrants a search for gamma-ray burst phenomena. A search for 400 GeV gamma-ray bursts on a 1 s time-scale using archival data taken between 1988 and 1992 with the Whipple Collaboration 10 m reflector is presented. No evidence of such bursts is found. Bursts of TeV gamma rays have been predicted from exotic astrophysical objects such as Primordial Black Holes and Cosmic Strings. An upper limit to the number density of exploding PBH of $3.0 \pm 1.0 \times 10^6$ pc^{-3} yr^{-1} is calculated. © 1998 Elsevier Science B.V.

PACS: 95.75.-z; 95.85.Pw; 98.70.Rz; 98.62.Nx
Keywords: TeV astronomy; Gamma-ray bursts; Primordial black holes

1. Introduction

The detection of gamma-ray bursts with peak luminosity at MeV energies has been one of the most exciting discoveries in high-energy astrophysics [9]. Although still unexplained after 30 years of intense research, the phenomenon has inspired searches for counterparts at a variety of wavelengths [14]. It has also opened the possibility that there might be similar phenomena that have peak luminosity at other wavelengths; here we consider a TeV search for such phenomena on time-scales of one second using the Imaging Atmospheric Cherenkov Technique.

The Whipple Observatory Gamma Ray Collaboration has been involved in searches for gamma-ray bursts since 1978; initially, multi-element first generation systems over long baselines were used [17]. The development of the Imaging Atmospheric Cherenkov

* Corresponding author. ES84, Marshall SpaceFlight Center, AL 35812, USA; E-mail: vc@msfc.nasa.gov.

0927-6505/98/$19.00 © 1998 Elsevier Science B.V. All rights reserved.
PII S0927-6505(97)00055-8

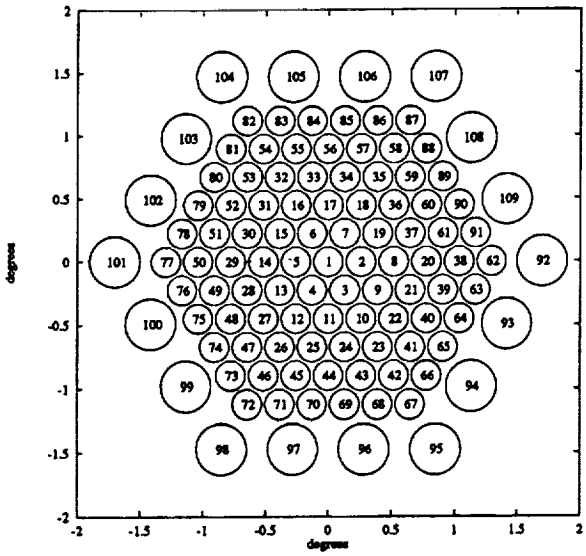

Fig. 1. Arrangement of photomultiplier tubes in focus box of 10 m reflector.

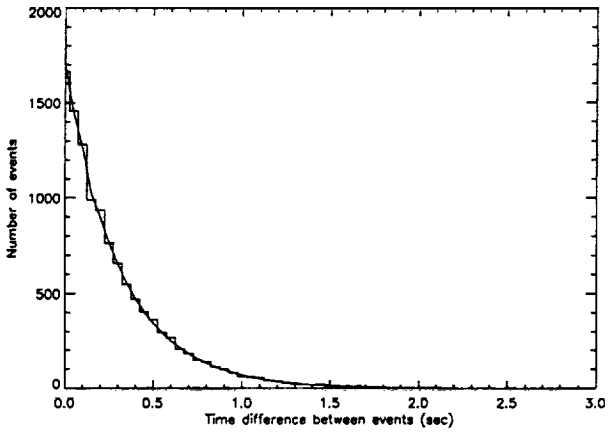

Fig. 2. Arrival time difference distribution of successive events in a 60 minute data file (histogram). The solid curve shows the expected Poisson distribution for this average event rate and total number of events.

Technique has significantly improved the sensitivity for the detection of point sources [25]. The Whipple 10 m imaging camera has successfully detected TeV emission from several point sources – the Crab Nebula [24], Markarian 421 [19], and Markarian 501 [20]. It has been the most sensitive instrument of its kind for source-centered observations but its off-axis sensitivity has not so far been fully characterized [1].

Here the response of the Whipple 10 m reflector to non-source-centered gamma rays is assessed using shower simulations, and a method is developed to search for gamma-ray bursts of one second duration. We report on a search through 4 years of the Whipple database.

There are a number of exotic suggestions that justify a search for gamma-ray bursts in this parameter space. These include emission from the decay of primordial black holes (PBHs) [13] and cosmic strings [22]. The cosmological and physical importance of PBHs is well established [12]. As the PBH evaporates, its temperature increases in proportion to the mass loss. Most models predict a final explosion of energy when all possible evaporation channels are available, but the number of degrees of freedom of emission is a highly controversial issue, and ranges from the conservative standard elementary particle model, where it reaches a maximum once the three generations of fermions are free to be produced, to the runaway Hagedorn model where the number of emission modes increases exponentially beyond this [12]. For the conservative model, an optimum time-scale of 1 s is found for observing the explosion of a PBH using the Whipple 10 m telescope. During this final second 9.1×10^{28} photons are emitted above 0.4 TeV.

The fluence sensitivity of the detector over this time-scale is of order 10^{-9} erg cm^{-2} which is comparable to or better than that achieved in most bands of the gamma-ray spectrum. The sensitivity of the technique is compared to that achieved in searches by other gamma-ray experiments, operating at energy thresholds higher than the Whipple instrument.

2. The Whipple 10 m telescope

Situated at an altitude of 2.3 km on Mt.Hopkins in Arizona, the telescope operated by the Whipple Collaboration has been used as an imaging device since 1982; the camera has been improved from a 37 to a 109 element imaging system during that time. The telescope consists of a 10-metre dish (with 248 front-coated mirrors) on an alt-azimuth mount and a camera containing 109 photomultipliers (PMTs). The inner 91 PMTs are 1.1 cm diameter tubes (Hamamatsu R1398) and are connected via amplifiers to trigger discriminators. An outer ring of 18 tubes is independent of the trigger logic and contributes only to the

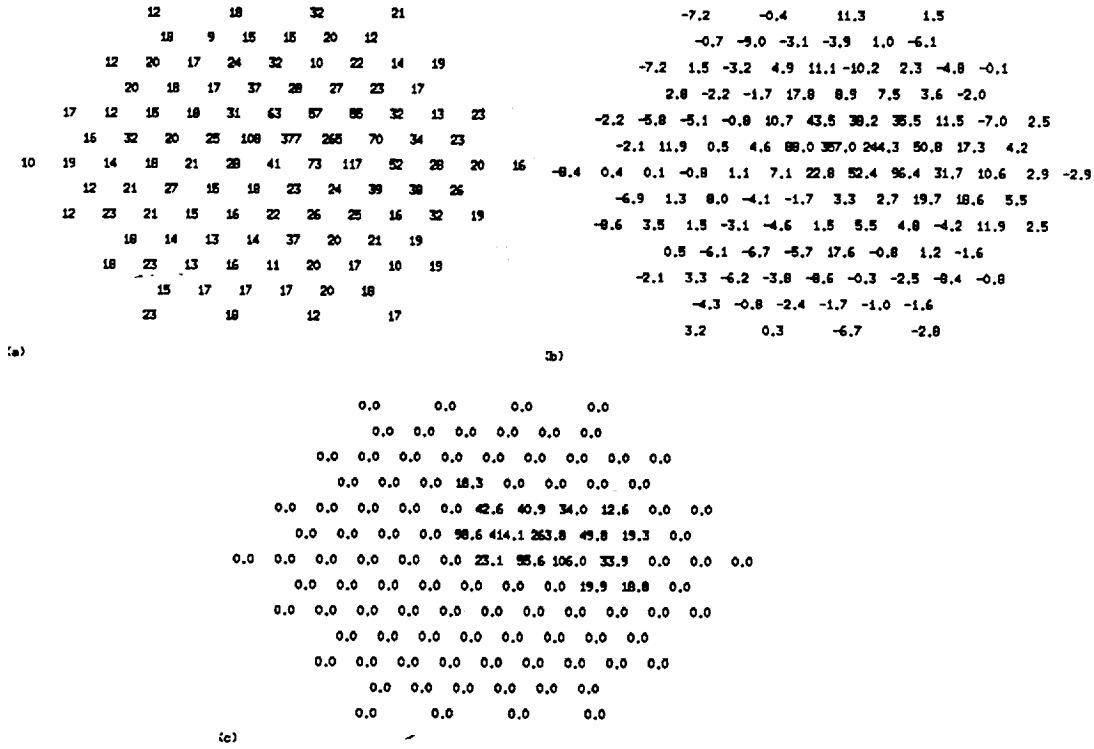

Fig. 3. 10 m image (a) before and (b) after flat-fielding, and (c) after cleaning.

imaging of the event. Until 1993, these outer tubes were 5 cm tubes giving a total field-of-view of 3.75°. They have been replaced by the smaller tubes so that the camera field-of-view is now 3°. The arrangement of PMTs in the focus box prior to 1993 is shown in Fig. 1 and a detailed description of the instrument can be found in [5].

The camera is triggered if the signal in two or more PMTs exceeds a preset threshold in a 10 nsec time interval. When the system is triggered, i.e. an event is registered, the light level in each PMT is recorded over a 25 nsec gate width. The trigger rate during the epoch of the observations reported here was typically 8 events per second. The time is derived from a GPS clock and is recorded with each event with an accuracy of 0.1 msec. The deadtime is 1.5 msec and the distribution of time differences of successive events from a 60 minute data file taken at a telescope elevation of 80° is shown in Fig. 2 (histogram). It is overlaid on the expected Poisson distribution for the same mean event rate (solid curve).

The digitized images of the Cherenkov light are analyzed off-line. A typical image recorded by the present

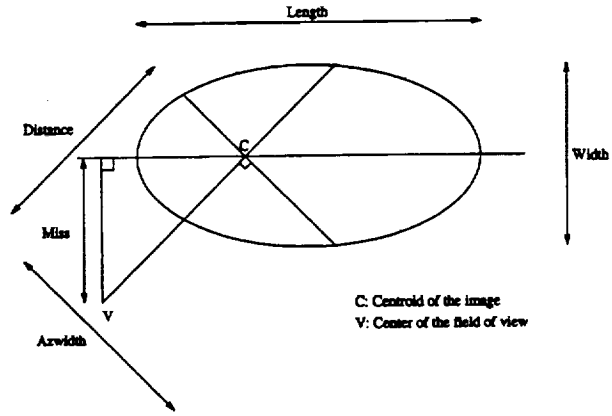

Fig. 4. Representation of image parameters.

camera is shown at various stages of processing in Fig. 3. Moment-fitting routines are used to define each image by an ellipse whose parameters define the event (shown in Fig. 4). The event is accepted as a potential gamma-ray event or rejected as a hadron-initiated event depending on the values of these parameters. The axis of the image is defined by minimizing the signal-weighted sum of the squares of the perpendicular angular distances of the pixels. The r.m.s. spread

of light perpendicular to and along this axis defines the semi-minor and semi-major axes of the ellipse and these are known as the *width* and *length* of the image. Image compactness is defined by *concentration*, which is the fraction of the sum over all nonzero pixels of the cleaned image in digital counts (known as *size*) contained in the two or three brightest pixels. The other parameters shown in Fig. 4 relate to the orientation of the image axis relative to the source position in the field-of-view.

If the position of the source is known (usually at the centre of the field of view), then the orientation of the image relative to that direction is important for source detection. A combination of shape and orientation parameters has been used by the Whipple Collaboration to reject 99.7% of recorded background while keeping 50% of gamma rays; the set of selection parameters that are most useful for observations of a point-source in the centre of the field of view are called Supercuts and are defined elsewhere [21]. A comparison of the *width* and *length* domains for photons (simulated) and real background (data taken with the telescope pointed at the zenith) can be seen in Fig. 5.

The success of Supercuts and the Imaging Atmospheric Cherenkov Technique in the detection of point sources owes much to Monte Carlo simulations of photon and background hadron-initiated cascades. Owing to the impossibility of testing the atmospheric Cherenkov detector at an accelerator, analytical models and simulation of phenomena are used to optimize instrumental design and in the development of analysis techniques. Data taken during observations of the Crab Nebula, which plays the role of a TeV gamma-ray standard candle, are used to perfect new techniques.

3. Off-axis sensitivity of 10 m reflector

The characteristics of the 10 m reflector in point-source mode of operation are well understood and defined [5]. What is less well characterized is the sensitivity of the instrument when an area of the sky is probed for a source without knowing its exact position, i.e., where each point in the field-of-view is a potential source. It has been demonstrated experimentally that the system is sensitive to a point source of gamma rays up to 1° off-axis [1,10]. In the work reported here, the response over the full field-of-view of the 10 m reflector is investigated, using simulations, in order to use the instrument as a relatively wide field burst detector.

3.1. The off-axis triggering and imaging of gamma rays

The geometrical field-of-view of the 10 m camera between 1988 and 1992 was 3.75°, but the imaging technique allows reconstruction of images whose origins lie outside this area. Conversely, some of the images of showers from sources on the edge of the camera face may fall outside the field-of-view so that the camera has reduced collection area for such sources.

In order to assess the sensitivity of the instrument for sources lying at various distances from the centre of the camera, a database of nearly 8000 simulated gamma-ray-induced showers of energies ranging from 0.2 TeV to 0.8 TeV was compiled using a simulation program based on the KASCADE code of Kertzmann and Sembroski [15]. The Whipple collaboration has used several different simulation codes in the various research institutions (e.g. MOCCA at the University of Leeds) and comparison of the simulations shows that they are in agreement with each other to within 10% in the Cherenkov light yields and image parameter distributions that they produce.

The response of the instrument to the simulated gamma-ray showers is gauged by mapping each Cherenkov photon in a shower from the mirrors onto the imaging camera and building up an event for each shower.

Displacing the focus box from its position at the focus of the reflector and constructing events as they appear to this displaced camera is equivalent to simulating the response of the camera to sources at an offset from the centre equal to the displacement of the camera but in the opposite direction. The response of the camera to gamma-ray showers from sources with 0° to 2.5° offsets from the centre was investigated by successively displacing the camera at 0.25° intervals along an arbitrary line, 17° from an axis through the centre of a row of PMTs. A different source displacement angle may be chosen without affecting the results. The treatment of simulated images is identical to that subsequently applied to real data. The parameterization and cutting procedures execute rapidly relative to the shower and instrument simulations, and it

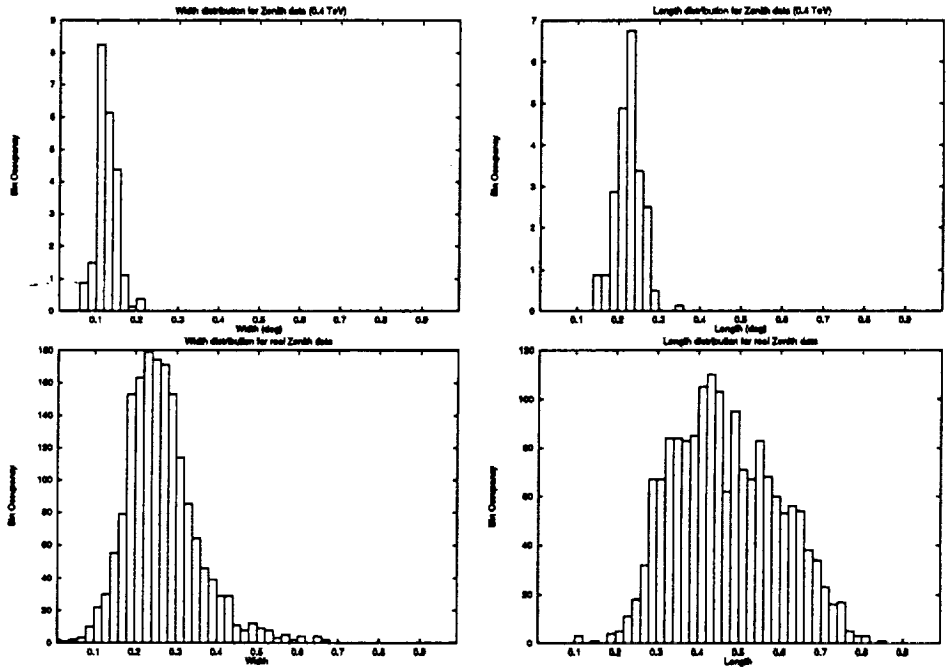

Fig. 5. Width (left) and length (right) distributions for simulated 0.4 TeV photon from the zenith (top) and real zenith (bottom) showers.

was possible to experiment with a variety of parameters and analysis methods before deciding on a suitable gamma-ray burst search method.

As the source position moves further away from the centre of the camera, less Cherenkov light falls on the detector at a given impact parameter. The software trigger is a requirement that two of the inner 91 tubes register at least 40 photo-electrons and the percentage of events triggering the system at each impact parameter is shown in Fig. 6 for source offsets of (a) 0°, (b) 0.75°, and (c) 1.5°.

By weighting the fraction according to the impact parameter value (the collection area is bigger at larger impact radii), a value for the trigger efficiency over the field of view, equivalent to the effective area of the detector for each source offset, is calculated,

$$\text{Trigger efficiency} = \frac{\sum_i 2\pi r_i \phi_i \, \delta r}{7 \times 10^4}, \qquad (1)$$

where r_i $(= i)$ is the radius of the annulus at impact parameter i, thickness $\delta r = 2$ metres, and ϕ_i is the fraction of the 20 showers at radius r_i which would trigger the telescope. The summing integer i is incremented from 12 to 200 in steps of 2. At impact parameters below 10 metres, the showers tend to saturate the central tube, and the Cherenkov light pool falls off rapidly beyond 150 metres, so that we define an ideal detector as one which is triggered by all showers with impact parameters between 10 and 150 metres, and which fails to register any events falling outside that area. The trigger efficiency is divided by 7×10^4 m^2 to give the efficiency relative to this arbitrary ideal detector. An efficiency of greater than 1 is, therefore, possible since showers lying beyond 150 metres may trigger the system. This procedure was implemented for all 4 shower energies, and the results are shown in Fig. 7. Above threshold (> 0.4 TeV) the instrument would register over half of the gamma-ray showers from sources out to 1° away from the centre, but it is obviously more efficient at detecting those nearer the centre than at large offsets.

Image parameters have traditionally been used, in some combination of shape and orientation cuts, to discriminate against the hadronic background. In this search, however, only the shape parameters are relevant since there is no preferred direction due to the unknown position of the source in the field-of-view. The most successful shape selection was found to involve cuts in *length* and *width*, using the values derived for Supercuts,

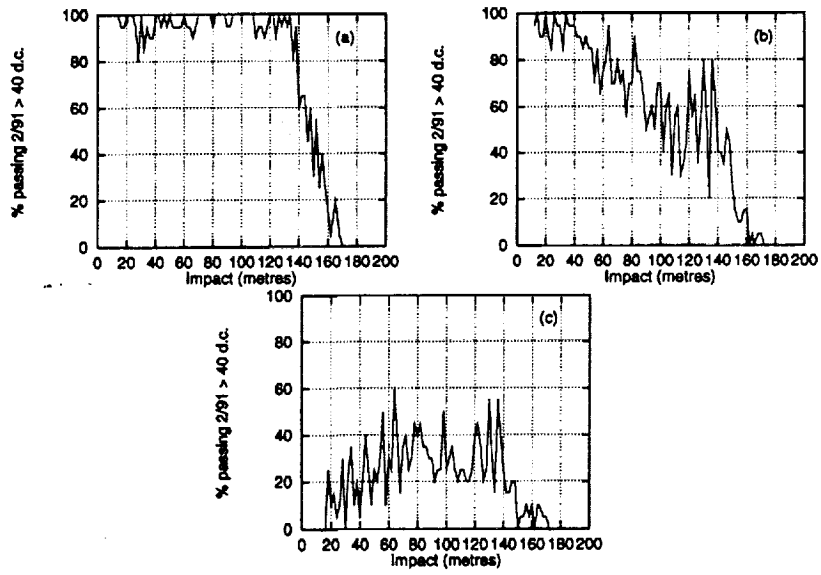

Fig. 6. Percentage of events which trigger the 10 m reflector as a function of impact parameter for source offsets (a) 0°, (b) 0.75°, (c) 1.5° for 0.4 TeV showers.

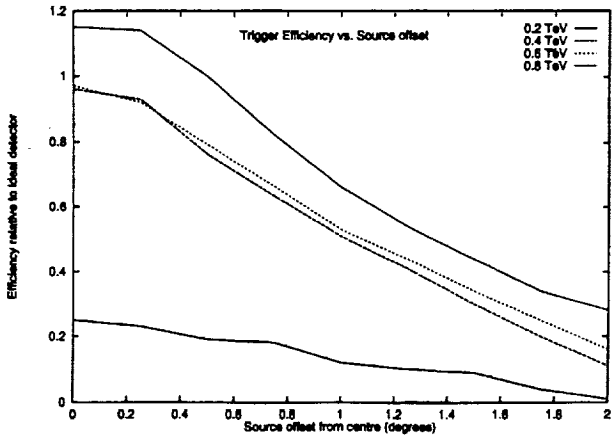

Fig. 7. Trigger efficiency of the 10 m reflector as a function of source offset and energy. An efficiency of 1 is that of an ideal detector which has a 100% trigger rate for showers of impact parameters between 10 and 150 metres, and no triggers outside this range. This is equivalent to a collection area of 7×10^4 m^2.

$$0.073° < width < 0.15°,$$

$$0.16° < length < 0.30°.$$

Fig. 8 shows the percentage of 0.4 TeV events at offsets (a) 0°, (b) 0.75° and (c) 1.5° which trigger the camera and satisfy these image shape requirements. Combining the percentages for each impact parameter produces the results which are shown in Fig. 9. Above the detector energy threshold, the collection area for gamma rays is fairly flat, and showers from sources which are up to half a degree off-axis are still selected over 50% of the time. There are two competing effects which explain the shape of the curves: at high energies, showers with large impact parameters produce enough Cherenkov light to trigger the telescope more often than distant low-energy showers, but the Supercuts selection is biased towards small showers, so that the higher energy showers are less likely than the low-energy events to survive the *width* and *length* cuts regardless of impact parameter. At large source offsets the fraction of events selected decreases with shower energy even though the high-energy events appear to trigger the camera more often than at lower energies. If the showers triggering the system at these large offsets are examined, it can be seen that they are the longest images in the high-energy databases.

Observations of the Crab Nebula at angular offsets from the centre of the field-of-view of the 10 m telescope were used to confirm the efficiency curves derived from these simulations. The Crab Nebula is a steady source of TeV gamma rays, and by comparing the rate of gamma rays measured after applying the Supercuts selection technique to data from September 1996 at offsets ranging from 0° to 1.5°, one obtains the efficiency for gamma ray collection displayed in Fig. 10. The errors in Fig. 10 reflect the variation in

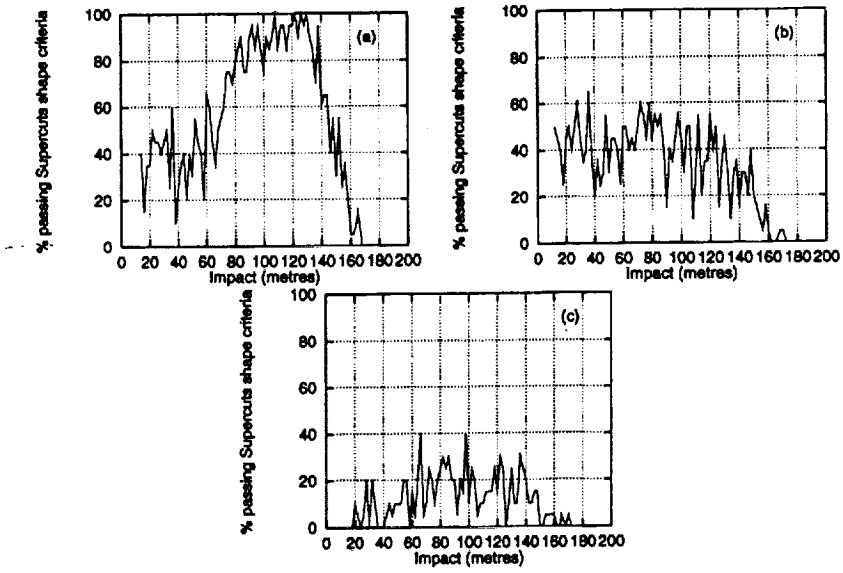

Fig. 8. Percentage of events which survive Supercuts shape cuts as a function of impact parameter for source offsets (a) 0°, (b) 0.75°, (c) 1.5° for 0.4 TeV showers.

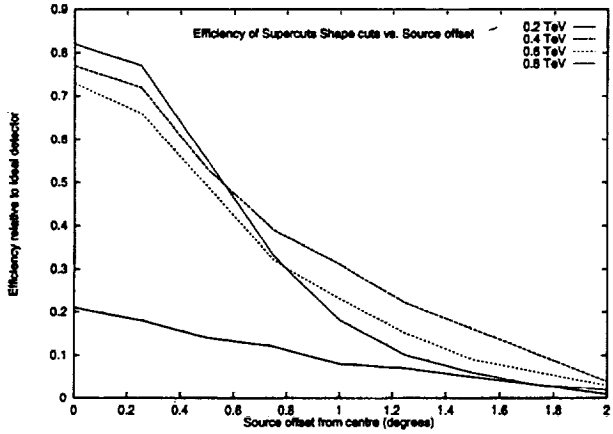

Fig. 9. Ability of 10 m reflector to detect gamma rays as a function of source offset and energy. *Width* and *Length* cuts are made on all events that trigger the system. An efficiency of 1 is that of an ideal detector which has a 100% trigger and image selection rate for showers with impact parameters between 10 and 150 metres and none outside. This is equivalent to a collection area of 7×10^4 m^2.

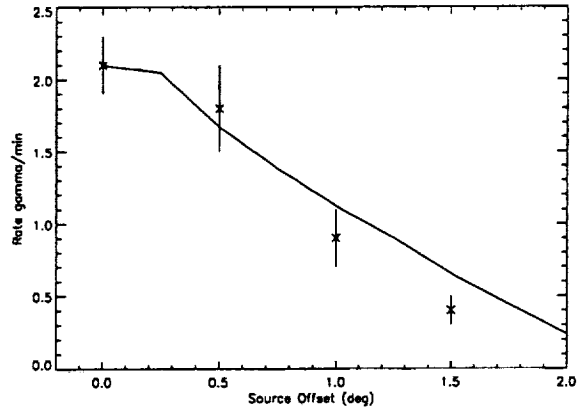

Fig. 10. Efficiency curve from simulations (solid line) compared to the gamma-ray rate measured from Crab Nebula (x) as a function of source offset.

event rates for the offset observations, and are large owing to the small exposure time: only 1 hour of source observations was made at a source offset of 0.5° from the centre of the field-of-view, 1.5 hours at 1.0°, and 2 hours at 1.5° offset. Because the field-of-view of the telescope was smaller when these offset observations were made compared to that simulated in this study, a perfect correlation is not expected, and one anticipates that the efficiency at larger source offsets be slightly lower relative to source-centered observations than in the simulations.

3.2. Orientation of gamma-ray images

The orientation of the ellipse fitted to each image is represented by its major axis, and the most likely point-of-origin of the shower progenitor on the field-of-view lies on this axis at a distance d in degrees

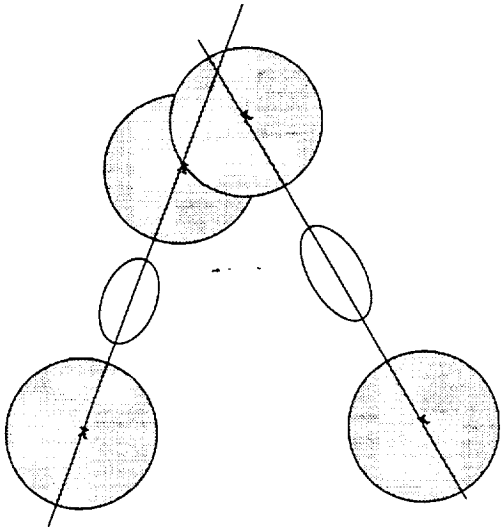

Fig. 11. Illustration of the most likely points-of-origin (x) along the major axes of two events (ellipses). The shaded circles indicate the uncertainty associated with these positions.

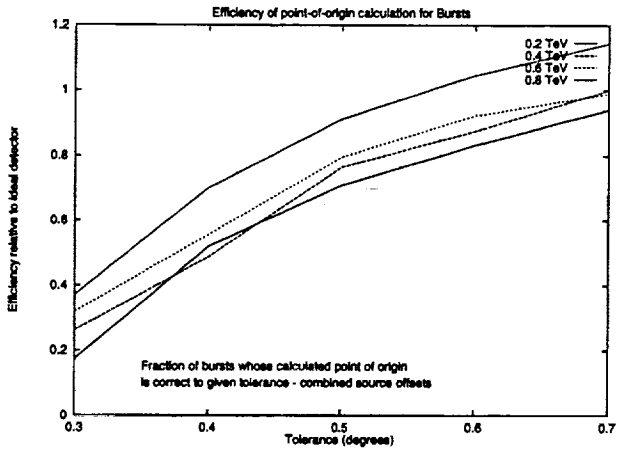

Fig. 12. Efficiency of point-of-origin determination from $d = 2 - 2 \times width/length$ along the major axis. The tolerance on the x-axis is the value by which this calculated point-of-origin is allowed to vary from the actual source position.

related to the ellipticity of the image,

$$d = 2 - 2(width/length)\,. \qquad (2)$$

This algorithm was developed based on simulations of gamma-ray showers from sources at the centre of the field-of-view, and was found to be accurate to about 0.3° either side of this point [1] for source-centered observations. The relation between the image, its centre, and the most likely point-of-origin are shown in Fig. 11.

Because the ellipses derived from the moment-fitting routines are symmetrical, the point-of-origin may lie either side of the centre of the image. The following equations are used:

$$\sqrt{(y_{or} - y_{cen})^2 + (x_{or} - x_{cen})^2} = 2 - 2 \times width/length\,,$$

$$y_{or} = m \times x_{or} + c\,,$$

to find the most likely points-of-origin x_{or}, y_{or} on both sides of the centre of light x_{cen}, y_{cen} along the major axis $y = m \times x + c$. The distance

$$\sqrt{(y_0 - y_{or})^2 + (x_0 - x_{or})^2}\,, \qquad (3)$$

where x_0, y_0 are the true positions of the simulated source, is a measure of how well Eq. (2) finds the point-of-origin of a shower. The tolerance is defined as the maximum allowed value of this distance, in degrees. A range of tolerance levels from 0.1° to 0.7° was explored to determine the off-axis efficiency of the point-of-origin determination, and the results are displayed in Fig. 12. The total efficiency Φ for each energy was obtained by combining source positions and weighting each efficiency (ϕ_r) according to source offset (r). The efficiency values featured are relative to an ideal detector with $\phi_r = 1$ at each source offset where the gamma-ray images are selected and their origin is correctly determined so that $\Phi = \sum \phi_r r / \sum r$, with r varying from 0.25° to 2.5°. The efficiency curve is fairly constant as the source is moved away from the centre and appears independent of impact parameter and photon energy.

Real background data were subjected to the same analysis so that the effect of varying the point-of-origin tolerance value on background acceptance could be assessed. It was found that in looking for bursts of 3 or more events over a 1-second time-scale, the highest signal to noise ratio could be obtained with a tolerance level of 0.425°. This selection criterion enables $66 \pm 5\%$ of shape-selected simulated events (over the impact parameter range 12 to 200 metres and source offset 0° to 2.5°) to be correctly located. The shaded areas in Fig. 11 show the regions from which the imaged events could have originated with this tolerance value.

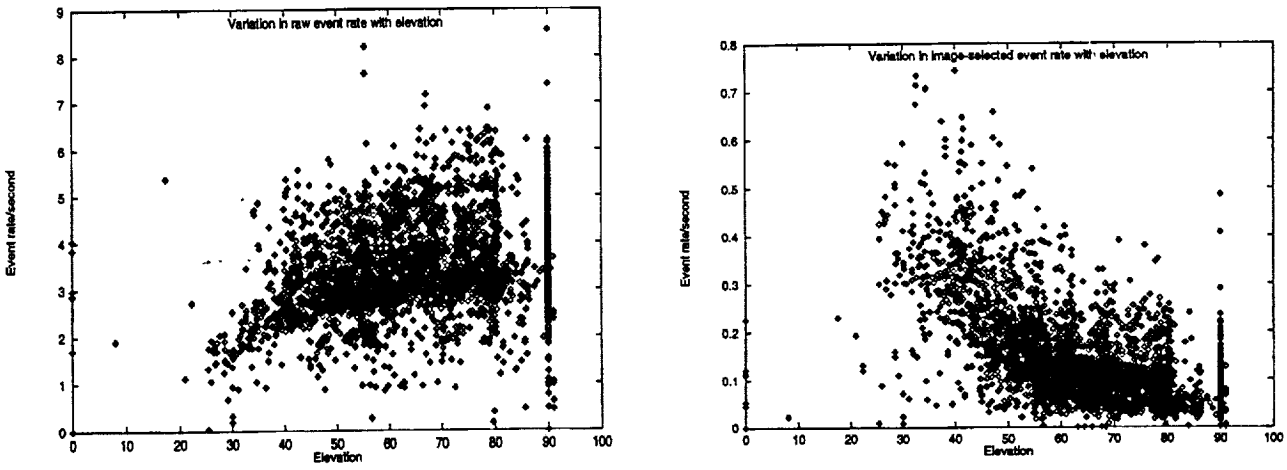

Fig. 13. Variation of event rate with elevation raw event rate (left) and event rate after selection via image *width* and *length* cuts (right).

It is then possible to apply this calculated off-axis response of the detector to the search for counterparts to the delayed component of BATSE bursts (reported elsewhere [7]) and to the serendipitious detection of gamma-ray bursts during the normal operation of the gamma-ray telescope (described below).

4. Searches for 1 s TeV gamma-ray bursts

The archival data of the Whipple Observatory taken with the 10 m reflector with an energy threshold above 0.4 TeV between September 1988 and September 1992 were used for this search. In general these observations were in the form of files of (approximately) 28 minute duration containing information on each event (the arrival time, the outputs of the 109 ADCs from the 109 pixels, and other housekeeping data). Examination of the observing logs allowed the identification and rejection of 1% of the data including (i) observations made when there were instrumentation problems, (ii) data taken with discriminator thresholds or high-voltage values significantly different from those used in normal operation, and (iii) observations made while testing new or experimental configurations (for example, experiments with filters). A further 1% of the files were rejected because of obvious anomalies, such as a large number of bright stars in the field-of-view, or because they were taken at a telescope elevation less than 35° above the horizon. Following rejection of unsuitable data, 2217 hours of observations comprised the database. The database was divided according to the event rate of candidate gamma rays. Variation in event rates was caused by differences in zenith angle, mirror reflectivity and discriminator settings. The elevation of the source under observation is known to affect the energy threshold of the detector, and also influences the appearance of both gamma and hadronic images. A larger depth of atmosphere must be penetrated by the extensive air shower particles if they are to produce light lower in the atmosphere, so that a telescope pointed close to the zenith is sensitive to lower energy showers than if it is operated nearer the horizon. Consequently, the raw event rates decrease with increasing zenith angle – this relationship is shown in Fig. 13 (left). Despite this overall fall in event rates at low elevations, the Cherenkov image on the camera face is narrower on the horizon than at the zenith, and this effect results in more hadronic events being selected as gamma rays on the basis of the *width* parameter. Fig. 13 (right) shows the variation of image-selected event rate with telescope elevation.

Nearly 80% of observations were made with the telescope elevation above 55°, where data rates and image characteristics are fairly homogeneous. These observations form the bulk of the 1759 hours of data which had an average rate of < 0.2 candidate gamma-ray events per second, and comprise the largest of the three subsets of the Whipple database. The rest of the data was divided according to the average event rate; rate = 0.2 to 0.4 per second (394 hours) and rate $>$ 0.4 events per second (64 hours). Standard routines were used to flat-field the data, tubes with bright stars

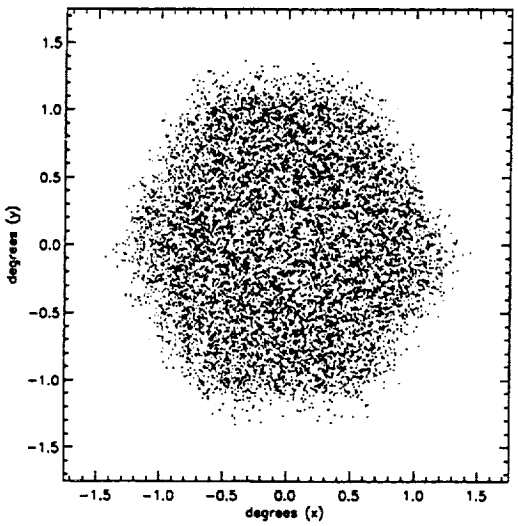

Fig. 14. Event centroid distribution of events in a 60 minute data file.

in their field-of-view were turned off in hardware or software, and the image parameters were calculated as described in [21]. The events were then characterized by these image parameters (and their arrival times). The evenness of the camera response across the field-of-view is illustrated in Fig. 14, showing the distribution of event centroids in camera coordinates (degrees from centre) for a 60 minute observation.

4.1. The burst search

Initially the events were culled to include only those events whose images satisfied the gamma-ray event criteria. Events which survived the *width* and *length* cuts described above were included in a reduced data set which was submitted to a search for bursts of 3 or more events in a 1 s time interval.

The arrival time of the first event was taken as the possible start of a 1 s burst and was compared to the time of the second event. If the time difference was under 1 s, the next event was examined. If not, the start of the time window was moved to the arrival time of the second event. The window was moved through the file until all events in a file have been processed, and the total number of bursts with from 3 to 10 shape-selected events in the file is obtained. No candidate bursts were found with more than 4 events. The number of 3- and 4-fold burst events are shown in Table 1 in the column headed "obs". A background (control) file was generated from each real data file by scrambling the events in each parameterized file, while maintaining the original time sequence. When the background file was subjected to the burst-search program, the image-selected events were the same as those picked from the real data file, but in a random order and attached to the original arrival times of other events. The number of 3- and 4-fold bursts thus found is shown in Table 1 headed "exp". The difference between the observed and the expectation is expressed in terms of the standard deviation, σ defined as $(\text{obs} + \text{exp})^{1/2}$. In no case is the difference statistically significant.

To this point no use has been made of the fact that the events in the putative 3- and 4-fold bursts must come from the same point in the sky. Hence all the bursts were subjected to the common origin selection described above. Less than 2% of the putative bursts passed this selection. These are listed as before in Table 2; the expectation is derived by applying the common origin selection to the scrambled events.

Again, no excess of 3- or 4-fold bursts of candidate gamma-ray events on a 1-second time-scale is found in the 2217 hours of the Whipple database. Two candidate four-fold events are shown in Fig. 15. If a TeV component to a background of bursters exhibiting activity on a 1 s time-scale exists, then the number of these bursts is low and below the sensitivity of the instrument in its current form.

5. Upper limit to density of exploding PBH

Based on the null results obtained in this search, an upper limit to the local density of exploding PBHs can be calculated using the flux of TeV photons predicted by the standard model and presented in [12].

Previous results of searches for exploding PBH by the Whipple Collaboration used extrapolated values of collection area and solid angle [18,16,23,6]. The work presented here involves a search over a larger archival database (2217 hours) for bursts on a longer time-scale (1 s) with a lower energy threshold (0.4 TeV); hence the sensitivity should be greater. In addition the sensitivity is calculated more rigorously than in previous experiments. In the earlier Whipple experiments the sampling distance was calculated from the trigger efficiency rather than gamma-ray collection area. Our new Monte Carlo simulations indicate that in calculat-

Table 1
Frequency of gamma-ray burst candidates in Whipple database vs expected burst frequency (no common origin sought)

Event rate/sec (cut)	Hours of data	3-event burst			4-event burst		
		exp	obs	σ	exp	obs	σ
0.0–0.2	1759	4747	4762	+0.15	234	245	+0.50
0.2–0.4	394	13463	13679	+1.31	1308	1286	−0.43
> 0.4	64	10597	10539	−0.40	1800	1724	−1.28
Total	2217	28807	28980	+0.72	3342	3255	−1.07

Table 2
Frequency of gamma-ray burst candidates in Whipple database vs expected burst frequency (with common origin)

Event rate/sec (cut)	Hours of data	3-event burst			4-event burst		
		exp	obs	σ	exp	obs	σ
0.0–0.2	1759	62	73	+0.95	0	2	1.41
0.2–0.4	394	230	232	+0.09	8	5	−0.83
> 0.4	64	236	257	+0.95	12	5	−1.70
Total	2217	528	562	+1.03	20	12	−1.41

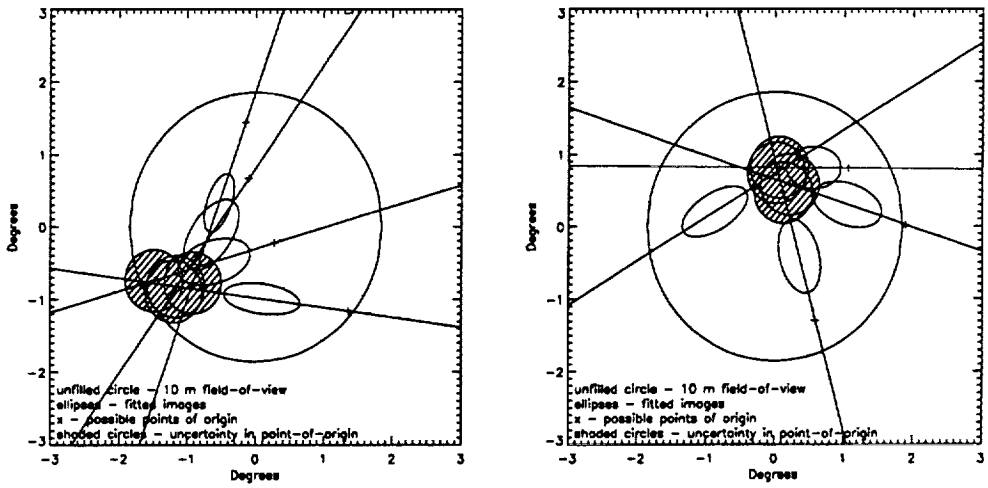

Fig. 15. Two bursts of four events from real data in 1 second with a possible common point-of-origin.

ing limits from data taken after 1988 (when the imaging system was introduced), the sampling distance was overestimated. In addition, a constant gamma-ray sensitivity over the field-of-view was assumed and the sensitive volume integrated the estimated sampling distance over the solid angle of the camera. A more realistic sensitive volume based on Monte Carlo simulations is used in this search. Table 3 shows the sampling distances and sensitive volumes for a 3-photon burst in the 10 m reflector for source offsets out to 2° given the gamma-ray flux calculated in [12]. The second column shows the collection area for a source at a particular point in the camera and column 3 shows the maximum distance at which a PBH can be detected. The volume probed, V_i, is calculated by integrating over the solid angle, Ω_i, covered by the annulus (or circle for a source at the centre) described by the source offset: $V_i = \frac{1}{3} r_i^3 (\Omega_i - \Omega_{i-1})$. This volume

Table 3
Sensitivity of 10 m reflector for 0.4 TeV γ after applying *width* and *length* cuts at source offsets out to 2°

Source offset from center (°)	Collection area (10^4 m^2)	Sampling distance (pc)	Sensitive volume ($\times 10^{-6}$ pc^3)
0.00	5.39 ± 0.89	0.38 ± 0.15	1.09 ± 0.07
0.25	5.07 ± 0.89	0.37 ± 0.15	3.03 ± 0.20
0.50	3.69 ± 0.95	0.32 ± 0.16	3.27 ± 0.41
0.75	2.73 ± 0.94	0.27 ± 0.16	2.75 ± 0.57
1.00	2.14 ± 0.82	0.24 ± 0.15	2.48 ± 0.61
1.25	1.52 ± 0.78	0.20 ± 0.14	1.75 ± 0.60
1.50	1.15 ± 0.62	0.18 ± 0.13	1.51 ± 0.57
1.75	0.70 ± 0.48	0.14 ± 0.11	0.82 ± 0.40
2.00	0.31 ± 0.37	0.09 ± 0.10	0.25 ± 0.34
Total sensitive volume			16.95 ± 3.77

Table 4
Upper limits to exploding PBH frequency from archival search

Hours of data	3-event burst		4-event burst	
	volume $\times 10^{-5}$ pc^3	limit $\times 10^6$ pc^{-3} yr^{-1}	volume $\times 10^{-5}$ pc^3	limit $\times 10^6$ pc^{-3} yr^{-1}
1759	1.67 ± 0.38	14.13 ± 3.3	1.07 ± 0.26	3.0 ± 1.0
394		96.2 ± 23.0		20.4 ± 5.3
64		745 ± 170		117 ± 30

is nearly 8 times smaller than the volume estimate in Nolan et al. [16] although the hardware system is identical and the analysis and burst search methods used in this work are more sensitive.

The corresponding distances and volumes accessible to the reflector can be calculated for the detection of bursts of 4 photons in 1 s. The excess (or deficit) of bursts obtained over expectation in the sensitive volume in each of the three data groups in the archive is used to find the 99.9% maximum likelihood upper limit to the frequency of exploding PBH per year per cubic parsec (Table 4). More sensitive upper limits are obtained from air shower experiments which operate at higher energies and have longer exposure times; these are shown in Table 5.

Models other than those derived from standard elementary particle theory have also been invoked to describe the final stages of evaporation of a PBH. Those propose a faster process with more degrees of freedom than the standard model – the Hagedorn model, in which the number of degrees of freedom increases exponentially with the number of emitted particles, predicts the most catastrophic explosion, of 6.0×10^{34} erg, lasting only 10^{-7} seconds, and comprised mainly of 250 MeV photons. A larger volume is accessible to searches for this type of event than for PBH exploding according to the standard model. Upper limits to Hagedorn-type PBH explosions are, therefore, more restrictive, and are given in [17,8].

Table 5
Standard elementary particle upper limits to PBH density

Experiment	Energy (TeV)	Ref.	Limit (pc^{-3} yr^{-1})
CYGNUS	50	[2]	6.1×10^5
AIROBICC	20	[11]	8.9×10^5
Tibet	10	[3]	4.6×10^5

6. Conclusions

A method is described of using an atmospheric Cherenkov telescope to search for gamma-ray bursts on short time-scales. The application of this method to the search for counterparts to classical gamma-ray bursts detected by the BATSE experiment is described

elsewhere [7]. Here it is applied to a search through a four year database accumulated by the Whipple telescope in its routine discrete source observing program. The minimum detectable fluence (6×10^{-9} erg cm^{-2} in one second) is comparable with that of BATSE at much lower energies and compares favorably with all other gamma-ray experiments currently in operation.

Null results are obtained and an upper limit to the PBH density is derived, where the PBH is exploding via the standard model. This limit of $3.0 \pm 1.0 \times 10^6$ pc^{-3} yr^{-1} is better than that obtained from previous searches using the Whipple 10 m reflector. It is not, however, as stringent as the PBH limits obtained with wide field air shower experiments. The low duty cycle and small field-of-view of atmospheric Cherenkov telescopes makes them less efficient than air shower experiments like the MILAGRO water-Cherenkov telescope [4] which have a large field-of-view and longer exposures. Telescopes with rapid slew speeds are, nevertheless, well suited for the detection of very high-energy counterparts to BATSE-type bursts [7].

Acknowledgements

We acknowledge the technical assistance of Teresa Lappin and Kevin Harris. This research is supported by grants from the US Department of Energy and by NASA, by PPARC in the UK, and by Forbairt in Ireland.

References

[1] C. Akerlof et al., Ap. J. 377 (1991) L97.
[2] D. Alexandreas et al., Proc. 23rd ICRC, Calgary, Vol. 1 (1993) p. 428.
[3] M. Amenomori et al., Proc. 24th ICRC, Rome, Vol. 2 (1995) p. 112.
[4] S. Barwick et al., Proc. 24th ICRC, Rome, Vol. 2 (1995) p. 436.
[5] M.F. Cawley et al., Exp. Astron. 1 (1991) 173.
[6] V. Connaughton et al., AIP Conf. Proc. 307 GRB, G.J. Fishman, J.J. Brainerd, K. Hurley, eds. (Huntsville, AL, 1993) p. 470.
[7] V. Connaughton et al., Ap. J. 479 (1997) 859.
[8] C. Fichtel et al., AIP Conf. Proc. 384 GRB, C. Kouveliotou, M.S. Briggs, G.J. Fishman, eds. (Huntsville, AL, 1995) p. 368.
[9] G.J. Fishman, C. Meegan, Annu. Rev. Astron. Astrophys. 33 (1995) 415.
[10] V.P. Fomin et al., Astropart. Phys. 2 (1994) 137.
[11] B. Funk et al., Proc. 24th ICRC, Rome, Vol. 2 (1995) p. 104.
[12] F. Halzen et al., Nature 353 (1991) 807.
[13] S.W. Hawking, Nature 248 (1974) 30.
[14] K. Hurley, Space Sc. Rev. 75 (1996) 43.
[15] M.P. Kertzmann, G.S. Sembroski, Nucl. Inst. Meth. A 343 (1994) 629.
[16] K. Nolan et al., Proc. 21 st. ICRC, Adelaide, Vol. 2 (1990) 150.
[17] N.A. Porter, T.C. Weekes, MNRAS 183 (1978) 285.
[18] N.A. Porter, T.C. Weekes, Nature 277 (1979) 199.
[19] M. Punch et al. Nature 358 (1992) 477.
[20] J. Quinn et al., Ap. J. 452 (1996) 588.
[21] P.T. Reynolds et al., Ap. J. 404 (1993) 206.
[22] T. Samura, K. Kobayakawa, Proc. 23rd ICRC, Calgary, Vol. 1 (1993) p. 128.
[23] P. Sommers, J.W. Elbert, J. Phys. G 13 (1987) 553.
[24] G. Vacanti et al., Ap. J. 377 (1991) 467.
[25] T.C. Weekes, Space Sci. Rev. 75 (1996) 1.

(3)

SEARCH FOR TeV COUNTERPARTS IN GAMMA RAY BURSTS

P.J.Boyle[1], J.H.Buckley[2], A.M. Burdett[3], J.Bussóns Gordo[1], D.A.Carter-Lewis[4], M.Catanese[4], M.F.Cawley[5], V.Connaughton[6], D.J.Fegan[1], J.P.Finley[7], J.A.Gaidos[7], K.Harris[2], A.M.Hillas[3], R.C.Lamb[8], F.Krennrich[4], R.W.Lessard[7], C.Masterson[1], J.E.McEnery[1], G.Mohanty[4], N.A.Porter[1], J.Quinn[1,2], A.J.Rodgers[3], H.J.Rose[3], F.W.Samuelson[4], G.H.Sembroski[7], R.Srinivasan[7], T.C.Weekes[2], J.Zweerink[4],

[1] *Physics Department, University College, Dublin, Ireland*
[2] *Whipple Observatory, Harvard-Smithsonian CfA, USA*
[3] *Physics Department, University of Leeds, United Kingdom*
[4] *Department of Physics and Astronomy, Iowa State University, USA*
[5] *Physics Department, St.Patrick's College, Maynooth, Ireland*
[6] *Marshall Space Flight Center, Alabama, USA*
[7] *Department of Physics, Purdue University, Indiana, USA*
[8] *Space Radiation Laboratory, Caltech, Pasadena, USA*

ABSTRACT

Based on BACODINE network notification the Whipple Observatory gamma-ray telescope has been used to search for the delayed TeV counterpart to BATSE-detected gamma-ray bursts. In the fast slew mode, any point in the sky can be reached within two minutes of the burst notification. The search strategy, necessary because of the uncertainty in burst position and limited FOV of the camera, is described.

INTRODUCTION

The Whipple collaboration has an active observational program which is dedicated to searching for TeV counterparts of classical gamma ray bursts. Since May 1994, the Whipple Observatory 10 meter gamma-ray telescope (Cawley, et al., 1990) has made 16 follow-up observations of BATSE burst notifications, but to date no positive identifications have been made (Connaughton, et al., 1995, Connaughton, et al., 1997a). The field of view of our current instrument is limited to 3.5 degrees and the error box for the BATSE position of gamma-ray bursts is 10 degrees in diameter. Therefore, more than a single pointing has to be used for the TeV follow up after a gamma-ray burst. The current observation technique is to take a 28 minute exposure at the initial location and 4 more exposures 3 degrees away, with a final exposure taken again at the initial position as in Figure 1a (Connaughton, et al., 1997a). In order to find any associated TeV component a two dimensional (2D) search strategy has been developed in order to locate the precise region of emission (Akerlof, et al., 1993, Connaughton, et al., 1997a, Lessard, et al., 1997).

Assuming gamma ray bursts have an associated TeV component, it is uncertain as to just how long after the BATSE notification of a gamma-ray burst that this emission would last. At present, we cover less than 50% of the actual BATSE error box in 2.5 hours and of the 16 follow-ups observed to date, only 6 had full observations of all positions (Table 1). All other follow-ups were terminated after an hour due to sun/moonrise or the position being too low to track. Owing to the uncertainty in the timescale of bursts and the lack of coverage of the whole error box, a non-detection cannot be used as an argument against the possibility of gamma-ray burst emission extending up to TeV-emission energies.

Table 1: Whipple Observations of BACODINE Positions

Date	BATSE Trig.[a]	BACODINE Intensity Cts/s[b]	Difference BACO-Hunts. (deg)[c]	Durat. BATSE (s)[d]	Whipple delay (min)[e]	Elev-ation (deg)[f]	Cycles observed (1-6)[g]
940516	2980	630	N/A	N/A	19	24-14	1 (1 hour)
950208	3408	778	1.64	N/A	16	N/A	1,2
950405	3494	704	9.5	N/A	8	27-33	1,2,3+cont
950524	3598	8726	1.37	6	5	56-31	complete
950625	3649	1661	3.84	40	18	28-41	1-6
950701	3658	9134	2.3	15	56	41-69	complete
951117	3909	1955	10.1	25	5	30-24	1 (1 hour)
951119	3911	801	6.98	60	20	45-54	complete
951124	3918	1231	5.98	150	2	59-76	complete
951220	4048	6698	2.88	17	27	71-37	complete
960521	5467	2919	9.13		14	80-68	1,2
961017	5634	3193	2.74	41	7	28-23	complete
961111[h]	5665	496	-	-	4	54-80	1-4
961206	5706	1312	6.4	1.4	5	26-22	1-3
970304	6113	8842	3.1	11	3	28-42	1-4
970308	6117	1120	13.6	2	4	43-72	complete

[a]Trigger number of BATSE burst

[b]Number of counts/s measured by BATSE in the first 1 or 2 seconds of the burst.

[c]Angular difference between the burst coordinates provided through BACODINE and the final estimated burst position from Huntsville.

[d]Duration of the burst seen by BATSE.

[e]Length of time that elapsed between sending the BACODINE message and the start of the first Whipple run.

[f]Average elevations of the first and last positions covered by the 10-metre telescope.

[g]Whipple coverage of burst area. The numbers listed indicate the positions covered in the observations. The 6 positions are described in the text and are shown in Figure 1a. An entry of "complete" means all 6 positions and their control observations were completed.

[h]Trigger #5665 was a terrestial trigger

RASTER SEARCH TECHNIQUE

In order to achieve a better coverage of the 10 degree error box we now scan a circular region around the BATSE burst position with a constant angular velocity. A raster scan across parallel lines in declination (Figure 1b) with a spacing of 1 degree results in complete coverage of the BATSE error box. A continuous motor speed of 0.1 degree/s facilitates a scan of the whole error box within 400 seconds. The fast scanning method has the advantage that we may give a flux upper limit within the first 300-400 seconds or less depending on the final improved BATSE burst position. Although the sensitivity within the first 300 seconds is not great, a burst of the calibre of 910503 or 930131 would be easily detected if the spectrum extends from the GeV region up to TeV energies (Hurley 1996). The time scale of those two bursts was 84 and 100 seconds respectively and only if the burst positions are close to the actual telescope position can a resonable coverage of the BATSE error box be achieved.

Recent improvements have lowered the time for response to a BACODINE notification of the Whipple telescope to within 15 seconds of the BATSE trigger. A new tracking system for the telescope will be

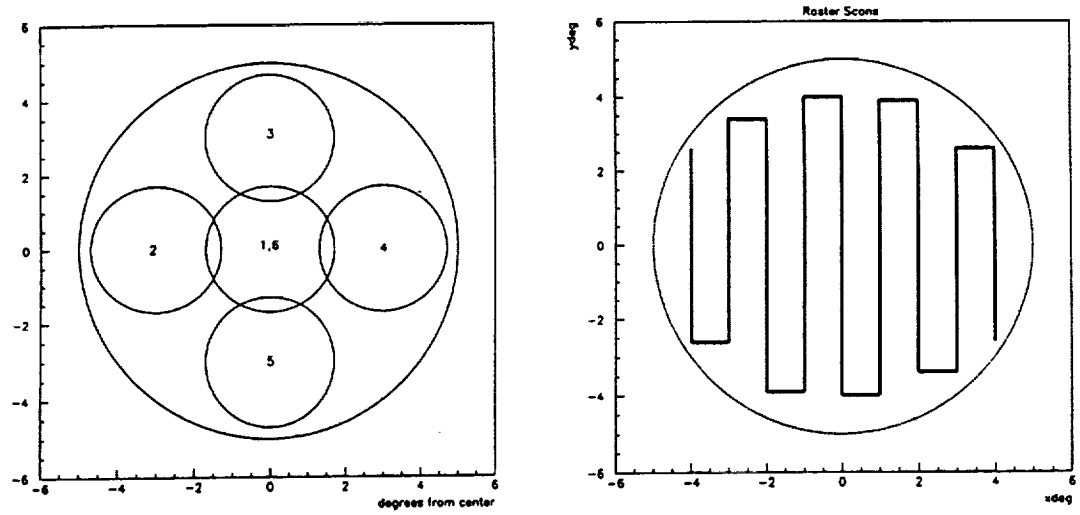

Fig. 1: (a): Current Response to BACODINE notifications. Each circle represents the field of view of the 10-meter reflector at the 5 different positions following a BATSE burst. (b): Raster Scan response. The reflector is moved at a constant velocity continuously along the track to cover the BATSE error box.

implemented in the fall of 1997, making the most distant point on the sky accessible within 2 minutes. A burst seen by BATSE and EGRET on 940217 lasted for some 1.5 hours at GeV energies. This class of gamma-ray burst might easily have been missed by the previous method but it could now be observed with a reasonable sensitivity (9 minutes effective observation time assuming a 3 degree FOV and a 10 degree error box).
The result of each raster scan will be analysed and displayed by a quicklook analysis to search for a strong excess. If there is no significant excess this scanning process can be continued for 2-5 hours if possible. If something significant is apparent, the telescope will be pointed at this position.

ANALYSIS

The Whipple high energy gamma-ray telescope images Čerenkov light from air showers onto an array of 151 photomultipliers covering a 3.5 degree field of view. The imaging technique uses information of the angular spread and orientation to reject more than 99.7% of the cosmic-ray induced showers while retaining over 50% of the possible gamma-ray induced events. For discrete objects the source is placed at the center of the field of view and candidate gamma-ray events (CGRE) are selected on the basis of the a combination of (a) image shape (*length & width*) and (b) orientation of the major axis of the shower (Reynolds, et al., 1993). However, as a burst source has an unknown position a 2-D search can determine the incident direction of the CGRE. The search makes use of the orienation, elongation and asymmetry of the image. Monte Carlo studies have shown that gamma-ray

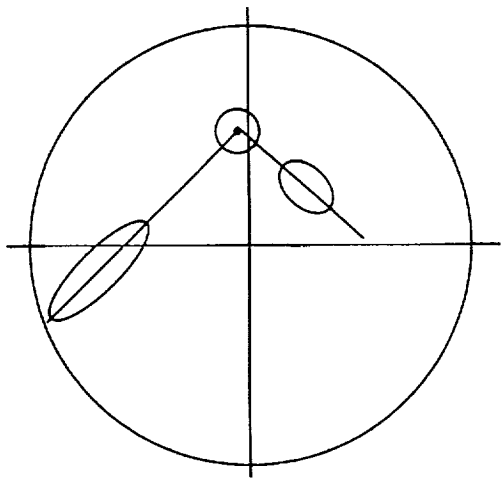

Fig. 2: 2-D reconstruction of points of origin of showers. For small impact parameters, the image has a structure close to that of a circle, whereas with increasing impact parameter it appears more elongated.

images are a) aligned towards the source position b) elongated in proportion to their impact parameter on the ground and c) asymetrical, images are weighted towards their point of origin (Figure 2). The distance between the image centroid and the true point of origin of a shower is represented by the imaging parameter *disp*:

$$disp = 1.85 - 1.85(width/length) \quad (1)$$

from which a unique point of origin can be calculated. As each event represents in itself a unique telescope position in Right Ascension (RA) and Declination (Dec), each point of origin must be translated into an absolute co-ordinate grid. Each point on the grid is then tested for an excess of gamma-ray-like events. The off center properties of the Whipple gamma-ray telescope are well established (Connaughton, et al., 1997b) and are used to determine a flux at any point in the camera.

ACKNOWLEDGEMENTS
We acknowledge the technical support of Emmet Roache. This research is supported by grants from the US Department of Energy and by NASA, by PPARC in the UK, and by Forbairt in Ireland.

REFERENCES
Akerlof, C.W., et al., 1991, Ap.J. 377, L97
Cawley, M.F., et al., 1990, Exp. Astron., 1, 185.
Connaughton, V., et al., 1995, Proc. 24th ICRC, 2, 96.
Connaughton, V., et al., 1997a, Ap.J., 479, 859.
Connaughton, V., et al., 1997b, Astroparticle Physics (submitted).
Hurley, K., Space Science Reviews, v.75, p.43-52.
Lessard, R.W., et al., 1997, Towards a Major Atmos. Cerenkov Detector - V.
Reynolds, P.T., et al., 1993, Ap.J. Letters 404, 206

OG 4.1.1

(4)

SPECTRUM OF TEV GAMMA RAYS FROM THE CRAB NEBULA

D.A.Carter-Lewis[1], S.Biller[2], P.J.Boyle[3], J.H.Buckley[4], A.Burdett[2], J.Bussons Gordo[3], M.A.Catanese[1], M.F.Cawley[5], D.J.Fegan[3], J.P.Finley[6], J.A.Gaidos[6], A.M.Hillas[2], F.Krennrich[1], R.C.Lamb[7], R.W.Lessard[6], C.Masterson[3], J.E.McEnery[3], G.Mohanty[1], J.Quinn[3], A.J.Rodgers[2], H.J.Rose[2], F.W.Samuelson[1], G.H.Sembroski[6], R.Srinivasan[6], T.C.Weekes[4], M.West,[2], J.A.Zweerink[1]

[1] *Iowa State University, U.S.A.*
[2] *University of Leeds, United Kingdom.*
[3] *University College, Dublin, Ireland*
[4] *Whipple Observatory, Harvard-Smithsonian CfA, U.S.A.*
[5] *St.Patrick's College, Maynooth, Ireland*
[6] *Purdue University, U.S.A.*
[7] *Space Radiation Lab, Caltech, U.S.A.*

ABSTRACT

The Crab Nebula has become established as the standard candle for TeV gamma-ray astronomy using the atmospheric Cherenkov technique. No evidence for variability has been seen. The spectrum of gamma rays from the Crab Nebula has been measured in the energy range 500 GeV to 8 TeV at the Whipple Observatory by the atmospheric Cherenkov imaging technique. Two methods of analysis involving independent Monte Carlo simulations and two databases of observations (1988-89 and 1995-96) were used and gave close agreement. Using the complete spectrum of the Crab Nebula, the spectrum of relativistic electrons is deduced and the spectrum of the resulting inverse Compton gamma-ray emission is in good agreement with the measured spectrum if the ambient magnetic field is about 25-30 nT.

1. INTRODUCTION

The Crab Nebula has become a standard candle in TeV astronomy; it has been detected by many groups and its integral flux appears constant. (We refer to the "steady" emission, not emission modulated at the pulsar period. We have not detected the latter at TeV energies. See paper by G. Gillanders et al., in these proceedings.) It is also well on the way to becoming a standard candle with regard to TeV spectral content. Synchrotron emission from the Crab covers a remarkably broad range terminating at about 10^8 eV, where a new component attributed to inverse Compton scattering begins. It is this component that we detect. The TeV spectrum is sensitive to the primary electron spectrum, the nebular magnetic field and the spatial distribution of electrons and magnetic field within the nebula.

In this paper we briefly describe two methods for extracting TeV spectra, compare results from the Whipple Observatory Imaging Cherenkov Telescope for the 1988/89 and 1995/96 observing seasons and comment on implications for the physics of the nebula. The methods, developed at Iowa State University and the University of Leeds, are based on Monte Carlo simulations using completely independent code and use different approaches in determining the overall gain of the Cherenkov telescope. In the ISU approach, the gains of the photomultiplier tubes, mirror reflectivities, etc., are measured and combined to find the overall gain. In the Leeds approach, the observed brightness distribution of cosmic-ray images is combined with cosmic-ray simulation results to determine the overall gain of the telescope. The methods are described in detail in "Paper I," Mohanty et al., (1997), and the resulting TeV spectrum is put into context of other observations with implications for the physics of the nebula in "Paper II," Hillas et al., (1997). The latter paper also compares our Crab TeV spectrum with those of other groups.

2. METHOD 1: A TRADITIONAL APPROACH

A straightforward approach to the determination of TeV spectra was developed at Iowa State University. Three components are required. First, a method of distinguishing gamma-ray images from background cosmic-ray images. The standard method is to use "supercuts" as described in, e.g., Punch et al. (1996). The images are characterized by second order moments giving the *width*, *length*, *distance* of the image centroid from the optic axis and *alpha*, the angle by which the image major axis misses passing through the optic axis. More that 99% of the background can be rejected by requiring small values of *width*, *length* and *alpha*. However, this procedure results in a strong bias against the images of higher energy gamma rays which tend to be longer and broader and hence more cosmic-ray like. Mohanty (1995) has modified the procedure so that the image selection criteria depend on the total brightness or *size* of the image as well. (The *size* can be used as an estimate of the energy.) The telescope collection areas for simulated gamma rays for the 1995/96 season using standard and "extended" supercuts is shown in Fig. 1.

The second component needed is a way to estimate the energy of each gamma-ray image. Two desirable criteria are (a) good resolution and (b) negligible bias. The former is important to detect small structures in the spectrum and the latter is important to avoid distortions. We obtained a resolution of $\Delta E/E \sim 0.36$ with negligible bias by using a second order polynomial in *size* and *distance* as described in Paper I. The energy resolution function is, to a good approximation, Gaussian in the variable $\log(E)$. It is plotted at an arbitrary energy in Fig. 1.

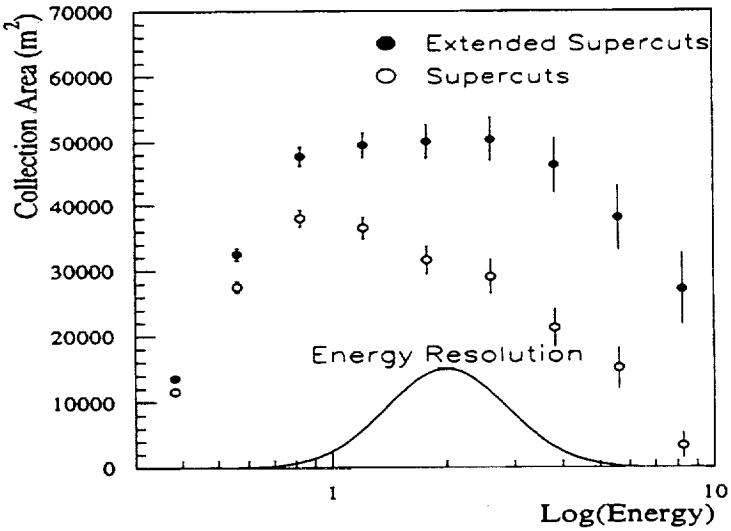

Fig. 1: The collection areas for standard and extended supercuts for the 1995/96 observing season are shown above. The resolution function is also plotted.

In data taken for spectral analysis, each on-source observation is followed by an "off-source" observation covering the same range of range of azimuth and elevation angles. The images for both types of observation are selected for gamma-like events. The estimated energies from corresponding observations are histogrammed and the difference ascribed to gamma rays from the source. This can then be fit by a power law or the fluxes extracted as described in Paper I.

3. METHOD 2: AN INTUITIVE APPROACH

A different approach with emphasis on verifiability was developed at the University of Leeds. There are two pieces to this approach, a method for selecting images likely to have been initiated by cosmic gamma rays and a method for determining the primary gamma-ray energy spectrum from the observed *size* spectra. Earlier descriptions of this approach are in (Hillas and West, 1991) and (West, 1994).

The selection criterion is a "cluster" or "spherical" method in which a single parameter is used to characterize the gamma-ray-like nature of an image and correlations between image parameters are incorporated naturally. Simulated gamma rays produce images with four parameters (*width*, *length*, *distance* and *alpha*) that populate a four-dimensional space. Each real image can be tested to see if it is likely to be a gamma-ray image by the value of the Mahalonobis distance between it and the centroid of the cluster. (This is equivalent to scaling and rotation of the axes so that the window is spherical and fluctuations uncorrelated.) The selection window is defined by the expected position and dimensions of the gamma-ray parameter cluster for several broad ranges of image *size*.

In order to extract a spectrum, a *size* histogram is then computed for on-source and off-source observations and the difference histogram is ascribed to gamma rays. A simulated *size* spectrum is then computed starting with a power-law primary energy spectrum for gamma rays. A weight is given to each simulated gamma ray and, by adjusting these weights, the spectrum can be varied so that its *size* spectrum matches that of the difference histogram. This method is simple, easy to implement and avoids the complexity of calculating collection areas and bias-free energy estimates. It is described in detail in Paper I.

4. RESULTS

The spectra obtained from the 1988/89 and 1995/96 seasons using Method 1 and 1988/89 season using Method 2 are in good agreement as shown in Fig. 2. As described in Paper I, we have tested the sensitivity of the results to uncertainties in the Monte Carlo simulations and have found that the results are relatively robust. The combined TeV fluxes from both seasons from Method 1 are well fit with the simple power law spectrum in which the differential flux ($J(E)$) is given by:

$$(3.3 \pm .2 \pm .7)\, 10^{-7} \left(\frac{E}{\mathrm{TeV}}\right)^{-2.45 \pm .08 \pm .05} \tag{1}$$

in units of $\mathrm{m^{-2} s^{-1} TeV^{-1}}$ where the first errors are statistical and the second are our estimate of systematic errors.

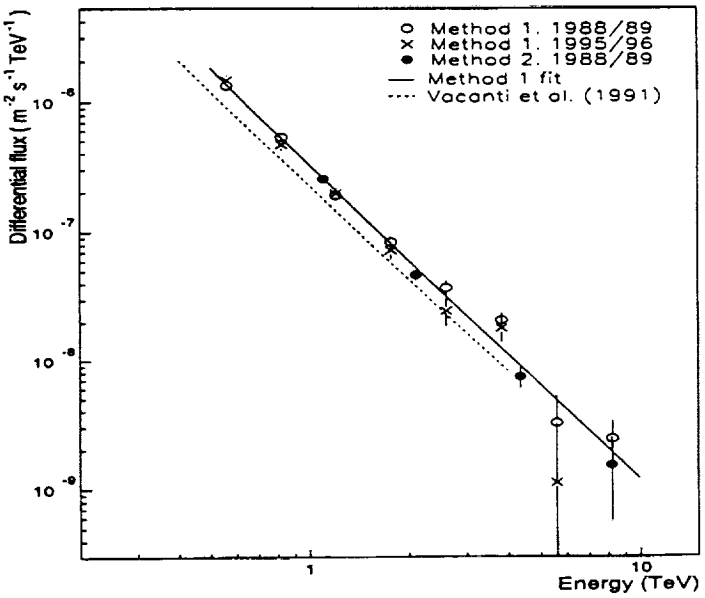

Fig. 2: The Crab spectrum in the range 0.3 to about 8 TeV extracted using Methods 1 (open circles) and 2 (solid circles) for the Whipple 1988/89 database and using Method 1 (x's) for the 1995/96 database are shown above. Also shown is a fit to the combined Method 1 results (solid line) as well as an earlier spectrum (dashed line) taken from Vacanti et al. (1991).

However, the simple extrapolation of this fit to lower energies yields fluxes far in excess of those observed by EGRET as is clear from Fig. 3 which shows a quadratic fit of $\log(J)$ vs. $\log(E)$ to our data and to an averaged point representing the EGRET flux (Nolan et al., 1993) at 2 GeV. This fit may be written:

$$J(E) = (3.25)\, 10^{-7} (E/\mathrm{TeV})^{-2.44 - 0.135 \log_{10}(E)} \mathrm{m^{-2} s^{-1} TeV^{-1}}. \tag{2}$$

5. COMMENTS ON INTERPRETATION

Most of the early inverse Compton models for TeV gamma rays assumed a constant magnetic field in the principal source region where these are produced (e.g., Gould 1965 or Rieke and Weekes 1969) whereas more recent models (De Jager and Harding, 1992 or Aharonian and Atoyan) incorporate hydrodynamic plasma/field flow making the calculations more complex and the results probably more realistic. Here, we try to stay close to the data and make the simpler assumption that the field is constant. The broad synchrotron emission band apparently extends up to 10^8 eV and is boosted to higher energies via inverse Compton scattering. The scattering giving rise to TeV gamma rays occurs in the Klein-Nishina rather than in the Thomson scattering regime. This implies that the electrons giving rise to our detected gamma rays must have energies in the range of 2-10 TeV and the corresponding scattered photons would mostly have energies of about 0.005 to 0.3 eV. This conclusion is only very weakly model dependent (see Paper II). Since electrons with energies of a few TeV generate synchrotron radiation at about 0.4 keV in a field of about 25 nT (see next paragraph), the

Einstein Observatory X-ray pictures of Harnden and Seward (1984) also show the part of the nebula emitting TeV gamma rays.

For assumed magnetic field values and the observed synchrotron flux, it is possible to deduce the spectrum of primary electrons, presumably generated in the shock at the termination of the pulsar wind (see, e.g., Coroniti and Kennel 1985). From the ambient photon density and deduced electron spectrum, the TeV flux can be calculated, and results for B fields of 10, 20 and 40 nT are shown in Fig. 3. The shaded regions reflect uncertainties arising from ill-defined UV to soft-X-ray region of the synchrotron photon spectrum. As can be seen from the figure, the effective B field must lie between 20 and 40 nT with 27 nT falling very near to our TeV data. Since even more energetic electrons only keep their energy for a short time, they should exist only near the pulsar wind shock. Hence, measurement of the TeV spectrum over a wider energy range may probe spatial variations in the nebular magnetic field (see Paper II).

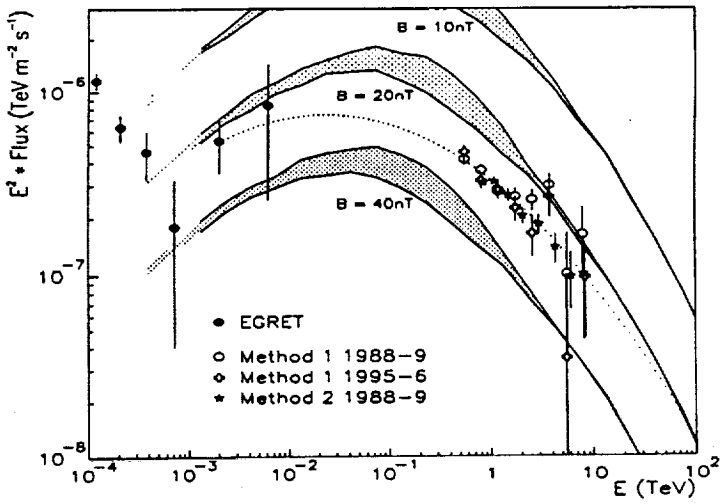

Fig. 3: Whipple and EGRET observations of the Crab gamma-ray spectrum. The dotted line is a fit to the WHipple points and a single 2 GeV flux value. Full-line curves are predicted inverse Compton fluxes for 3 differenct assumed B fields.

6. ACKNOWLEDGEMENT

This work is supported by grants from the US DOE and NASA, by PPARC in the UK and by Forbairt in Ireland.

7. REFERENCES

Aharonian, F.A. and Atoyan A.M, Astropart. Phys. **3**, 275 (1995)

Atoyan, A.M. and Aharonian, F.A., MNRAS **278** 525 (1996).

Coroniti, F.V. and Kennel, C.F., in "The Crab Nebula and related supernova remnants," ed. M.C.Kafatos and R.B.C. Henry, CUP, p 25 (1985).

De Jager, O.C., and Harding, A.K., Ap. J., **396**, 161 (1992).

Gould, R.J., Phys. Rev. Lett., **15**, 577 (1965).

Harnden, F.R.,Jr. and Seward, F.D., Ap. J. **283** 279 (1984).

Hillas, A.M. and West, M., Proc. 22nd ICRC Dublin **6** 472 (1991).

Hillas, A.M., et al, "Paper II," to be submitted to Ap. J. (1997).

Mohanty, G., PhD Thesis Iowa State University (1995).

Mohanty, G., et al., "Paper I," Astroparticle Physics, submitted (1997).

Nolan, P.L. et al., Ap. J., **409**, 697 (1993).

Punch, M., et al., Proc. 22nd ICRC Dublin **1** 464 (1991).

Rieke, G.H., and Weekes, T.C., Ap. J., **155**. 429 (1969).

Vacanti, G., et al., Ap. J. **377**, 467 (1991).

West, M., PhD Thesis University of Leeds (1994).

5

A SEARCH FOR TeV GAMMA-RAY EMISSION FROM THE CRAB PULSAR

G.H. Gillanders[1], P.J. Boyle[2], J.H. Buckley[3], A.C. Burdett[4], J. Bussons Gordo[2], D.A. Carter-Lewis[5], M. Catanese[5], M.F. Cawley[6], D.J. Fegan[2], J.P. Finley[7], J.A. Gaidos[7], A.M. Hillas[4], F. Krennrich[5], R.C. Lamb[8], M.J. Lang[1], R.W. Lessard[7], C. Masterson[2], J.E. McEnery[2], G. Mohanty[5], P. Moriarty[9], J. Quinn[2], A.J. Rodgers[4], H.J. Rose[4], F.W. Samuelson[5], G.H. Sembroski[7], R. Srinivasan[7], T.C. Weekes[3], J. Zweerink[5]

[1] *Department of Physics, University College, Galway, Ireland*
[2] *Physics Department, University College, Dublin 4, Ireland*
[3] *Whipple Observatory, Harvard-Smithsonian CfA, P.O. Box 97, Amado, AZ 85864-0097, USA*
[4] *Department of Physics & Astronomy, University of Leeds, Leeds LS2 9JT, Yorkshire, UK*
[5] *Department of Physics & Astronomy, Iowa State University, Ames, IA 50011-3160, USA*
[6] *Physics Department, St. Patrick's College, Maynooth, County Kildare, Ireland*
[7] *Department of Physics, Purdue University, West Lafayette, IN 47907-1396, USA*
[8] *Computer Sciences Corporation, Space Telescope Science Institute, Pasadena, CA, USA*
[9] *Department of Physical Sciences, Regional Technical College, Galway, Ireland*

ABSTRACT

We present results of the analysis of 35.4 hours of observation of the Crab Nebula taken with the Whipple Observatory high resolution gamma-ray imaging telescope between October 1995 and March 1996. Although we see a steady flux of gamma rays from the nebula, we find no statistically significant evidence in the data for emission pulsed at the period of the pulsar. Analysis of 10 hours of data obtained for Geminga during the 1996-97 season is in progress and will also be presented at the conference.

INTRODUCTION

The pulsar in the Crab Nebula and the surrounding nebula is one of the most closely studied astrophysical sources. It has been studied extensively in regions of the electromagnetic spectrum as diverse as radio waves and TeV gamma rays. In most regions of the spectrum, the 33 ms pulsar period is clearly visible when emission from the Crab Nebula is studied. The study of the pulsed emission, with its double peaked profile, in different energy ranges is of central importance in the development of pulsar models (Eikenberry and Fazio, 1997). The EGRET experiment has shown that there is pulsed gamma-ray emission at GeV energies (Ramanamurthy et al. 1995). The Crab Nebula is firmly established as a persistent dc source of TeV gamma radiation (Weekes et al. 1989; Vacanti et al. 1991; Akerlof et al. 1990; Baillon et al. 1991; Goret et al. 1993). However, these observations show no modulation of the signal at the period of the pulsar. In contrast to these reports of steady emission from the source, other groups have reported TeV emission modulated at the 33 ms period of the Crab pulsar. Some of these reports describe episodic activity (Gibson et al. 1982; Bhat et al. 1986; Acharya et al. 1992) while weak pulsed emission persistent over a year has also been reported (Dowthwaite et al. 1984).

OBSERVATIONS AND SELECTION OF GAMMA-LIKE EVENTS

The database analyzed comprised 77 on-source scans with a total duration of 35.4 hours. 55 of these scans were taken in an ON/OFF mode under good sky conditions and were used in both the dc analysis and the periodicity analysis. The remaining 22 scans, taken in a tracking mode where there were no off-source control observations made, were used in the periodicity analysis only.

All observations were made using the Whipple Observatory 109 element high resolution camera at the focus of the 10m optical reflector (Cawley et al. 1990). The camera recorded a digitised image of the Cherenkov light pool of each detected shower along with the arrival time of the shower which was recorded with a resolution of 0.25 ms. After the standard Whipple methodology for flat fielding, gains, normalisation and noise rejection was applied (Fegan et al. 1995), gamma-ray-like showers were selected on the basis of their shape and orientation using the gamma-ray selection procedures discussed below. The selection criteria used in the Supercuts-95 and small events analyses used are listed in Table 1 while those used in the Extended Supercuts analysis are described in detail in Mohanty et al. (1997).

Table 1. Summary of Event Selection Criteria

Selection type	**Supercuts-95**	**Small events cuts**
Pre-selection	*size* $\geq$ 400 d.c. *max1* > 100 d.c. *max2* > 80 d.c. *frac3* < 0.975	*size* < 400 d.c. *max1* > 40 d.c. *max2* > 40 d.c. *frac3* < 0.975
Distance cut	0.51° - 1.10°	0.51° - 1.10°
Shape cut	0.16° < *length* < 0.30° 0.073° < *width* < 0.15°	*length/size* < 7.41×10^{-4} °/d.c. 0.159° < *length* < 0.269° 0.080° < *width* < 0.142°
Orientation cut	*alpha* < 15°	*alpha* < 14.7°
Energy	> ~300 GeV	~200 - ~300 GeV
Reference	Catanese et al. (1996)	Moriarty et al. (1997)

The standard gamma-ray selection procedure for this data, known as Supercuts-95, was optimised on data taken on the Crab Nebula in the 1994-95 season to give the optimum ratio of gamma-ray showers selected to statistical fluctuation in the numbers of hadronic images selected (Catanese et al. 1996). This procedure incorporates a pre-selection filtering which raises the effective threshold energy of the telescope to ~300 GeV.

While the introduction of such a pre-selection filter is desirable from the point of view of optimising overall signal to noise ratio, it automatically rejects all small showers. In the context of a search for periodic emission from the Crab pulsar which is a source of gamma rays at GeV energies (Ramanamurthy et al. 1995) this is clearly undesirable. Accordingly, a separate analysis technique, developed to study events in the ~200 GeV to ~300 GeV region (Moriarty et al. 1997), was used to study events with *size* less than 400 d.c. (digital counts). The most notable difference between this small event selection process and Supercuts-95 is the introduction of a *length* over *size* cut to reject arcs of Cherenkov light rings arising from single muons which are prominent in smaller events.

Supercuts-95 is optimised to maximise the overall signal to noise ratio but in doing so it rejects many of the larger gamma-ray events. A third selection process known as Extended Supercuts (Mohanty et al. 1997) was used to help improve the sensitivity of the system to these higher energy events. This procedure is quite similar to Supercuts-95 but scales the various cuts used with the shower *size* and passes more of the gamma-ray-like events at higher energies. Since the purpose of using Extended Supercuts here was specifically to improve the sensitivity at higher energies, a non-standard pre-selection filter of *size* greater than 400 digital counts was applied. Use of Extended Supercuts is appropriate in the context of a Crab pulsar periodicity search since the published detections of pulsed emission by Cherenkov telescopes are at energies greater than 1 TeV.

ANALYSIS AND RESULTS

DC analysis

The 55 ON/OFF pairs were analyzed to establish the presence of a steady unpulsed TeV gamma-ray signal from the direction of the source over the period of observation. The excess obtained in the ON data over the OFF data after the selection criteria were applied was spread through all ON/OFF pairs. The results of this analysis are summarised in Table 2. The on-source observing time was 1521 sidereal minutes and the detector collection area was $3.5 \times 10^8 cm^2$.

Table 2. Results of dc analysis

	Raw data	Supercuts-95	Small events	Extended Supercuts
N_{ON}	1321593	3923	2374	7414
N_{OFF}	1311351	1607	1555	4825
$N_{ON} - N_{OFF}$	10242	2316	819	2589
Effect	6.3σ	31.1σ	13.1σ	23.4σ
Integral flux ($x10^{-11} cm^{-2} s^{-1}$)		7.3		8.1
Energy		> ~300 GeV	~200-300 GeV	>~300 GeV

Barycentering and periodicity analysis

All event arrival times were corrected to the Solar System barycentre using the JPL DE200 ephemeris (Standish, 1982). The absolute Crab pulsar phase of each event relative to the maximum of the radio pulse was then computed using the Jodrell Bank Crab pulsar radio ephemeris (Lyne & Pritchard, 1997). The precision of the barycentering process and the fidelity of GPS times appended to events were checked using optical observations of the Crab pulsar made on December 2 1996 using an infrared photometer on the Multiple Mirror Telescope. The output pulses from the photometer were fed to the Cherenkov telescope data acquisition system where a scaler counted the number of photometer pulses in 1 ms intervals. The Crab pulsar phase for each of the times attached to the 1 ms counts was calculated as outlined above. Figure 1 shows the phaseogram obtained when the distribution of counts are sorted in a 50 bin phaseogram. The clear detection of the pulsar signal, with the main peak in phase with the radio pulse, demonstrates the validity of the GPS clock system, data acquisition system and barycentring procedures.

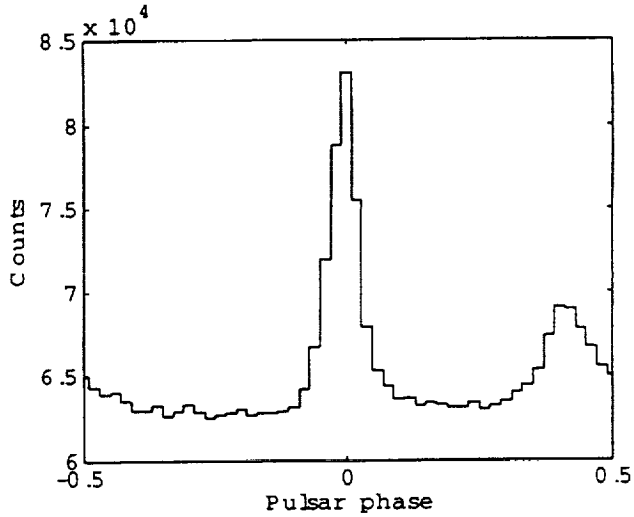

Fig. 1. Optical light curve obtained after event times are corrected to the Solar System barycentre.

The different gamma-ray selection criteria discussed above were applied separately to each of the 77 on-source scans. Separate 50 bin phaseograms were constructed for each type of cut for each data file and for various combinations of data file for each cut (nightly, dark run, full season). Each phaseogram was tested for non-uniformity using a χ^2 test. There was no statistically significant evidence of pulsar activity found in any of the light curves. The lowest chance probability obtained for any of the 50 bin phaseograms was 0.006. This was for an Extended Supercuts selection from a single run. Given the number of light curves (77 scans, 24 nights, 6 dark runs, full season) and the number of different cuts, this value is not statistically significant. Analyses using 25 bin and 10 bin phaseograms also yield no significant excesses.

To calculate upper limits for pulsed emission some assumption has to be made as to the pulsar duty cycle. If VHE emission occurs only at phases within the main peak and the EGRET main pulse width is 0.1 in phase, the duty cycle is 10%. A 10% duty cycle centred on phase 0.0 was assumed and the method of Helene (1983) was used to calculate 99.9% confidence level upper limits for persistent pulsed emission over the season of observation. The 99.9% upper limits for Supercuts-95 and Extended Supercuts were 76.5 and 95.6 events respectively. The on-source observing time was 2125 sidereal minutes. This gave upper limits of 1.7×10^{-12} $cm^{-2}s^{-1}$ for Supercuts-95 and 2.1×10^{-12} $cm^{-2}s^{-1}$ for Extended Supercuts with E > ~300 GeV in both cases. Thus the 99.9% confidence limits based on a 10% duty cycle give a pulsed fraction of less than ~2.5% of the dc flux.

DISCUSSION

The upper limits for pulsed emission presented in this paper improve on the results of an analysis of data taken during the 1993-94 observing season and reported at the 24th ICRC by Gillanders et al. (1995). Incorrect 3σ upper limits for pulsed emission inadvertently appeared in the text of that paper. The correct values presented at the conference for two separate datasets were 3.8×10^{-12} $cm^{-2}s^{-1}$ (E > ~400 GeV) and 4.1×10^{-12} $cm^{-2}s^{-1}$ (E > ~250 GeV). The 3σ upper limit on the pulsed fraction for the 1993-94 observations was ~4% of the detected dc flux. The low upper limits obtained for TeV pulsed fraction in both these analyses are consistent with results from EGRET (Ramanamurthy et al. 1995) where the pulsed fraction falls off with increasing energy at energies greater than 1 GeV.

ACKNOWLEDGEMENTS

We acknowledge the support of the US Department of Energy, NASA, FORBAIRT (Ireland) and PPARC (United Kingdom). We also acknowledge the provision of a Crab infrared signal from the Multiple Mirror Telescope by Steve Eikenberry.

REFERENCES

Acharya, B.S. et al., *A&A*, **258**, 412 (1992)
Akerlof, C.W. et al., *Proc. 21st Int. Cosmic Ray Conf. (Adelaide)* **2**, 135 (1990)
Baillon, P. et al., *Proc. 22nd Int. Cosmic Ray Conf. (Dublin)* **1**, 220 (1991)
Bhat, P.N. et al., *Nature*, **319**, 127 (1986)
Catanese, M. et al., in *Towards a Major Atmospheric Cherenkov Detector IV*, Padua, ed. M. Cresti, p. 335, (1996)
Cawley, M.F. et al., *Experimental Astron.*, **1**, 173 (1990)
Dowthwaite, J.C. et al., *ApJ*, **286**, L35 (1984)
Eikenberry, S.S. and Fazio, G.G., *ApJ*, **476**, 281 (1997)
Fegan, D.J. et al., in *Towards a Major Atmospheric Cerenkov Detector III* (Ed. T. Kifune),149 (1995)
Goret P., et al., *A&A*, **227**, 401 (1993)
Gibson, A.I., et al., *Nature*, **296**, 833 (1982)
Gillanders, G.H. et al., *Proc. 24th Int. Cosmic Ray Conf. (Rome)* **2**, 323 (1995)
Helene, O., *Nucl. Instr. Methods*, **212**, 319 (1983)
Lyne, A.G. and Pritchard, R.S., Private communication (1997)
Moriarty, P., et al., submitted to *Astroparticle Phys.*, (1997)
Mohanty, G., et al., submitted to *Astroparticle Phys.*, (1997)
Ramanamurthy, P.V. et al., *ApJ* **450**, 791 (1995)
Standish, M., *A&A* **114**, 297 (1982)
Vacanti, G., et al., *ApJ*, **377**, 467 (1991)
Weekes, T.C., et al., *ApJ*, **342**, 379 (1989)

(6)

VERY HIGH ENERGY OBSERVATIONS OF PSR B1951+32

R.Srinivasan[1], P.J.Boyle[2], J.H.Buckley[3], A.M.Burdett[4], J.Bussons Gordo[2], D.A.Carter-Lewis[5], M.F.Cawley[6], M.Catanese[5], E. Colombo[8], D.J.Fegan[2], J.P.Finley[1], J.A.Gaidos[1], A.M.Hillas[4], R.C.Lamb[6], F.Krennrich[5], R.W.Lessard[1], C.Masterson[2], J.E.McEnery[2], G.Mohanty[5], P. Moriarty[7], J.Quinn[2], A.J.Rodgers[4], H.J.Rose[4], F.W.Samuelson[5], G.H.Sembroski[1], T.C.Weekes[3], and J.Zweerink[5]

[1] *Department of Physics, Purdue University, West Lafayette, IN 47907*
[2] *Physics Department, University College, Dublin 4, Ireland*
[3] *Whipple Observatory, Harvard-Smithsonian CfA, P.O. Box 97, Amado, AZ 85645-0097*
[4] *Department of Physics and Astronomy, University of Leeds, Leeds, LS2 9JT, Yorkshire, UK*
[5] *Department of Physics and Astronomy, Iowa State University, Ames, IA 50011-3160*
[6] *Space Radiation Lab, California Institute of Technology, Pasadena, CA 91125*
[7] *Regional Technical College, Galway, Ireland*
[8] *Present address: CONAE, Paseo Colon 751, Argentina*

ABSTRACT

PSR B1951+32 is a γ-ray pulsar detected by the *Energetic Gamma Ray Experiment Telescope* (EGRET) and identified with the 39.5 ms radio pulsar in the supernova remnant CTB 80. The EGRET data shows no evidence for a spectral turnover. Here we report on the first observations of PSR B1951+32 beyond 30 GeV. The observations were carried out with the 10m γ-ray telescope at the Whipple Observatory on Mt. Hopkins, Arizona. In 8.1 hours of observation we find no evidence for steady or periodic emission from PSR B1951+32 above $\sim$ 260 GeV. FLux upper limits are derived and compared with model extrapolations from lower energies and the predictions of emission models.

INTRODUCTION

The pursuit of Very High Energy (VHE) astrophysics has resulted in the discovery of five sources, of which three are associated with young spin-powered pulsars. VHE emission has been detected from the direction of the Crab Nebula (Vacanti et.al., 1991), the Vela pulsar (Takanori 1996) and PSR B1706-44 (Kifune et al., 1995) but no evidence has been found for periodic emission at these energies in these experiments.

PSR B1951+32 has been detected as a pulsating X-ray source (Safi-Harb et al., 1995) and as a high energy γ-ray pulsar at E $\geq$ 100 MeV at the radio period (Ramanamurthy et al., 1995). It can be inferred from the five pulsars seen in the MeV to GeV γ-ray region that longer period or older ($\sim 10^5$ years) pulsars have a greater fraction of spin down energy emitted as high energy γ-rays. The best fit outer gap model of Zhang and Cheng (1997) suggests that PSR B1951+32 should emit detectable levels of TeV γ-rays (Figure 2). The multiwavelength spectrum of PSR B1951+32 (Figure 1b) indicates a maximum power per decade at energies consistent with a few GeV and still rising at 10 GeV. These factors make PSR B1951+32 a good candidate for observations with the ACT above 100 GeV.

OBSERVATIONS

The observations of PSR B1951+32 reported here were acquired with the 10m reflector located at the Whipple Observatory on Mt. Hopkins in Arizona. A total of 14 *Tracking* runs and 4 *On/Off* pairs taken between 13th May, 1996 and 17th July, 1996 constitute the database for all subsequent discussion. The total *On* source observing time is 8.1 hrs. The radio position (J2000) of PSR B1951+32 (α = $19^h\ 52^m\ 58.25^s$, δ= 32° 52′ 40.9″) was assumed for the subsequent timing analysis.

Table 1: Pulsar Parameters

PSR	P	$\dot{P}$	Distance	$\log_{10}$B	$\mathrm{Log}_{10}\dot{E}$
	msec	$10^{-15}ss^{-1}$	kpc	Gauss	ergs/s
B1951+32	39.53	5.8494	2.5	11.69	36.57

ANALYSIS AND RESULTS

Standard Analysis

The event selection criteria are collectively called *Supercuts95* and a detailed description can be found elsewhere (Catanese et al., 1995). *Supercuts95* raises the effective energy threshold of the detector with its software trigger and *size* cuts. PSR B1951+32 appears to have a steep spectrum at EGRET energies and since the pulsar spectrum is expected to cut off, it behooves us to reduce the threshold of our analysis to search for a lower energy signal. The dominant background at lower energies is due to muons whose images appear in the camera as arcs and can be discriminated by a cut on their large *length/size* values. Hence the selection criteria used *Supercuts95* on images with sizes larger than 400 p.e. and *Smallcuts* (Table 2) for images with sizes less than 400 p.e. No steady emission is

Table 2: Parameter ranges for selecting γ-ray images

Parameter	Supercuts95	Smallcuts
length	0°16 - 0°30	unchanged
width	0°073 - 0°15	unchanged
distance	0°51 - 1°1	unchanged
alpha	$< 15^{\circ}$	unchanged
max1	$>$ 100 p.e.	45 p.e. - 100 p.e.
max2	$>$ 80 p.e.	45 p.e. - 80 p.e.
size	$\geq$ 400 p.e.	0 - 400 p.e.
length/size	not used	$< 7.5 \times 10^{-4}$ °/p.e.

Table 3: Selected Events for Steady Emission analysis

Selection	Source Events $\alpha < 15°$	Background Events $\alpha < 15°$	Excess	Significance
Supercuts95	292	254	38	1.16σ
Smallcuts	618	672	-54	-1.10σ
Supercuts95 + Smallcuts	910	926	-16	-0.24σ

detected from PSR B1951+32 and 3σ flux upper limits are displayed in Table 4. The effective area for *Supercuts95*, that was used to calculate the upper limit, was taken as $A_{eff} \sim 3.5 \times 10^8$ cm^2: the same area was used for the dataset that resulted from a combination of *Supercuts95* and *Smallcuts* although here there is more systematic uncertainty. The energy threshold was obtained from simulations and extrapolating the Crab Nebula γ-ray rate for each set of cuts used assuming a spectrum $\sim E^{-2.4}$.

Periodic Analysis

The arrival times of the Čerenkov events were registered by a GPS clock with an absolute resolution of 250 μsec. An oscillator calibrated by GPS second marks was used to interpolate to a resolution of

0.1 μsec. After an oscillator drift correction was applied, all arrival times were transformed to the solar system barycenter and folded to produce the phases, ϕ_j, of the events modulo the pulse period. The ephemeris frequency parameters used were ν= 25.2963719901267 s^{-1} and $\dot{\nu}$=-3.73940$\times 10^{-12} s^{-2}$, at the epoch t_0=JD 2450177.5. This frequency was extrapolated 72 days to obtain a timing solution relevant to the epoch of observation. The datasets, however, were taken within the validity interval of the above ephemeris.

To check the Whipple Observatory timing systems an *optical* observation of the Crab pulsar was undertaken on December 2nd (UT) 1996 using the 10m reflector. The phase analysis of the event arrival times yielded a clear detection of optical Crab pulsar signal which is in phase with the radio pulse and demonstrates the validity of the timing, data acquisition and software in the presence of a pulsed signal. No evidence of pulsed emission from PSR B1951+32 at the radio period exists. To calculate a pulsed flux upper limit we assumed the same pulse profile as seen at EGRET energies, i.e. with the phase range for the main pulse and secondary pulse as 0.12 - 0.22 and 0.48 - 0.74 respectively (Ramanamurthy et al., 1995).

Table 4: Integral Flux Upper limits

	Steady Emission $cm^{-2}s^{-1}$)	Periodic Emission ($cm^{-2}s^{-1}$)	Threshold (GeV)
Supercuts95	0.97×10^{-11}	3.7×10^{-12}	≥ 370
Supercuts95 + Smallcuts	1.95×10^{-11}	6.7×10^{-12}	≥ 260

DISCUSSION

PSR B1951+32 is surrounded by a compact nebula which gives a plerionic nature to the supernova remnant, CTB80. X-ray plerions are good candidates for VHE emission since the electrons responsible for nebular synchrotron X-rays should also create VHE γ-rays via the inverse Compton (IC) process. It is expected that for plerions, such as that associated with PSR B1951+32 where the density of nebular synchrotron photons is too low for SSC to take place, detectable VHE emission should be produced by the IC scattering of the 2.7K cosmic microwave background by the same electrons radiating synchrotron X-ray photons. Interpreting the unpulsed X-ray emission form CTB80 as the synchrotron emission from a plerion, the estimated IC flux > 1 TeV is 6.6×10^{-13} TeV/cm^2/s/TeV (De Jager et. al., 1995). This represents the lower limit on the IC flux since there can be other sources of soft photons in addition to the microwave background.

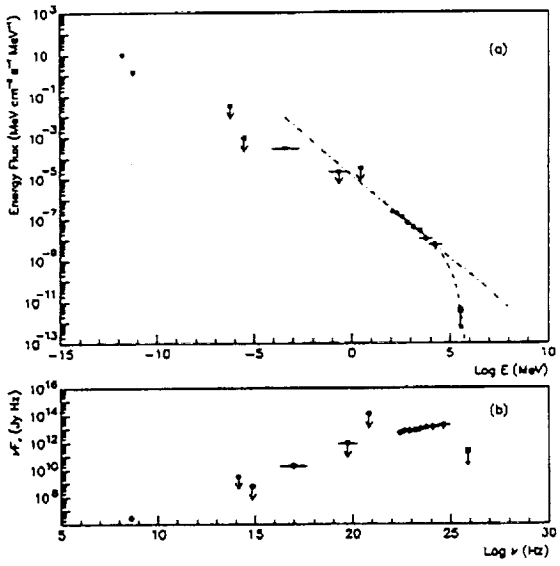

Fig. 1: The pulsed energy spectrum of PSR B1951+32. The Whipple limit is indicated as a filled square at 370 GeV. (See text for details).

To model the pulsed high energy spectrum, a function of the form

$$dN_\gamma/dE = KE^{-\Gamma}e^{(-E/E_0)} \quad (1)$$

was used where E is the photon energy, Γ is the photon spectral index and E_0 is the cut off energy. The pulsed upper limit reported here is two orders of magnitude lower than the extrapolated EGRET power law. Equation (2) was used to extrapolate the EGRET spectrum to VHE energies constrained

by the TeV upper limit reported here and indicates a cut off energy of $E_0 \leq 75$ GeV for pulsed emission (Figure 1a).

The strength of the cut off provides a good discriminant between the various pulsar emission models. The status of current observations and the derived cutoff discussed above indicates that the cutoff is beyond 10 GeV. In polar cap models this would indicate a sharp cutoff since the pair production optical depth increases exponentially with photon energy (Harding 1997). However, it is not possible to constrain the shape of the cut off with the non detection of pulsed TeV flux reported here. The most relavant comparison of the Whipple upper limit with emission models is the outer gap model of Zhang and Cheng (see Figure 2). This model includes the effect of geometry in the treatment of pulsed emission via a parameter $\alpha = r/r_L$, the radial distance to the synchrotron emitting region near the outer gap, r, as a function of the light cylinder radius r_L. Our pulsed upper limits are consistent with the outer gap model if $\alpha > 0.6$ implying an emission region far out in the magnetosphere.

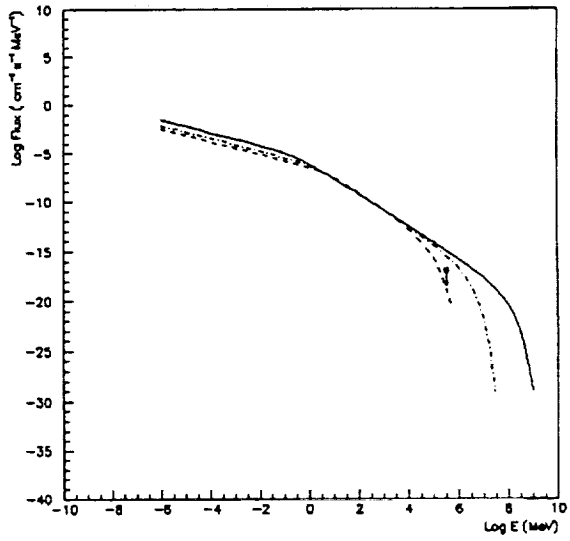

Fig. 2: Predicted pulsed γ-ray flux of PSR B1951+32 from the Zhang and Cheng outer-gap model. The solid, dot-dash and dashed curves correspond to α=0.5, 0.6, 0.7 respectively. (See text for details).

The result reported here is the first observation of PSR B1951+32 beyond 30 GeV. PSR B1951+32 exhibits very similar spectral behavior and morphological features, such as an associated synchrotron nebula, to PSR B1706-44 (Finley et al., 1997). If these factors are any indication of similar emission mechanisms in pulsars then the lack of unpulsed emission from PSR B1951+32 is puzzling considering that PSR B1706-44 was detected as a VHE source of unpulsed emission > 1 TeV (Kifune et al., 1995). Lack of pulsed emission indicates that the processes producing pulsed high energy photons over two decades of energy in the EGRET energy range somehow become ineffective over a decade of energy to result in a lack of VHE γ-rays. The low magnetic field of PSR B1951+32 relative to the average pulsar field implies that attenuation of γ-rays by magnetic absorption is not a likely explanation for the non-detection.

ACKNOWLEDGEMENTS

We acknowledge the technical assistance of K. Harris. This research is supported by grants from the U.S. Department of Energy, NASA, PPARC in the UK and by Forbairt in Ireland. The authors wish to thank A. Lyne for providing the radio ephemeris of PSR B1951+32 and D. J. Thompson for providing the multiwavelength spectrum for PSR B1951+32.

REFERENCES

Catanese, M. et al. 1995, Towards a Major Atmospheric Cherenkov Detector -IV, Padova, 335
De Jager, O.C. et al. 1995, in Proc. 24th ICRC (Rome), 2, 528
Finley, J.P. et al. 1997, ApJ, in preparation
Kifune, T. et al. 1995, ApJ, 438, L91
Ramanamurthy, P.V., et al. 1995, ApJ, 447, L109
Safi-Harb, S., Oğelman, H., & Finley, J.P. 1995, ApJ, 439, 722
Harding, A. 1997, private communication
Takanori, Y. 1996, Ph.D. thesis, University of Tokyo
Vacanti, G., 1991, ApJ, 377, 467
Zhang, L. and Cheng, K.S. 1997, ApJ, submitted

OG 4.2.6

(7)

CONSTRAINTS ON COSMIC-RAY ORIGIN THEORIES FROM TEV GAMMA-RAY OBSERVATIONS

R.W.Lessard[1], P.J.Boyle[2], S.M. Bradbury[4], J.H.Buckley[3], A.C.Burdett[4],J.Bussons Gordo[2], D.A.Carter-Lewis[5], M.Catanese[5], M.F.Cawley[6], D.J.Fegan[2], J.P.Finley[1], J.A.Gaidos[1], A.M.Hillas[4], F.Krennrich[5], R.C.Lamb[7], C.Masterson[2], J.E.McEnery[2], G.Mohanty[5], J.Quinn[2], A.J.Rodgers[4], H.J.Rose[4],F.W.Samuelson[5], G.H.Sembroski[1], R.Srinivasan[1], T.C.Weekes[3] and J.Zweerink[5]

[1]*Department of Physics, Purdue University, West Lafayette, IN 47907-1396, U.S.A.*
[2]*Department of Experimental Physics, University College Dublin, Belfield, Dublin 4, Ireland*
[3]*Whipple Observatory, Harvard-Smithsonian CfA, P.O. Box 97, Amado, AZ 85645-0097, U.S.A.,*
[4]*Department of Physics, University of Leeds, Leeds, LS2 9JT, Yorkshire, U.K.,*
[5]*Department of Physics and Astronomy, Iowa State University, Ames, IA 50011-3160 USA,*
[6]*Department of Physics, Saint Patrick's College, Maynooth, Co. Kildare, Ireland,*
[7]*Space Radiation Laboratory, California Institute of Technology, Pasadena, CA 91125 USA*

ABSTRACT

If supernova remnants (SNRs) are the sites of cosmic-ray acceleration, the associated nuclear interactions should result in observable fluxes of TeV gamma-rays from the nearest SNRs. Measurements of the gamma-ray flux from six nearby, radio-bright, SNRs have been made with the Whipple Observatory gamma-ray telescope. No significant emission has been detected and upper limits on the >300 GeV flux are reported. Three of these SNRs (IC443, gamma-Cygni and W44) are spatially coincident with low latitude unidentified sources detected with EGRET. These upper limits weaken the case for the simplest models of shock acceleration and energy dependent propagation.

INTRODUCTION

It is generally believed that cosmic rays with energies less than $\sim$ 100 TeV originate in the galaxy and are accelerated in shock waves in shell-type SNRs. This hypothesis is supported by several strong arguments. First, supernova blast shocks are one of the few galactic sites capable of sustaining the galactic cosmic ray population against loss by escape, nuclear interactions and ionization energy loss assuming a SN rate of about 1 per 30 years and a 10% efficiency for converting the mechanical energy into relativistic particles. Second, models of diffuse shock acceleration provide a plausible mechanism for efficiently converting this explosion energy into accelerated particles with energies $\sim 10^{14} - 10^{15}$ eV and naturally give a power-law spectrum similar to that inferred from the cosmic ray data after correcting for energy dependent propagation effects. Finally, observations of non-thermal X-ray emission in SN1006 (Koyama, et al., 1995) and IC443 (Keohane, et al., 1997) suggest the presence of electrons accelerated to $\sim$ 100 TeV and $\sim$ 10 TeV respectively.

If SNRs are sites for cosmic ray production, there will be interactions between the accelerated particles and the local swept-up interstellar matter. Drury, Aharonian and Volk (1994) (DAV) and Naito and Takahara (1994) have calculated the expected gamma-ray flux from secondary pion production using the model of diffusive shock acceleration. The expected intensity (DAV) is

$$F(>E) = 9\times 10^{-11}\left(\frac{E}{1\mathrm{TeV}}\right)^{-1.1}\left(\frac{\theta E_{SN}}{10^{51}\mathrm{erg}}\right)\left(\frac{d}{1\mathrm{kpc}}\right)^{-2}\left(\frac{n}{1\mathrm{cm}^{-3}}\right)\mathrm{cm}^{-2}\mathrm{s}^{-1} \qquad (1)$$

where E is the photon energy, θ is the efficiency for converting the supernova explosion energy, E_{SN}, into accelerated particles, d is the distance to the SNR and n is the density of the local ISM.

OBSERVATIONS

We report on the results of observations of six nearby SNR (W44, W51, gamma-Cygni, W63, Tycho and IC443) by the Whipple Observatory's high energy gamma-ray telescope situated on Mount Hopkins in southern Arizona. The telescope (Cawley et al., 1990) employs a 10 m diameter optical reflector to focus Čerenkov light from air showers onto an array of 109 photmultipliers covering a 3 degree field of view. By making use of distinctive differences in the lateral distribution of gamma-ray induced showers and hadronic induced showers, images can be selected as gamma-ray like based on their angular spread. The determination of the incident direction of the selected gamma-ray like events is accomplished by making use of the orientation, elongation and asymmetry of the image. Monte Carlo studies have shown that gamma-ray images are a) aligned towards their source position on the sky b) elongated in proportion to their impact parameter on the ground and c) have a cometary shape with their light distribution skewed towards their point of origin in the image plane. Results on the Crab Nebula indicate that the angular resolution function for the telescope using this technique is a Gaussian with a standard deviation of 0.13 degrees. (Lessard et al., 1997). A combination of Monte Carlo simulations and results on the Crab Nebula indicate that the energy threshold of the technique is 300 GeV and the effective collection area for a point source located at the center of the field of view is $2.1 \times 10^8 \mathrm{cm}^2$ and is reduced for offset sources (Lessard et al., 1997).

The analysis of data from extended sources involves binning the event arrival directions. We define the source region for the SNR by a circular aperture which matches the maximum extent of the radio shell (Green, 1995) plus twice the width of the angular resolution function to account for the smearing of the edge of the remnant. The number of gamma-ray candidate events is obtained by subtracting the number of events in the OFF-source observations from the number of events in the ON-source observations.

RESULTS

The observations were made over three observing seasons, from 1993 to 1996. Two dimensional images of the excess events for the Crab Nebula (which was deliberately offset from the center of the camera, to demonstrate the veracity of the technique) and the SNR W51 are shown in Figure 1. In each frame, the statistical significance is displayed in grayscale. The black contours are from the 4850 MHz radio survey by Condon et al., 1994, showing the extent of the radio shell. The circle shows the circular aperture used to derive the excess counts from the entire remnant (see Table 1).

Of the six remnants observed, W 51 showed the greatest excess at an offset location which is spatially consistent with hard x-ray emission and peak radio intensity. More data are required to determine if this excess is signicant. No significant excess has been recorded for the other remnants and 99.9% confidence upper limits on the flux have been calculated (see Table 1). The upper limit assumes uniform emission from the remnant in the absence of *a priori* knowledge of a more defined emission region.

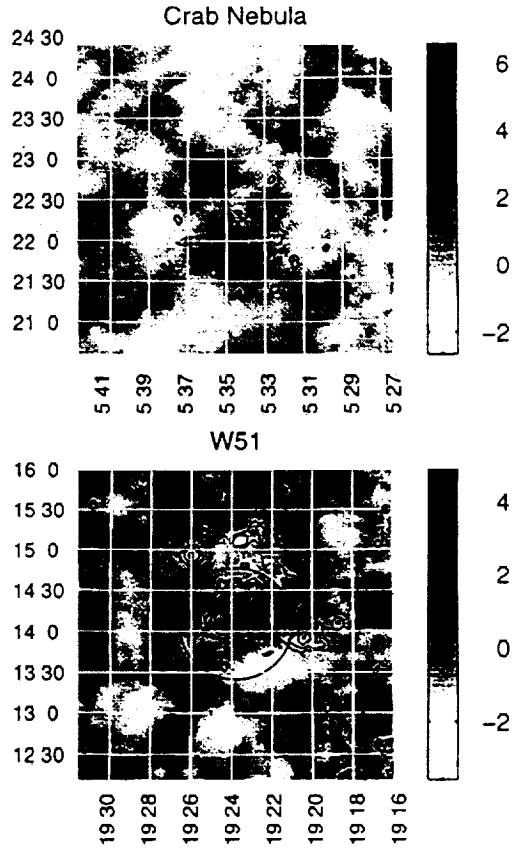

Fig. 1: Observations of the Crab Nebula and W51. We have applied a boxcar smoothing method which maximizes the point source sensitivity. The statistical significance of the excess selected events is shown in grayscale. The overlayed contours are proportional to the 4850 MHz radio intensity.

DISCUSSION

In Figure 2 the Whipple upper limits and EGRET data (Es-

posito et al., 1996, for gamma-Cygni and IC443, Fierro, 1995, for W44, and Thompson et al., 1995 for the remaining) are compared with an $E^{-2.1}$ extrapolation of the EGRET data using the contribution to the gamma-ray spectrum from secondary pion decay as derived by Buckley et al. (1997) using the model of DAV. The upper dotted curve assumes a source spectrum of $E^{-2.1}$ and a reasonable maximum value of the product $E_{SN}\theta/d^2$ used in the model. The lower dotted curve assumes a source spectrum of $E^{-2.3}$ and a reasonable minimum value of the product $E_{SN}\theta/d^2$.

We interpret our results in the context of two hypotheses, (1) that the EGRET data gives evidence for acceleration of cosmic ray nuclei in SNR and that the observed gamma-ray emission comes not from primary electrons but from nuclear interactions of cosmic rays with ambient material or (2) that the EGRET flux is produced by some other mechanism.

Under the assumption that the contribution from electron bremsstrahlung and inverse Compton (IC) scattering are neglible, it is reasonable to compare the high energy gamma-ray upper limits to an extrapolation of the integral EGRET fluxes using the model by DAV. In the case of gamma-Cygni, IC443 and W44 the Whipple upper limits lie a factor of ~ 25, 10 and 10 respectively below the extrapolation and require either a spectral break or a source spectrum steeper than $E^{-2.5}$ for gamma-Cygni and $E^{-2.4}$ for IC443.

Another plausible explanation for the results is that the EGRET flux is produced by high energy electrons accelerated in the vicinity of pulsars. If this is the case, then the Whipple upper limits must be compared with the *a priori* model predictions. There is enough uncertainty in the parameters of the SNR that the upper limits are not in strong conflict with these predictions, but it is still strange that in these objects which show strong evidence for interactions with molecular clouds (corresponding to the upper dotted curve) in no case is there an observable TeV gamma-ray flux. Evidence of an X-ray point source embedded in gamma-Cygni (Brazier et al., 1996) and IC443 (Keohane et al., 1997) and the observation of a pulsar, B1853+01, in W44 (Wolszczan, et al. 1991), all provide support to a pulsar origin for the EGRET flux.

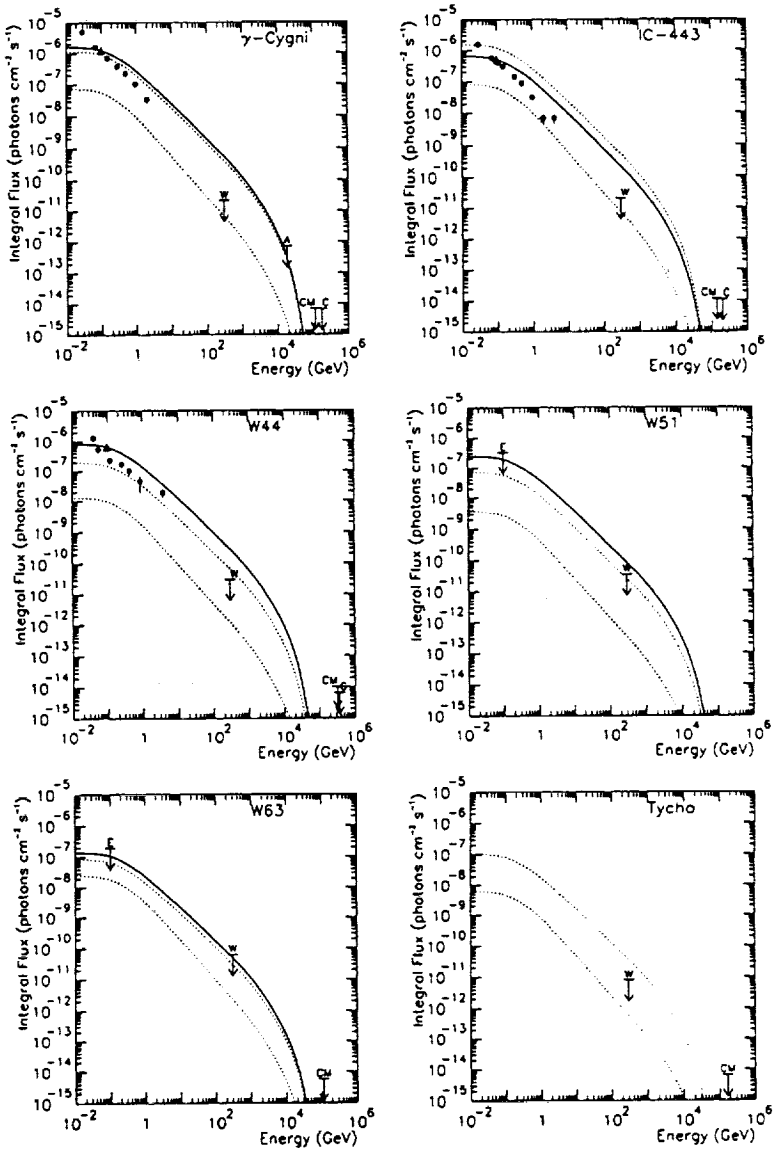

Fig. 2: Whipple upper limits shown along with EGRET integral fluxes, and integral spectra. These are compared to extrapolations from the EGRET integral data points (solid curves), as well as a conservative estimate of the allowable range of fluxes from the model of DAV (dotted curves). Also shown are CASA-MIA upper limits from Borione et al., 1995, CYGNUS upper limits from Allen et al., 1995, and the AIROBIC upper limit from Prosch et al., 1996.

Table 1: Results of Observations.

Source Name	Pointing α, δ (1950)	Aperture Radius (deg)	ON Source Counts	OFF Source Counts	Total Time (min)	Upper Limit $\times 10^{-11}$ ($cm^{-2}s^{-1}$)
W44	18:53:29, 01:14:57	0.55	450	426	360.1	3.0
W51	19:21:30, 14:00:00	0.68	619	559	468.0	3.6
γ-Cygni	20:18:59, 40:15:17	0.76	1040	1104	560.0	2.2
W63	20:17:15, 45:24:36	1.05	452	501	140.0	6.4
Tycho	00:22:28, 63:52:11	0.29	315	302	867.2	0.8
IC443	06:14:00, 22:30:00	0.64	1565	1522	1076.7	2.1

ACKNOWLEDGEMENTS

We acknowledge the technical assistance of Kevin Harris and Teresa Lappin. This research has been supported in part in the U.S. by the Department of Energy and NASA, Forbairt in Ireland and PPARC in the UK.

REFERENCES

Allen, G.E., et al., 1995, ApJ, 448, L25.

Borione, A., et al., 1995, in Proc. 24th Int. Cosmic Ray Conf. (Rome), 2,439.

Brazier, K.T., et al., 1996, MNRAS, 281, 1033.

Buckley, J.H., et al., 1997, in preparation.

Cawley, M.F., et al., 1990, Exper. Astr., 1, 173.

Condon, J.J., et al., 1994, AJ, 107, 1829.

Drury, L.O'C., et al., 1994, AA, 287, 959.

Esposito, J.A., et al., 1996, ApJ, 461, 820.

Fierro, J.M., 1995, PhD Thesis.

Green, D.A., 1995, A Catalog of Galactic Supernova Remnants (1995 July version), Cambridge, UK, Mullard Radio Astronomy Observatory, Available on the World Wide Web at http://www.phy.cam.uk.ac/www/research/ra.SNRs/snrs.intro.html.

Keohane, J.W., et al., 1997, accepted by ApJ.

Koyama, K., et al., 1995, Nature, 378, 255.

Lessard, R.W., 1997, Ph.D thesis, National University of Ireland.

Naito, T. and Takahara, F., 1994, J.Phys. G:Nucl.Part.Phys.,20,477.

Prosch, C., et al., 1996, AA, 314, 275.

Thompson, D.J., et al., 1995, ApJS, 101, 259.

Wolszczan, A., et al., 1991, ApJ, 372, L99.

8

A SEARCH FOR TEV EMISSION FROM UNIDENTIFIED SOURCES IN THE GALACTIC PLANE

J.H. Buckley[1], P.J. Boyle[2], S.M. Bradbury[3], A.M. Burdett[3], J. Bussóns Gordo[2], D.A. Carter-Lewis[4], M. Catanese[4], M.F. Cawley[5], D.J. Fegan[2], J.P. Finley[6], J.A. Gaidos[6], A.M. Hillas[3], F. Krennrich[4], R.C. Lamb[7], R.W. Lessard[6], C. Masterson[2], J.E. McEnery[2], G. Mohanty[4], J. Quinn[1,2], A.J. Rodgers[3], H.J. Rose[3], A.C. Rovero[8], F.W. Samuelson[4], G.H. Sembroski[6], R. Srinivasan[6], T.C. Weekes[1], and J. Zweerink[4]

[1]*F. L. Whipple Observatory, Harvard-Smithsonian CfA, P.O. Box 97, Amado, AZ 85645, USA*
[2]*Dept. of Exp. Physics, University College Dublin, Belfield, Dublin 4, Ireland*
[3]*Department of Physics, University of Leeds, Leeds, LS2 9JT, Yorkshire, England, UK*
[4]*Dept. of Physics and Astronomy, Iowa State University, Ames, IA 50011, USA*
[5]*Physics Department, St. Patrick's College, Maynooth, County Kildare, Ireland*
[6]*Department of Physics, Purdue University, West Lafayette, IN 47907, USA*
[7]*Space Radiation Laboratory, California Institute of Technology, Pasadena, CA 91125, USA*
[8]*Instituto de Astronomía y Físca del Espacio, CC 67, Suc. 28, (1428) Buenos Aires, Argentina*

ABSTRACT

The ~70 unidentified sources of the EGRET sky survey may be one of its most important legacies. The identification of these sources at other wavelengths is critical to understanding their nature. Many have flat spectra out to 10 GeV which, if extrapolated to TeV energies, would be easily detectable relative to the steeply falling diffuse background. The Whipple Observatory γ-ray telescope has been used to observe a number of these which were selected based on their position, intensity and spectrum and in some cases based on a possible association with a supernova remnant or pulsar. No significant emission has been detected from these sources, and upper limits are given.

INTRODUCTION

Despite extensive searches for counterparts to the ~30 low-lattitude unidentified EGRET sources, the nature of these objects is still largely unknown. Kaaret & Cottam (1996) have suggested that the low latitude unidentified sources show a correlation with OB associations, the sites of massive star formation. Since nearly half of all supernovae occur as the core collapse of young massive stars which explode into star formation regions (e.g., Huang & Thaddeus 1986) a correlation with the positions of pulsars and with supernova remnants also follows. Kaaret & Cottam argue that pulsars emit γ-rays over a significantly longer lifetime than SNR, so that the number of γ-ray pulsars is expected to be significantly larger than the number of γ-ray SNR. However, Esposito et al. (1996), Sturner & Dermer (1994) and Sturner, Dermer and Mattox (1996) have presented evidence for associations of a number of these objects with SNRs (γ-Cygni, IC443, W44, Monoceros) for which there is no pulsar within the 95% confidence error contour (Sturner, Dermer & Mattox 1996). Attempts to detect radio pulsars in the error boxes of EGRET unidentified sources have been unsuccessful (e.g., Nice & Sayer 1997) and provide some constraints on models in which all of the Galactic unidentified sources are pulsars. Since EGRET generally lacks the spatial resolution to distinguish the point-like emission from pulsars and AGNs from the extended emission expected to arise in the vicinity of supernova shells, variability has been used to distinguish compact sources. Dramatic transient sources such as the enigmatic 2CG 135+1 and newly discovered GRO J1838+04 are difficult to interpret as either arising from AGNs or from pulsars, and are possibly representatives of a new class of Galactic γ-ray source distinct from isolated pulsars (e.g., Tavani et al. 1997).

Detection of these objects at high energies using ground based γ-ray detectors would aid in the identification of these objects in two important ways. First, the contribution from the diffuse γ-ray background falls as a steeper power of energy ($\sim E^{-2.7}$) than the source spectrum ($\sim E^{-2}$) for many of these objects, implying a smaller effect from uncertainties in the diffuse background model in determining the position, flux and spectra of these sources. Second, the 0.13° angular resolution of the Whipple 10m γ-ray telescope (Lessard and Buckley 1997) provides the ability to resolve extended sources such as SNRs and offers the potential to narrow the error box for bright sources.

OBSERVATIONS AND ANALYSIS

The high-energy γ-ray telescope (Cawley et al. 1990) at the Whipple Observatory employs a 10 m diameter optical reflector to image Čerenkov light from air showers onto an array of 109 fast photomultipliers covering a 3° field of view (FOV). By making use of the distinctive differences in the angular distribution of light and orientation of the shower images a γ-ray signal can be extracted from the large background of hadronic showers.

Data are generally taken in a differential mode where each 28 min ON-source run is followed by a 28 min OFF-source control run which is offset in right ascension to ensure that the same range of azimuth and zenith angles are sampled. While this cancels the zenith angle dependence of the cosmic-ray rate as well as other systematic effects in the camera, differences in sky brightness between the ON-source and OFF-source regions can lead to biases. For some galactic plane sources, such differences are substantial due to either diffuse emission from the galactic plane or bright stars.

Systematic effects arising from such brightness differences can be largely canceled by the procedure of software padding (Cawley et al. 1983). This procedure consists of adding noise to all pixels of each event so that matching PMTs in ON-source and OFF-source runs have identical noise pulse height spectra. Only PMT signals which exceed some multiple of this noise level are included in the subsequent analysis of the shower images (Punch et al. 1993).

The technique used to generate the two-dimensional plots and upper limits is a simple extension of the standard Whipple data analysis (Reynolds et al. 1993) and is described in more detail in Lessard and Buckley (1997). After initial processing of the shower images including pedestal subtraction, gain correction and image cleaning (e.g., Punch et al. 1993) individual Čerenkov shower images are subjected to a moment analysis to determine a set of parameters that characterize the roughly elliptical images. Each point on a two dimensional grid covering the 3° FOV is considered as the potential source position. For each event, the RMS width and length, centroid position, orientation, ellipticity and the skew of the shower image are calculated about this point of origin and tested for consistency with the parameter values expected for a γ-ray event coming from the corresponding direction in the sky. For each grid point the number of candidate events ON-source and OFF-source are calculated, and the significance of the excess, S_λ, is derived using the likelihood ratio method of Li & Ma (1983). In the two-dimensional plots presented in Figures 1, the gray-scale indicates the number of excess counts (candidate γ-rays) consistent with each grid point and the contours shown correspond to the statistic S_λ in steps of 1. Note that due to the large number of trials associated with the 30×30 grid, approximately one S_λ=3 excess is expected for each two-dimensional plot.

While it is desirable to have one control (OFF-source) run for each run ON-source, for some of the data presented here the number of exposures taken OFF-source is less than the number of ON-source runs. In this case, the background level is determined by normalizing the OFF-source data to the ON-source data in a 0.25° band around the perimeter of the field of view. The resulting normalization factor α enters into the calculation of the significance and the upper limit following the procedure of Li and Ma (1983). For the sources J0542+26, J0635+0521, and J1825-1307, little or no OFF-source data was taken and a background template was formed using contemporaneous control data taken for other sources. This results in an additional systematic error for these sources.

In calculating upper limits, we are testing the hypothesis that the emission is coming from a

Table 1: Results of Observations.

Name	Position l	Position b	Nearby Objects	EGRET (> 100 MeV) Flux (10^{-8} $cm^{-2}s^{-1}$)	EGRET (> 100 MeV) Spectral Index	Prediction (> 400GeV) ($10^{-11}cm^{-2}s^{-1}$)	Whipple (> 400 GeV) Exposure (min)	Whipple (> 400 GeV) Flux Limit ($10^{-11}cm^{-2}s^{-1}$)
J0241+6119	135.74	1.22	2CG135+01	87.0±6.7	-2.2±0.1	4.14	972	1.02
J0542+26	181.92	-2.00	S147	17.6±3.5	-3.3±0.5			
J0545+3943	170.79	5.65		12.7±2.8	-3.0±0.3		108	6.72
J0618+2234	189.13	3.19	IC443	45.7±3.8	-1.8±0.1	70.8	1188	0.911
J0635+0521	206.30	-1.20	Monoceros	24.5±4.1	-2.4±0.3	3.09	108	5.59
J0749+17			PSR 0751+1807				486	0.813
J1746-2852	0.17	-0.15	Sgr A*	110.9±9.4			270	0.45†
J1825-1307	18.38	-0.43	PSR B1823-13	84.0±7.9	-2.3±0.1	1.48	702	1.55
J1857+0118	34.80	-0.76	W44	52.1±8.7	-1.9±0.2	29.9	351	2.79
J2020+4026	78.12	2.23	PSR B1853+01 γ-Cygni SNR	122.9±6.8	-2.0±0.1	33.8	513	0.990

† Integral flux above 2.0 TeV.

point source within the EGRET error box. Upper limits calculated for the extended regions corresponding to the IC443, W44 and γ-Cygni SNRs (for 2EG J0618+2234, 2EG J1857+0118, and 2EG J2020+4026 respectively) are reported elsewhere (Buckley et al. 1997). 99.9% confidence-level upper limits are calculated for each grid point lying within the EGRET 95% confidence interval using the method of Helene (1983) and accounting for the declining γ-ray detection efficiency away from the camera center (Lessard & Buckley 1997). The maximum upper limits for each error box are shown in Table 1.

RESULTS AND CONCLUSIONS

Table 1 shows preliminary Whipple upper limits for a number of unidentified sources together with the extrapolated EGRET flux derived from the EGRET spectrum. Fluxes and spectral indices are from Fierro et al. (1996). In addition to sources from the first (Fichtel et al. 1994) or second EGRET catalogs (Thompson et al. 1995), we also include the source J0749+17 from the initial list of unidentified sources by Hartman et al. (1992). This object was not included in the first EGRET catalog because of its low significance ($< 4\sigma$), but is of interest since it prompted the radio pulsar search by Lundgren, Zepka and Cordes (1995) that led to the discovery of the binary millisecond pulsar PSR 0751+1807. Also on our list is the source J0542+26 which was on the list of high confidence unidentified sources in the first but not the second EGRET catalog. This source has a 158 arcmin error radius which could not be shown in Figure 1. This source is of interest since it is coincident with the position of the old, nearby (0.8-1.4kpc, Kundu et al. 1980) SNR S 147 as pointed out by Sturner and Dermer (1994).

These data were taken over the period December 1994 to May 1997. Two-dimensional plots for these sources are shown in Figure 1 excluding results for J0618+2234, J1857+0118 and J2020+4026 which are shown elsewhere (Buckley et al. 1997). Upper limits are at energies above 400 GeV unless otherwise indicated. 2EG 1746-2852 transits at an elevation of <30° resulting in an increase of the effective area and energy threshold by a factor of approximately 5.0 compared with observations at the zenith (Krennrich et al. 1997). While 2EG J1746-2852 shows a small (2.5σ) excess at the position of Sgr A* and within the EGRET error box, this excess is not considered significant given the additional systematic errors present for galactic plane sources. 2EG J0241+6119 shows a similar excess near the position of 2CG135+01 and within the EGRET error box. The excess in J0542+26 lies outside and to the south of the radio shell of S147 and approximately 0.5° away from the X-ray binary 4U0535+262, too far to make an association. The other sources show no significant emission within the EGRET error boxes. Further deep observations with the GRANITE-III high resolution camera should provide better sensitivity given the extended FOV and finer pixelization, and correlations with data taken at other wavelengths should improve chances for detecting variable unidentified sources.

ACKNOWLEDGEMENTS

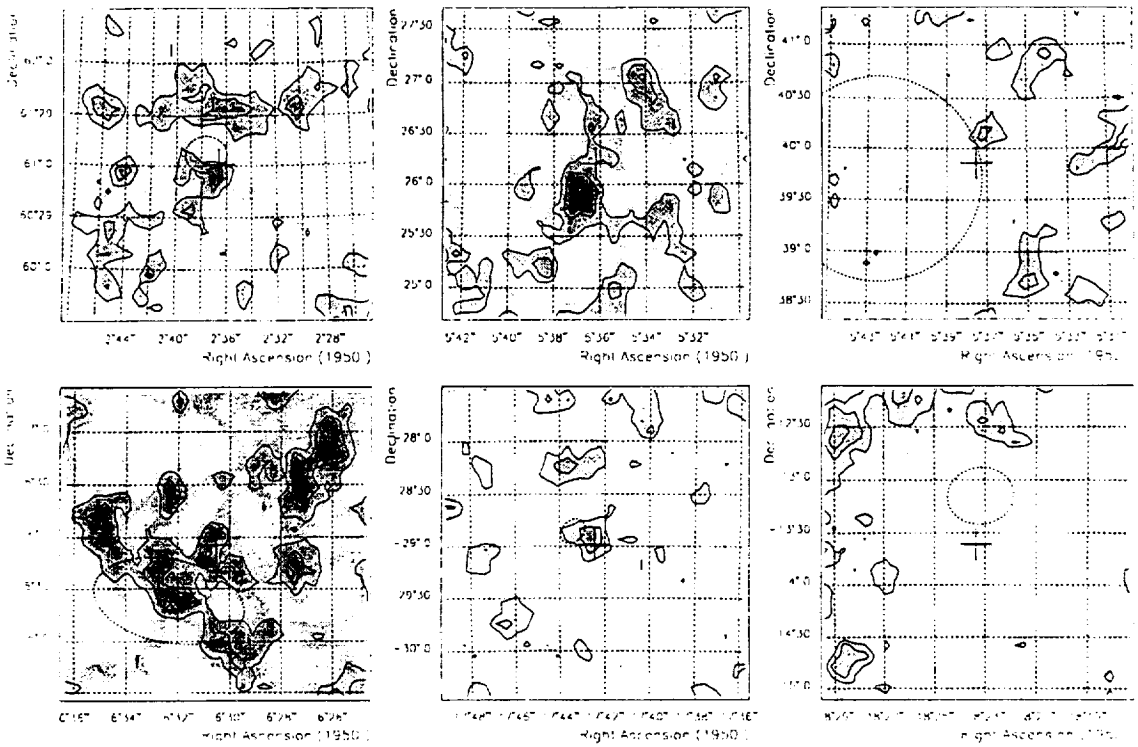

Fig. 1: Plots of two-dimensional distributions of candidate gamma-ray events and contours of S_λ for (a) J0241+6119 (cross at the position of 2CG135+01), (b) J0542+26, (c) J0545+3943, (d) J0635+0521, (e) J1746-2852 (cross at Sgr A) and (f) J1825+2234 (cross at the position of PSR B1823-13). Dotted contours show the elliptical fit to the EGRET 95% confidence intervals. .*

This research is supported by grants from the U. S. Department of Energy and NASA, by PPARC in the UK and by Forbairt in Ireland.

REFERENCES

Buckley, J.H., et al., in preparation (1997).
Cawley, M.F, et al., *Exper. Astr.*, 1, 173 (1990).
Esposito, J.A., et al., *ApJ*, 461, 820 (1996).
Fichtel, C.E., et al., *ApJS*, 94, 551 (1994).
Fierro, J., Ph.D. Dissertation, Stanford University (1996).
Hartman, R.C., et al., *BAAS*, 24, 1155 (1992).
Helene, O., *Nucl. Instr. Meth.*, 212, 319 (1983).
Huang, Y.-L., & Thaddeus, P., *ApJ*, 309, 804 (1986).
Kaaret, P., & Cottam, J., *ApJ*, 462, L35 (1996).
Krennrich, F., et al., *ApJ*, in press (1997).
Kundu, Angerhofer, P.E., Fürst, E., & Hirth, W., *A&A*, 92, 225 (1980).
Lessard, R.W., & Buckley, J.H., in preparation (1997).
Li, T.-P., & Ma, Y.-Q., ApJ, 272, 317 (1983).
Lundgren, S.C., Zepka, A.F., & Cordes, J.M., *ApJ*, 453, 419 (1995).
Nice, D.J., & Sayer, R.W., *ApJ*, 476, 261 (1997).
Punch, M., Ph.D. thesis, National University of Ireland (1993).
Reynolds, P. T., et al., *ApJ*, 404, 206 (1993).
Sturner, J.A., Dermer, C.D., *A&A*, 293, L17 (1994).
Tavani, M., et al., *ApJ*, 479, 109 (1997).
Thompson, D.J., et al., *ApJS*, 101, 259 (1995).